EXPLORING LOCAL NEURONAL CIRCUITRY WITH CONTROLLED IONTOPHORESIS

Anna Marie Belle

A dissertation submitted to the faculty of the University of North Carolina at Chapel Hill in partial fulfillment of the requirements for the degree of Doctor of Philosophy in the Department of Chemistry

Chapel Hill
2013

Approved by:

Mark Wightman

James Jorgenson

Royce Murray

Regina Carelli

Dorothy Erie

ABSTRACT

Anna Marie Belle: EXPLORING LOCAL NEURONAL CIRCUITRY WITH CONTROLLED IONTOPHORESIS
(Under the direction of R. Mark Wightman)

Understanding how neurochemical messengers propagate neuronal signals and ensure delivery of nutrients to fuel this process is the first step to proper treatment and prevention of disorders involving neurological dysregulation. Here, the technique of controlled iontophoresis is coupled to electrochemical detection of dopamine, serotonin, and molecular oxygen (O_2) and concurrent monitoring of cell firing to begin to probe the mechanics of local neural circuits. Iontophoresis is a drug delivery technique where application of current causes charged molecules to migrate through a glass capillary. In controlled iontophoresis these capillaries are coupled to a carbon-fiber microelectrode and ejections are monitored electrochemically. The ability to control and modify iontophoretic ejections in real-time makes controlled iontophoresis a significant advancement over previous iterations of iontophoresis as explained and demonstrated herein. Use of this technique first established that we can in fact selectively modulate electrically evoked dopamine release in the striatum of anesthetized rats with local application of an autoreceptor antagonist. Then, the technique was used to examine functional hyperemia, the link between cerebral blood flow and neurochemical release, by monitoring local changes in O_2. Direct glutamate application, known to cause vasodilation, increased local O_2 concentration linking these O_2 changes to blood flow. Additionally, with controlled iontophoresis the relative concentrations of glutamate applied could be compared. This led to the discovery that application of high concentrations of glutamate induced ionic

oscillations that are attributed to calcium. Next, the role of serotonin in functional hyperemia is examined in two regions with different serotonergic topography. Unlike glutamate, serotonin application is shown have a much more complex role in functional hyperemia, inducing increases, decreases, and no change in O_2. Finally, in order to really understand neuronal signaling, it must be given a context. This work concludes with collection of concurrent electrochemical/electrophysiological data while controlled iontophoresis is used to selectively modulate dopamine release and cell firing in freely-moving animals engaged in behavioral tasks. Preliminary application of this technique has confirmed the existence of subpopulations of medium spiny neurons in the nucleus accumbens and shown that each of these subpopulations plays a unique role in intracranial self-stimulation.

ACKNOWLEDGEMENTS

The work presented herein was directly and indirectly influenced and its author nurtured by many people over the years. First, to my advisor, Mark Wightman, your guidance, support, and enthusiasm for learning has shaped me into the scientist I am now and for that I am truly grateful. You have provided a chemistry laboratory full of endless opportunities limited only by my own creativity and need for sleep. To Dr. Natalie Rios Herr, thank you for teaching me the ways of the Wightman Lab as a young first year and for your own work on controlled iontophoresis, without which this dissertation would not be possible. To Dr. Catarina Owesson-White, thank you for confronting the seemingly impossible project of iontophoresis in freely-moving animals with me and giving me a Zumba buddy. Our efforts are presented in Chapters 5 and 6. To Kevin Wood, you were a fantastic undergraduate researcher and thank you for collecting the serotonin data in Chapter 4. To Preethi Gowrishankar, thank you so much for all your help over the past 3 years, without your help there is no way I could have collected the data in Chapters 3 and 4. You continually went above and beyond as an undergraduate student! Finally, to former and current Wightmanites thank you so much for all of the encouragement, help, friendship and fun both during and after work.

There are also several people who have fostered my love of science in general and chemistry in particular over the years. To my extended family, thank you for all of the gifts and holiday projects, it's amazing the influence that Childcraft Encyclopedias and a crystal radio can have on a child. I will always remain gratefully to my high school chemistry

teacher, Marilyn Theisen. While there's a chance that I would still love chemistry without her instruction, I am not willing to risk it. Thanks also to Dr. Kevin Chambliss and Dr. Jason Belden, for their support and mentorship during my undergraduate research. Finally, I will be forever gratefully to Kevin Chambliss, not only for mentorship over the years but for suggesting I look into 'Chapel Hill' for graduate school.

There have been a number of folks near and far who have helped me through this experience as well. To Natalie, Kristi and Kristen, thanks for the free therapy and laughs over the years. And, to Michael, my friend-for-life, thanks for making this whole experience a bit more fun. Finally, thanks to my family for all of your support over the years. Justin thanks for being my first collaborator and the best brother ever. My gratitude and love also goes to my parents Joseph and Deborah Belle who are mentioned last simply because they should be mentioned in every paragraph above!

TABLE OF CONTENTS

LIST OF TABLES

LIST OF FIGURES

LIST OF ABBREVIATIONS AND SYMBOLS

*	probability less than 0.05
**	probability less than 0.01
***	probability less than 0.001
$[O_2]_{max}$	maximal evoked O_2 concentration
µA	microamperes
μ_{app}	mobility due to applied current
μ_{eo}	electroosmotic mobility
μ_{ep}	electrophoretic mobility
µM	micromolar
µs	microsecond
4-MC	4-methylcatechol
5-HT	serotonin
aCSF	artificial cerebral spinal fluid
Ag/AgCl	silver/silverchloride
AP	acetaminophen
AP	anterior-posterior
B_{max}	drug concentration at maximal binding
BOLD	blood-O_2-level-dependent
Ca^{2+}	calcium ion
CB_1	cannabinoid receptor type 1
CBF	cerebral blood flow
CE	capillary electrophoresis
CMOS	complementary metal–oxide–semiconductor
CV	cyclic voltammogram

D1R	D1 receptor
D2R	D2 receptor
DA	dopamine
DC	direct current
DV	dorsal-ventral
E	applied electric field
ε	permittivity
EC_{50}	effective concentration for 50% of full effect
EGTA	ethylene glycol tetraacetic acid
EOF	electroosmotic flow
eVTO	extended variable-time out
F	Faraday's constant (96,485 C/mol)
fMRI	functional magnetic resonance imaging
FR	fixed-ratio
FSCV	fast-scan cyclic voltammetry
g	gram
GABA	*gamma*-aminobutyric acid
GPe	external capsule of the globus pallidus
GPi	internal capsule of the globus pallidus
H^+	hydrogen ion
HDCV	high definition cyclic voltammetry
Hz	hertz
i	applied current
i.p.	intraperitoneal injection
ICSS	intracranial self stimulation

K^+	potassium ion
K_d	drug concentration at 50% maximal binding
kg	kilogram
kHz	kilohertz
kV	kilovolt
L	distance between CE inlet and dectector
L_t	length of CE capillary
M	molar
MFB	medial forebrain bundle
mg	milligram
Mg^{2+}	magnesium ion
min	minute
ML	medial-lateral
mL	milliliter
mm	millimeter
ms	millisecond
MSN	medium spiny neuron
N	nomifensine
n	transport number
η	viscosity
nA	nanoampere
Na^+	sodium ion
NAc	nucleus accumbens
NaCl	sodium chloride
nM	nanomolar

NPE	2-(4-nitrophenoxy) ethanol
O_2	molecular oxygen
PBS	phosphate buffered saline
PEH	peri-event histogram
PET	Positron emission tomography
QL	quinlorane
QP	quinpirole
R	raclopride
s	second
SNr	substantia nigra pars reticulata
T	ejection time
$t_{neutral}$	time for neutral species to reach detector
t_r	time for analyte to reach detector
TRIS	tris(hydroxymethyl)aminomethane
U	uric acid
UNC	University of North Carolina
UV-VIS	ultraviolet-visible light
V	applied voltage
V	volt
v_{eo}	electroosmotic flow velocity
v_{ep}	rate of electrophoretic migration
v_{obs}	observed linear velocity
VTA	ventral tegmental area
VTO	variable-time out
z	charge

ζ	zeta-potential at glass capillary-solution interface
Ω	Ohm

Chapter 1

Monitoring and modulating dopamine release and unit activity in real-time

INTRODUCTION

A vital step in creating effective treatments for addiction and learning disorders is to understand the neuronal circuitry that drives voluntary reward-directed behaviors and how drugs may hinder, help or hijack this system. Intracranial self stimulation (ICSS) is a well established behavioral paradigm in which an animal learns to press a lever to stimulate a region in their own brain and is considered a robust method to study learning and reward (Olds and Milner, 1954). Use of this technique combined with selective lesions and pharmacological manipulation of selected brain regions has indicated that the nucleus accumbens (NAc) is an important junction for the transmission of information during ICSS (Saddoris et al., 2013).

The role of dopamine in circuits that control learning, goal-oriented behaviors, and addiction has been of interest to neuroscientists for many decades. It is known that dopaminergic neurons, many of which terminate in the NAc, change their firing patterns in response to rewards and cues that predict reward (Mirenowicz and Schultz, 1994) and that dopamine neurotransmission is vital for reinforcing a behavior (Di Chiara and Imperato, 1988). However, these discoveries were made using electrophysiology to monitor the firing pattern of neurons or microdialysis to look at prolonged changes in extracellular dopamine concentration, not dopamine concentration changes on the timescale of cell firing. Dopaminergic neurons generally fire several times per second with periodic bursts of

increased frequency (Grace and Bunney, 1984) so a technique that can distinguish changes in dopamine concentration on this timescale is essential.

Fast-scan cyclic voltammetry (FSCV) can measure changes in local dopamine concentrations up to 60 times per second (Kile et al., 2012), making it the perfect technique to monitor dopamine release in freely moving animals (Garris et al., 1997; Rebec et al., 1997, Robinson and Wightman, 2007). Thanks to technical advances over the past decade FSCV can now be combined with electrophysiological recordings and iontophoresis, allowing researchers to monitor and manipulate pre- and postsynaptic activity during behavior. The technical considerations and resulting discoveries from the combination of these techniques are discussed here.

DOPAMINE NEUROTRANSMISSION

Neurons are brain cells responsible for the integration and transmission of information throughout the brain; they receive, process, and transmit information to and from discrete populations of neurons within specific circuits in the brain. Classic neurotransmission occurs when the activation of receptors on dendrites of a cell begins a cascade of intracellular processes that often include the generation and propagation of an action potential, a voltage difference across the neuronal membrane. The frequency of the firing of action potentials of a cell is referred to as its unit activity, and the modulation of unit activity is the way in which information is encoded. When an action potential propagates along the neuron's axon to its terminals, it triggers the release of neurotransmitter into the extracellular space. There the neurotransmitters can bind to specific receptors on a proximal neuron. The modulation of target neurons via neurotransmitter release is central to the regulation of an organism's behavior.

Dopamine release in the NAc plays an extensive role in governing motivated behaviors (Salamone and Correa, 2012) and we have shown that its release coincides with learned associations for rewarding stimuli and drugs of abuse (Phillips et al., 2003; Robinson and Wightman, 2007; Owesson-White et al., 2009; Beyene et al., 2010; Day et al., 2010). There is a high density of dopamine cell bodies in the ventral tegmental area (VTA) that send their axonal projections to many regions of the brain including the striatum. The ventral striatum is divided into two subregions: the NAc core and NAc shell. In both NAc subregions, dopamine terminals form synapses onto spines found on the dendrites of medium spiny neurons (MSNs) (Yung et al., 1995). MSNs comprise 95% of the cell bodies in the NAc and release GABA, an inhibitory neurotransmitter, upon firing (Chang and Kitai, 1985). Neurons with cell bodies located in regions other than the VTA, including other NAc MSNs, also synapse onto these MSNs, making their activation a complex process known to be essential for movement, learning, and motivation, and that is facilitated by dopamine release in the region.

When dopamine is released from terminals it can then bind to any of the 5 types of dopamine receptors (D1-D5). The predominant dopamine receptors in the NAc, are the D1 receptor (D1R) and D2 receptor (D2R). Both of these receptors are G-protein linked, but D1Rs activate G-proteins that stimulate adenylyl cyclase while D2Rs activate G-proteins that inhibit adenylyl cyclase. D1Rs also have a lower binding affinity for dopamine than D2Rs. This difference in binding affinities supports the idea that normal basal levels of dopamine in the brain constantly ensure the activation of the majority of D2Rs, while sudden phasic increases in dopamine release activate D1Rs (Dugast et al., 1997; Berke and Hyman, 2000).

D2Rs are found on both pre- and postsynaptic terminals. Pre-synaptic receptors are commonly referred to as D2 autoreceptors (Roth, 1979) and are found to have inhibitory effects on DA release from terminals. D2-autoreceptors have been linked to short term

modulation of dopamine release (Kita et al., 2007) making them an ideal target when attempting to manipulate evoked dopamine release quickly. Additionally, there are biochemical (Helmreich et al., 1982; Martin et al., 1982; Claustre et al., 1985), electrophysiological (Skirboll et al., 1979), and behavioral (Bradbury et al., 1984) data suggesting that dopamine agonists exhibit greater potency at D2 autoreceptors than at postsynaptic D2Rs. While both pre- and postsynaptic D2 receptors exhibit similar pharmacology (Elsworth and Roth, 1997), they differ in the G-proteins they use to inhibit adenylyl cyclase (Montmayeur et al., 1993; Guiramand et al., 1995). Functionally, this means more binding may be required at post-synaptic receptors to elicit comparable adenylyl cylase inhibition. The net effect of dopamine release on MSNs is dependent on a balance between the binding of D1Rs, postsynaptic D2Rs and D2 autoreceptors. Indeed, it appears that the more we know about dopamine neurotransmission the more subtle and yet complex its signaling capabilities seem.

While the different effects of D1R and D2R activation on MSNs has long been recognized, it was recently discovered that D1Rs and D2Rs are in fact segregated onto two different MSN populations (Valjent et al., 2009; Gerfen and Surmeier, 2011). In the dorsal striatum approximately half of MSNs contain D1Rs and project axons to the output nuclei of the basal ganglia (substantia nigra and internal capsule of the globus pallidus). These D1 MSNs are termed the “direct pathway.” Other MSNs contain exclusively D2Rs and project to the external capsule of the globus pallidus. These D2 MSNs are termed the “indirect pathway” because they synapse with neurons that also project back to the output nuclei. Although this circuitry was originally characterized in the dorsal striatum, it is also found in the NAc (Ikemoto, 2007).

EVOLUTION OF A WAVEFORM

A number of electrochemical techniques can be used to detect neurotransmitters *in vivo* (Robinson et al., 2008) but cyclic voltammetry has the unique ability to provide a distinct current trace (cyclic voltammogram) for the oxidation and/or reduction of electroactive compounds. This allows identification and quantification of compounds, a critical feature that prevents incorrect conclusions about the role of a substance in a particular behavior (Wightman and Robinson, 2002). FSCV has become the electrochemical technique of choice for monitoring changes in neurotransmitter levels in the brain because it adds high temporal resolution to the chemical selectivity and high sensitivity of cyclic voltammetry (Millar et al., 1985). The detection of monoamines with FSCV has been optimized over the years to allow detection of low nanomolar concentrations of dopamine (Keithley et al., 2011). However, the detection limit is not the only factor that must be considered when deciding on a waveform. By varying the rate and range of potentials applied to the carbon-fiber microelectrode the detection limit of a neuroactive species and the temporal response of the electrode can be optimized.

The first studies in freely moving rats detected dopamine with a waveform that held the carbon fiber at -0.4 V, increased linearly up to 1.0 V and back to -0.4 V in 9.3 ms once every 100 ms. This potential waveform is less frequently used today for the detection of neurotransmitters in freely moving animals because of its lack of sensitivity. However, many important discoveries were made with its use because of its temporal resolution. These include studies of rapid dopamine release in response to reward delivery and how the magnitude of the dopamine changes as an animal learns a behavior (Garris et al., 1999; Kilpatrick et al., 2000). This high speed recording of dopamine release during behavioral tasks supported the hypothesis that dopamine release is required for learning a rewarding task, but it does not signal the reward itself.

The lack of sensitivity of the original waveform used for dopamine detection limited FSCV to the measurement of "extracellular dopamine changes after electrical stimulation of cell bodies in the substantia nigra compact, rather than spontaneous or gradual changes in extracellular dopamine" (Budygin et al., 2001). Fortunately, extension of the original waveform increased dopamine sensitivity 9-fold *in vivo* allowing detection of 5 nM, a level seen for some naturally occurring changes in dopamine (Heien et al., 2003). The improved detection limit was achieved by holding the electrode at -0.6 V and linearly increasing voltage to 1.4 V and back to -0.6 V in 10 ms once every 100 ms. Increased sensitivity resulted from two consequences of this extended waveform: adsorptive pre-concentration of dopamine occurs when the electrode is held at a more negative potential between scans, and the reactive carbon fiber surface is constantly cleaned as a consequence of over-oxidation of its functional groups. This extended waveform decreased the temporal response of the technique by 1.2 s, however, and decreased the selectivity of the electrode for the oxidation and reduction of dopamine over other species. Thus this waveform is most useful for experiments carried out in regions where only a single electroactive compound is present and when the detection limit of dopamine is of higher priority than the electrode's temporal response. This waveform allowed monitoring of naturally occurring increases in dopamine release the NAc (Phillips et al., 2003) and allowed detection of basal dopamine level changes over 90 s periods (Heien et al., 2005).

The waveform now used for dopamine detection *in vivo* combines the detection limit of the extended waveform and the temporal response of the original waveform. The scan starts at -0.4 V and linearly increases to 1.3 V at the same rate as the extended waveform, taking 8.5 ms to complete (Heien et al., 2004). This is repeated every 100 ms. This "dopamine waveform" allows detection of 8 nM DA without the sacrifice in temporal response seen with pre-adsorption at -0.6 V. This is the waveform of choice in experiments

where FSCV is used to monitor dopamine or norepinephrine and pH changes in the brain of freely-moving animals.

With the development of methods to quantitatively measure the dynamics of several analytes simultaneously (Heien et al., 2004) and to display thousands of cyclic voltammograms simultaneously to qualitatively monitor the temporal dynamics of each analyte (Michael et al., 1998), we were able to begin to ask and answer increasingly complex questions about dopamine signaling dynamics in behavior. One of these questions was how the dynamics of dopamine signaling affected the balance between cerebral blood flow and metabolism in a region. A waveform was designed that allows for the reduction of oxygen at the carbon fiber when biased to a negative potential (-1.4 V). By scanning up to 1.0 V we can also see the oxidation of dopamine and any changes in hydrogen ion concentrations within the same scan, but the sensitivity of this waveform for monoamines is greatly reduced due to the reduced magnitude of the positive scan and a holding potential of 0.0 V (Zimmerman and Wightman, 1991; Kennedy et al., 1992). Monitoring oxygen, pH, and dopamine simultaneously has allowed the discoveries that dopamine seems to have little effect on the balance between cerebral blood flow (oxygen changes) and metabolism (pH changes) in both anesthetized (Zimmerman and Wightman, 1991; Venton et al., 2003) and awake animals (Cheer et al., 2006; Ariansen et al., 2012). The information about metabolic dynamics during neurotransmission that this waveform allows us to monitor also allowed us to be the first to show with the temporal and spatial resolution of our microelectrodes that the endocannabinoid CB_1 receptor mediates changes in the balance between cerebral blood flow and metabolism in the brain of awake animals (Cheer et al., 2006). This finding has implications for the development of new treatments for cerebral vascular disorders and is an excellent example of the sorts of questions FSCV can answer about the brain.

SEEING THE BRAIN COMMUNICATE: A COMBINATION OF MEASUREMENT PROCEDURES

Development of the FSCV method that is optimized for monitoring neuronal processes was a task that analytical chemists with an interest in neuroscience could confidently undertake. However, the design of small animal behavioral experiments to probe the role of dopamine dynamics encompassed concepts far beyond those normally addressed by chemists. We employed a number of unconventional stimuli such as the popping of bubble wrap outside of cages to monitor the startle response of rats (Robinson and Wightman, 2004). We made the unanticipated discovery that the presence of female rats induced subsecond dopamine increases in male rats. We also discovered that these dopamine transients were unrelated to sexual differentiation (Rebec et al., 1997; Robinson et al., 2001; Robinson et al., 2002). Nevertheless, the initial attempts at behavioral experiments turned out to be excellent proof-of-concept for this new measurement technique in freely moving rats.

In 2000, the Wightman lab partnered with the lab of Dr. Regina Carelli, a psychologist with demonstrated proficiency in small animal behavior. Carelli was known for using electrophysiology to monitor cell firing in behaviors involving reward-based learning and drugs of abuse (Carelli and Deadwyler, 1997; Carelli, 2000; Carelli, 2002). Extracellular electrophysiological recordings monitor voltage changes in the space around a cell that result from potential changes arising from propagation of an action potential. Carelli and coworkers had focused on the electrophysiology responses of dopaminergic neurons in rats and thus it was relatively straight forward to reexamine the same behaviors while monitor changes in dopamine release with FSCV (Carelli, 2002). The combined expertise brought by psychologists and chemists working in parallel allowed significant breakthroughs in understanding the dynamics of dopamine transmission in behavior and addiction. The temporal resolution of FSCV resolves distinct dopamine increases coinciding with the cue

indicating imminent lever availability from those that occur at the lever presentation 2 s later (Stuber et al., 2005a; Day et al., 2007). In addition, the temporal resolution of FSCV showed that the dopamine release occurred *before* the reward was presented once the animal knew to expect lever presentation at a fixed interval (Cheer et al., 2007). This directly supported earlier theories that hypothesized that dopamine is responsible for reward prediction or its expectation instead of being a component of the hedonistic aspect (Schultz, 1998).

The early experiments used a fixed time between lever availability so it was unclear whether dopamine was playing a role in the measurement of elapsed time or was signaling that the lever was present. We now use a variable time-out period between lever presentations to avoid teaching the animal that the timing of cue presentation is predictable (Owesson-White et al., 2008). FSCV used in a variety of reward-based behavioral paradigms established that in the NAc, dopamine release occurs during behavioral tasks with the same rapid dynamics as changes in cell firing (Phillips et al., 2003; Roitman et al., 2004; Stuber et al., 2005b; Stuber et al., 2005a; Owesson-White et al., 2008; Jones et al., 2010; Sugam et al., 2012).

Combining Electrochemistry with Electrophysiology

In a 2004 review, Carelli and Wightman reviewed the microcircuitry in the NAc involved in drug addiction (Carelli and Wightman, 2004). The review contained a single figure in which data from two separate experiments in two separate animals were overlaid to show cell firing and dopamine changes both rapidly occurred at the administration of cocaine. The modulation of cell firing in NAc MSNs during behavioral tasks appeared to be dopamine-dependent (Yun et al., 2004) but the relationship between the two was (and still is!) not fully understood. While the Wightman lab had previously ventured into simultaneous electrochemistry and single-unit recordings experiments in anesthetized preparations

(Ewing et al., 1983; Kuhr et al., 1987), the two techniques were carried out at separate electrodes positioned 500 µm apart (Ewing et al., 1983) or in completely different brain regions (Kuhr et al., 1987). The development of the electronics and methods to combine the two techniques on a single electrode in a freely-moving animal was first accomplished by the lab in 2005 (Cheer et al., 2005) and has been an ongoing area of research (Owesson-White et al., 2009; Cacciapaglia et al., 2011; Takmakov et al., 2011; Belle et al., 2013).

The key to this combined technique is the ability to use a carbon-fiber microelectrode both for electrochemistry and electrophysiology. This concept was first developed by Julian Millar and coworkers in anesthetized animals (Armstrong-James and Millar, 1979, 1988; Stamford et al., 1993). Several advantages arise from using the same electrode for both measurements, including the ability to measure action potentials from the neurons that are being influenced by the local neurotransmitter release sensed at the electrode (Su et al., 1990), the minimization of tissue damage, and the decreased complexity of surgeries. Rapidly alternating between these two techniques without glitches or artifacts requires complex circuitry and modified experimental parameters to freely-moving systems (Garris et al., 1997), a project that required the collaboration of chemists, neurobiologists, and electrical engineers (Cheer et al., 2005; Takmakov et al., 2011).

A switch is used to alternate the carbon fiber between a current amplifier for electrochemical detections and a voltage follower for single-unit recording. The headstage where this first stage of signal modification is completed is located on the rats' head within a few centimeters of the electrode, minimizing the noise in the amplified signal. Figure 1 shows the timing and output when switching between the two circuits. When the voltage follower is connected, voltage changes occurring at the carbon fiber are recorded. Alternatively when the current amplifier is connected to the carbon fiber, it is ramped through a potential window and the resulting currents recorded. The original design of this experiment included a solid-state switch that unfortunately would sometimes allow

electrochemical voltages to leak over into the single-unit recordings (Cheer et al., 2005). While these voltage changes looked distinct from unit activity, they often overwhelmed the recordings making it difficult to elicit firing changes in the unit of interest. Two improvements were made to help prevent this leakage.

The first modification was to the electrical circuit. There is now a new solid-state relay chosen for its low leakage, low charge transfer, low and matched input capacitance, low resistance (10 Ω), and fast (<1 μs) switching time (Takmakov et al., 2011). These characteristics prevent excess charging currents during the switch and current leakage between the two circuits. The second modification that helped prevent leakage of voltage between the two systems was the timing of the voltammetric scan to the carbon fiber. The unit-recording interval always has a 20 ms gap every 180 ms during which the 8.5 ms voltammetric scan occurs. In initial applications of this technique, the potential scan occurred at the very end of this 20 ms interval. This was done to maximize the adsorption of dopamine to the electrode while it was held at a negative potential; however, this resulted in current fluctuations when the electrode was switched over to electrophysiology. These fluctuations would manifest as large voltage changes in the single-unit data. To correct for this, a potential of -0.4 V is applied for pre-concentration of dopamine and current stabilization of the electrode for only the first 5 ms of the 20 ms interval. The electrode is then ramped to 1.3 V and back to -0.4 V where it remains for ~5 ms before the mode is switched. This timing is shown in Figure 1.1. The ability to look at these changes concurrently and with respect to external stimuli or behavioral patterns allows us to begin to directly tease apart the effects of dopamine neurotransmission by monitoring dopamine release from terminals and the unit-activity of the cell with dopamine receptors in the vicinity. The required modifications of the dopamine waveform result in some sacrifices in electrochemical detection however. The sampling rate is doubled to once every 200 ms

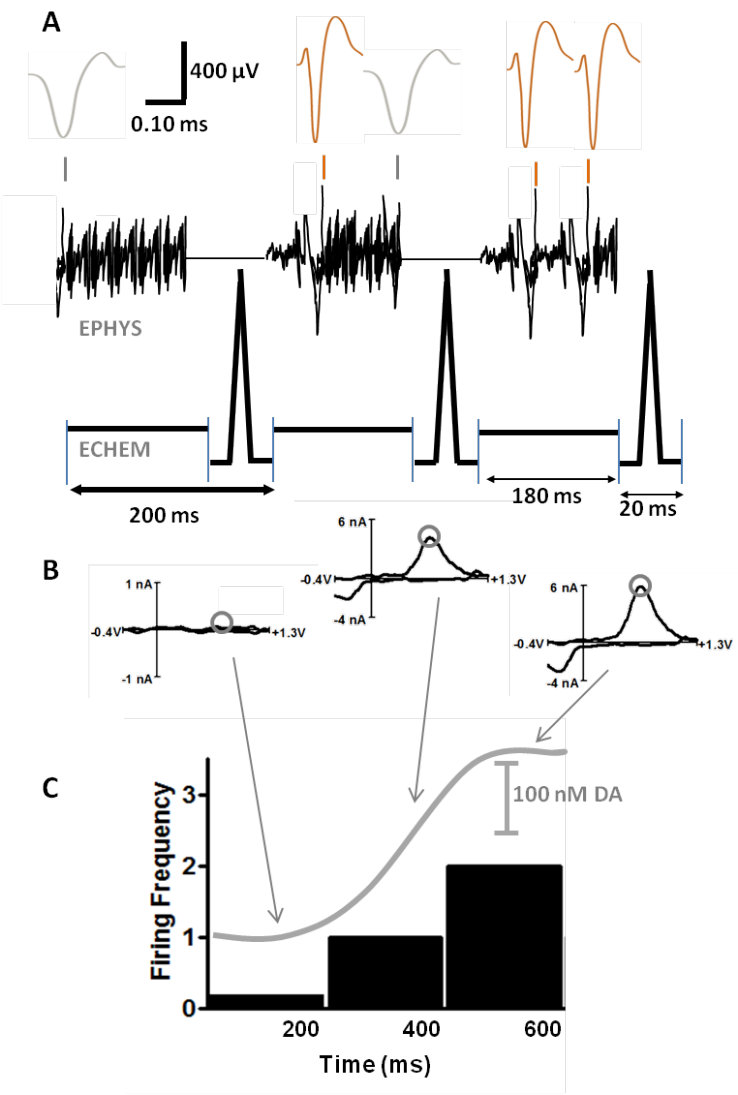

Figure 1.1. Data output from combined fast-scan cyclic voltammetry/electrophysiology experiments. A) The output of the carbon-fiber electrode was connected to a voltage follower to monitor cell firing, seen at voltage changes over time (upper circuitry). The lines above the voltage read out indicate regions of the 180 ms recording interval that have been expanded above. The dark grey spikes are firing of the MSN of interest. The light grey spikes are an example of an excluded event. Every 200 ms the electrode was switched from the electrophysiology circuit to the lower voltammetry circuitry for 20 ms. In this position, the amplifier controlled the electrode potential and the current was monitored. When the lower circuit was completed, the electrode was held at -0.4 V then over 8.5 ms scanned from to +1.3 V and back to -0.4 V. During this time, there were no voltage changes seen in the electrophysiology (when circuit was open but program still recorded data). B) The cyclic voltammograms resulting from changes each of the three sequential potential scans. C) The simultaneous presentation of electrophysiological and electrochemical data. The histogram shows the frequency with which the cell fired during the 200 ms bins and the trace superimposed over the graph shows changes in the concentration of dopamine detected over the same time period.

and the dopamine detection limit is only 62% of the traditional dopamine waveform (Cheer et al., 2005).

This dual technique's first discovery was to show that in the same location dopamine release and changes in cell firing were both synchronized to lever pressing in trained animals. MSNs that showed increases OR decreases at lever press (and electrical stimulation), showed a simultaneous increase in dopamine (Cheer et al., 2005). This study also showed that cell firing (but not dopamine release) changed with the administration of GABAergic antagonists; supporting the idea that dopamine altered the probability of a cell firing but was not the neurotransmitter directly responsible for NAc MSNs firing. Later work demonstrated a positive correlation between the concentration of dopamine and magnitude of cell firing change and observed that dopamine release was seen in all locations with MSNs responsive to behavioral stimuli (Owesson-White et al., 2009). MSNs that were unresponsive during the behavior were all in locations with no dopamine release during the behavior (Owesson-White et al., 2009; Cacciapaglia et al., 2012). The difference between correlation of dopamine release and cell firing in the two subregions of the NAc, the core and the shell, was also investigated. Dopamine in the core was closely timelocked to the reinforced response of the lever press. In the shell, dopamine was released over a longer duration and did not coincide as greatly with lever pressing (Owesson-White et al., 2009). The same subregion specific dopamine dynamics were seen for natural rewards as well (Cacciapaglia et al., 2012). These results demonstrate the heterogeneity of dopamine release and suggest this release is positioned to selectively modulate specific MSNs.

After establishing the link between dopamine release and cell firing during ICSS (Cheer et al., 2005; Cheer et al., 2007; Owesson-White et al., 2009), we investigated whether this link was also seen with natural rewards (Cacciapaglia et al., 2011). Rats were trained to press a lever for a sucrose pellet instead of a direct electrical stimulation. The lever was made available at a variable interval and preceded by a 2 s cue. Locations with a

surge in dopamine concentration at the onset of the cue and (to a lesser extent) with lever press, showed one of four alterations in MSN firing: inhibition at cue presentation, excitation at cue presentation, inhibition at lever press, and excitation at lever press. To see if this surge of dopamine was in fact responsible for the coincident changes in cell firing, NMDA receptors were blocked in the VTA attenuating the burst firing of dopamine cells in the region (Chergui et al., 1993). This decreased dopamine release in the NAc. MSNs that showed an excitation to the cue onset or lever press became non-phasic, while cells that were inhibited at either the cue or the lever press were unaffected by the diminished in dopamine release. This showed dopamine's ability to selectively modulate discrete pathways within the NAc and suggested that this was a selective modulation of the direct (D1 MSNs) or indirect (D2 MSNs) pathway.

Controlled Iontophoresis

Iontophoresis is a technique that uses current to induce the migration of a solution of ions through a glass pipette. It was developed in the early 1950s by W.L. Natsuk, a student of A.L. Hodgkin (Nastuk, 1953). While attempting to understand how ions contributed to the actions of acetylcholine at the neuromuscular junction, he noticed that acetylcholine would naturally leak out of a glass pipette pulled to a fine tip and that application of current to the pipette solution ejected even more acetylcholine onto the junction (Hicks, 1984). From there, iontophoresis increased in popularity and extensive studies on the technique were carried out (Krnjevic et al., 1963a; Krnjevic et al., 1963b; Crawford and Curtis, 1964; Curtis and Nastuk, 1964; Bradley and Candy, 1970; Bloom, 1974; Simmonds, 1974; Freedman et al., 1975; Purves, 1977, 1979). The technique's popularity for studying receptor dynamics *in vivo* is due to the fact that drugs can be quickly, selectively, and locally delivered to the site of action with minimal disruption of tissue. Systemic drug administration is only useful for drugs that can pass the blood-brain barrier without metabolic degradation. Even in cases

where the drug can cross the blood-brain barrier, the drug affects the entire brain making it difficult to study discrete brain region effects (Bloom, 1974). Additionally, systemic drug administration can alter animal behavior, making it difficult to look at the drug effects in the brain during behavior (Hernandez and Cheer, 2012). These problems are avoided by using iontophoresis to study the pharmacology of the brain.

A drawback to iontophoresis was the inability to monitor or quantify the amount of drug delivered. This made it impossible to differentiate a null response to drug application from a clogged glass pipette. Additionally, too little drug delivered could result in a false negative whereas excessive application could lead to nonspecific effects. Applied pump currents are commonly used to compare ejections (Pierce and Rebec, 1995; Kiyatkin and Rebec, 1996, 1999b), but the same pump current ejects different drug concentrations from barrel to barrel (Herr et al., 2008). Modifications to the design of Millar and co-workers, which coupled iontophoresis barrels to carbon-fiber microelectrodes, allow detection of electroactive compounds ejected with iontophoresis at the neighboring electrode (Armstrong-James et al., 1981).

Using these coupled iontophoresis probes, electroosmosis was found to contribute significantly to the observed drug delivery (Herr et al., 2008). Electroosmosis is a phenomenon caused by the attraction between the cations in solution and the ionizable silanol groups on the glass capillary surface. When a positive current is applied to the capillary, the cations along the wall migrate toward the anode, inducing a bulk movement of solution, termed electroosmotic flow. The variability in iontophoretic ejections is associated with variability of electroosmotic flow from barrel to barrel, while electrophoretic mobility (ionic migration) for a given species is consistent. Using an electroactive neutral molecule as an internal standard to monitor the variability in electroosmotic flow, and subsequently the amount of drug delivered from different barrels, allows us to control for this variability. These insights into iontophoresis enable quantitative delivery of electroactive and

electroinactive drugs by monitoring the coejection of an electroactive molecule from the same barrel (Herr et al., 2008). When the relative mobilities of the coejected substances are known, monitoring the concentration of the electroactive molecule with the carbon-fiber electrode provides an indirect measure of the relative concentration of the coejected nonelectroactive substance (Herr et al., 2008; Herr et al., 2010).

While FSCV had previously been coupled to iontophoresis to monitor modulation of cell firing by electroactive compounds (Kiyatkin and Rebec, 1996, 1997; Rebec, 1998; Kiyatkin and Rebec, 1999a, b; Kiyatkin et al., 2000; Kiyatkin and Rebec, 2000), it was not until 2010 that the technique was used *in vivo* to alter release from dopamine terminals in the region of drug application (Herr et al., 2010). These papers established that controlled iontophoresis could be used to quickly (<60 s) modulate dopamine release by affecting D2 autoreceptors and the dopamine transporter in anesthetized (Herr et al., 2010) and freely-moving animals (Belle et al., 2013). Monitoring iontophoresis ejections eliminates the fear of ionic and electrical artifacts from the ejection current altering the neuronal environment as well. With controlled iontophoresis coupled to the simultaneous electrochemistry/electrophysiology technique we can watch for these problems during an experiment. While changes to the neuronal environment are not seen from ejection of saline or the electroactive marker molecule, if the ejection current is seen to affect the electrode, electrical connections can be altered or a different barrel on the probe used to prevent any data collection problems (Belle et al., 2013).

With the discovery of the discrete location of D1Rs and D2Rs on separate populations of MSNs (Valjent et al., 2009; Gerfen and Surmeier, 2011) came a huge breakthrough in how neuronal networks in the brain work together in reward, behavior and addiction. In the NAc core, only 6% of MSNs have both D1Rs and D2Rs, while 53% of MSN's have D1Rs exclusively (D1 MSNs) and 41% of MSNs have D2Rs exclusively (D2 MSNs) (Valjent et al., 2009). While the role each receptor during learning and reward has

been investigated (Surmeier et al., 2007), direct electrophysiological evidence has been lacking, partly because of the difficulties in differentiating D1 MSNs and D2 MSNs *in vivo* (Venance and Glowinski, 2003).

Coupling controlled iontophoresis to the same microelectrode in a combined FSCV and single-unit recording experiment allows for pharmacological identification of MSNs based on their responses to D1R and D2R antagonists (Belle et al., 2013). The firing rates of NAc MSNs in awake animals were monitored before, during and after a 15 s iontophoretic ejection of specific dopamine receptor antagonist. Changes in response to these antagonists were seen both immediately and on a prolonged timescale (as an overall change in the firing rate of a neuron after application). Looking at prolonged changes, 40% of MSNs increased their firing rate after local application of a D2R antagonist, 46% of MSNs exhibited a decreased firing rate after local application of the D1R antagonist, and only 11% of MSNs responded to both antagonists. These results are in agreement with previously reported distributions for dopamine receptor subtypes on MSNs (Valjent et al., 2009) supporting the method as a way to discriminate between and selectively modulate D1 MSNs and D2 MSNs *in vivo*.

CONCLUSIONS

As our knowledge of the subtle and complex signaling required for the brain to encode reward-directed behaviors increases, the ability to selectively modulate and monitor dopamine release and MSN firing in freely-moving animals engaged in behavioral tasks becomes even more essential. The development of a technique to monitor subsecond dopamine fluctuations in freely-moving animals has allowed the study of naturally and electrically evoked dopamine during reward-motivated tasks and provided the ability to watch slower, tonic changes in dopamine. Furthermore, combining this ability with

concurrent observation of cell firing patterns *in vivo* is essential for understanding neurotransmission. The technique has shown that MSNs alter their firing during a behavioral task, receive dopaminergic inputs during the behavior and that dopamine release is required for excitations of MSNs during behavior. This combined technique is a passive way to 'listen in' on neurotransmission and the ability to selectively and locally modulate this neuronal conversation will allow an even greater understanding of the purpose of dopaminergic pathways in learning and reward.

DISSERTATION OVERVIEW

While the final two chapters of this dissertation directly report the development and first insights from the combined electrochemical/electrophysiological with iontophoretic modulation discussed here, other applications of controlled iontophoresis in anesthetized animals are first discussed in Chapters 2, 3 and 4. These Chapters lay the ground work for further iontophoretic investigations in awake animals. Chapter 2 presents the utility and methodology of controlled iontophoresis for pharmacological manipulation of neurotransmission. Controlled iontophoresis is then used to probe the relationship between cerebral metabolism (neurotransmission) and blood flow. First, in Chapter 3 this relationship is examined for glutamate, a neurotransmitter with a known vasoactive role in the brain. Then, in Chapter 4 methodology from Chapter 3 is used to investigate the role of serotonin in regulation of cerebral blood flow. Finally, controlled iontophoresis is modified for use in conscious animals (Chapter 5) to elicit the role of dopamine in ICSS (Chapter 6). These projects all demonstrate the utility and improvements of controlled iontophoresis to look at the inner workings of neurotransmission in whole, conscious animals.

REFERENCES

Ariansen JL, Heien MLAV, Hermans A, Phillips PEM, Hernadi I, Bermudez M, Schultz W, Wightman RM (2012) Monitoring extracellular pH, oxygen, and dopamine during reward delivery in the striatum of primates. Front Behav Neurosci 6.

Armstrong-James M, Millar J (1979) Carbon fibre microelectrodes. J Neurosci Methods 1:279-287.

Armstrong-James M, Millar J (1988) High-speed cyclic voltammetry and unit recording with carbon fibre microelectrodes. In: Measurement Of Neurotransmitter Release in vivo (Marden C, ed), pp 209-224. New York: John Wiley and Sons Ltd.

Armstrong-James M, Fox K, Kruk ZL, Millar J (1981) Quantitative ionophoresis of catecholamines using multibarrel carbon fibre microelectrodes. J Neurosci Methods 4:385-406.

Belle AM, Owesson-White C, Herr NR, Carelli RM, Wightman RM (2013) Controlled Iontophoresis Coupled with Fast-Scan Cyclic Voltammetry/Electrophysiology in Awake, Freely Moving Animals. ACS Chem Neurosci 5:761-71.

Berke JD, Hyman SE (2000) Addiction, dopamine, and the molecular mechanisms of memory. Neuron 25:515 -532.

Beyene M, Carelli RM, Wightman RM (2010) Cue-evoked dopamine release in the nucleus accumbens shell tracks reinforcer magnitude during intracranial self-stimulation. Neuroscience 169:1682-1688.

Bloom FE (1974) To spritz or not to spritz: The doubtful value of aimless iontophoresis. Life Sciences 14:1819-1834.

Bradbury AJ, Cannon JG, Costall B, Naylor RJ (1984) A comparison of dopamine agonist action to inhibit locomotor activity and to induce stereotyped behaviour in the mouse. Eur J Pharmacol 105:33-47.

Bradley PB, Candy JM (1970) Iontophoretic release of acetylcholine, noradrenaline, 5-hydroxytryptamine and D-lysergic acid diethylamide from micropipettes. Br J Pharmacol 40:194-201.

Budygin EA, Phillips PE, Robinson DL, Kennedy AP, Gainetdinov RR, Wightman RM (2001) Effect of acute ethanol on striatal dopamine neurotransmission in ambulatory rats. J Pharmacol Exp Ther 297:27-34.

Cacciapaglia F, Wightman RM, Carelli RM (2011) Rapid Dopamine Signaling Differentially Modulates Distinct Microcircuits within the Nucleus Accumbens during Sucrose-Directed Behavior. J Neurosci 31:13860-13869.

Cacciapaglia F, Saddoris MP, Wightman RM, Carelli RM (2012) Differential dopamine release dynamics in the nucleus accumbens core and shell track distinct aspects of goal-directed behavior for sucrose. Neuropharmacology 62:2050-2056.

Carelli RM (2000) Activation of accumbens cell firing by stimuli associated with cocaine delivery during self-administration. Synapse 35:238-242.

Carelli RM (2002) Nucleus accumbens cell firing during goal-directed behaviors for cocaine vs. 'natural' reinforcement. Physiol Behav 76:379-387.

Carelli RM, Deadwyler SA (1997) Cellular mechanisms underlying reinforcement-related processing in the nucleus accumbens: electrophysiological studies in behaving animals. Pharmacol Biochem Behav 57:495-504.

Carelli RM, Wightman RM (2004) Functional microcircuitry in the accumbens underlying drug addiction: insights from real-time signaling during behavior. Curr Opin Neurobiol 14:763-768.

Chang HT, Kitai ST (1985) Projection neurons of the nucleus accumbens: an intracellular labeling study. Brain Res 347:112-116.

Cheer JF, Wassum KM, Wightman RM (2006) Cannabinoid modulation of electrically evoked pH and oxygen transients in the nucleus accumbens of awake rats. J Neurochem 97:1145-1154.

Cheer JF, Heien ML, Garris PA, Carelli RM, Wightman RM (2005) Simultaneous dopamine and single-unit recordings reveal accumbens GABAergic responses: implications for intracranial self-stimulation. Proc Natl Acad Sci USA 102:19150-19155.

Cheer JF, Aragona BJ, Heien ML, Seipel AT, Carelli RM, Wightman RM (2007) Coordinated accumbal dopamine release and neural activity drive goal-directed behavior. Neuron 54:237-244.

Chergui K, Charlety PJ, Akaoka H, Saunier CF, Brunet JL, Buda M, Svensson TH, Chouvet G (1993) Tonic activation of NMDA receptors causes spontaneous burst discharge of rat midbrain dopamine neurons in vivo. Eur J Neurosci 5:137-144.

Claustre Y, Fage D, Zivkovic B, Scatton B (1985) Relative selectivity of 6,7-dihydroxy-2-dimethylaminotetralin, N-n-propyl-3-(3-hydroxyphenyl)piperidine, N-n-propylnorapomorphine and pergolide as agonists at striatal dopamine autoreceptors and postsynaptic dopamine receptors. J Pharmacol Exp Ther 232:519-525.

Crawford JM, Curtis DR (1964) The Excitation and Depression of Mammalian Cortical Neurones by Amino Acids. Br J Pharmacol Chemother 23:313-329.

Curtis DR, Nastuk WL (1964) Micro-electrophoresis. In: Physical Techniques in Biological Research, pp 144-190. New York: Academic Press.

Day JJ, Roitman MF, Wightman RM, Carelli RM (2007) Associative learning mediates dynamic shifts in dopamine signaling in the nucleus accumbens. Nat Neurosci 10:1020-1028.

Day JJ, Jones JL, Wightman RM, Carelli RM (2010) Phasic nucleus accumbens dopamine release encodes effort- and delay-related costs. Biol Psychiatry 68:306-309.

Di Chiara G, Imperato A (1988) Drugs abused by humans preferentially increase synaptic dopamine concentrations in the mesolimbic system of freely moving rats. Proc Natl Acad Sci USA 85:5274-5278.

Dugast C, Brun P, Sotty F, Renaud B, Suaud-Chagny MF (1997) On the involvement of a tonic dopamine D2-autoinhibition in the regulation of pulse-to-pulse-evoked dopamine release in the rat striatum in vivo. Naunyn Schmiedebergs Arch Pharmacol 355:716-719.

Elsworth JD, Roth RH (1997) Dopamine Synthesis, Uptake, Metabolism, and Receptors: Relevance to Gene Therapy of Parkinson's Disease. Exp Neurol 144:4-9.

Ewing AG, Alloway KD, Curtis SD, Dayton MA, Wightman RM, Rebec GV (1983) Simultaneous electrochemical and unit recording measurements: characterization of the effects of D-amphetamine and ascorbic acid on neostriatal neurons. Brain Res 261:101-108.

Freedman R, Hoffer BJ, Woodward DJ (1975) A quantitative microiontophoretic analysis of the responses of central neurones to noradrenaline: interactions with cobalt, manganese, verapamil and dichloroisoprenaline. Br J Pharm 54:529-539.

Garris PA, Christensen JR, Rebec GV, Wightman RM (1997) Real-time measurement of electrically evoked extracellular dopamine in the striatum of freely moving rats. J Neurochem 68:152-161.

Garris PA, Kilpatrick M, Bunin MA, Michael D, Walker QD, Wightman RM (1999) Dissociation of dopamine release in the nucleus accumbens from intracranial self-stimulation. Nature 398:67-69.

Gerfen CR, Surmeier DJ (2011) Modulation of striatal projection systems by dopamine. Annu Rev Neurosci 34:441-466.

Gratton A, Wise RA (1994) Drug- and behavior-associated changes in dopamine-related electrochemical signals during intravenous cocaine self- administration in rats. J Neurosci 14:4130-4146.

Grace AA, Bunney BS (1984) The control of firing patterns in nigral dopamine neurons: burst firing. J Neurosci 4:2877-2890.

Guiramand J, Montmayeur J-P, Ceraline J, Bhatia M, Borrelli E (1995) Alternative Splicing of the Dopamine D2 Receptor Directs Specificity of Coupling to G-proteins. J Biol Chem 270:7354-7358.

Heien ML, Johnson MA, Wightman RM (2004) Resolving neurotransmitters detected by fast-scan cyclic voltammetry. Anal Chem 76:5697-5704.

Heien ML, Phillips PE, Stuber GD, Seipel AT, Wightman RM (2003) Overoxidation of carbon-fiber microelectrodes enhances dopamine adsorption and increases sensitivity. Analyst 128:1413-1419.

Heien ML, Khan AS, Ariansen JL, Cheer JF, Phillips PE, Wassum KM, Wightman RM (2005) Real-time measurement of dopamine fluctuations after cocaine in the brain of behaving rats. Proc Natl Acad Sci USA 102:10023-10028.

Helmreich I, Reimann W, Hertting G, Starke K (1982) Are presynaptic dopamine autoreceptors and postsynaptic dopamine receptors in the rabbit caudate nucleus pharmacologically different? Neuroscience 7:1559-1566.

Hernandez G, Cheer JF (2012) Effect of CB1 receptor blockade on food-reinforced responding and associated nucleus accumbens neuronal activity in rats. J Neurosci 32:11467-11477.

Herr NR, Kile BM, Carelli RM, Wightman RM (2008) Electroosmotic flow and its contribution to iontophoretic delivery. Anal Chem 80:8635-8641.

Herr NR, Daniel KB, Belle AM, Carelli RM, Wightman RM (2010) Probing presynaptic regulation of extracellular dopamine with iontophoresis. ACS Chem Neurosci 1:627-638.

Hicks TP (1984) The history and development of microiontophoresis in experimental neurobiology. Prog Neurobiol 22:185-240.

Ikemoto S (2007) Dopamine reward circuitry: Two projection systems from the ventral midbrain to the nucleus accumbens-olfactory tubercle complex. Brain Res Rev 56:27-78.

Jones JL, Day JJ, Aragona BJ, Wheeler RA, Wightman RM, Carelli RM (2010) Basolateral amygdala modulates terminal dopamine release in the nucleus accumbens and conditioned responding. Biol Psychiatry 67:737-744.

Keithley RB, Takmakov P, Bucher ES, Belle AM, Owesson-White CA, Park J, Wightman RM (2011) Higher sensitivity dopamine measurements with faster-scan cyclic voltammetry. Anal Chem 83:3563-3571.

Kennedy RT, Jones SR, Wightman RM (1992) Simultaneous measurement of oxygen and dopamine: coupling of oxygen consumption and neurotransmission. Neuroscience 47:603-612.

Kile BM, Walsh PL, McElligott ZA, Bucher ES, Guillot TS, Salahpour A, Caron MG, Wightman RM (2012) Optimizing the Temporal Resolution of Fast-Scan Cyclic Voltammetry. ACS Chem Neurosci 3:285-292.

Kilpatrick MR, Rooney MB, Michael DJ, Wightman RM (2000) Extracellular dopamine dynamics in rat caudate-putamen during experimenter-delivered and intracranial self-stimulation. Neuroscience 96:697-706.

Kita JM, Parker LE, Phillips PE, Garris PA, Wightman RM (2007) Paradoxical modulation of short-term facilitation of dopamine release by dopamine autoreceptors. J Neurochem 102:1115-1124.

Kiyatkin EA, Rebec GV (1996) Dopaminergic modulation of glutamate-induced excitations of neurons in the neostriatum and nucleus accumbens of awake, unrestrained rats. J Neurophysiol 75:142-153.

Kiyatkin EA, Rebec GV (1997) Iontophoresis of amphetamine in the neostriatum and nucleus accumbens of awake, unrestrained rats. Brain Res 771:14-24.

Kiyatkin EA, Rebec GV (1999a) Striatal neuronal activity and responsiveness to dopamine and glutamate after selective blockade of D1 and D2 dopamine receptors in freely moving rats. J Neurosci 19:3594-3609.

Kiyatkin EA, Rebec GV (1999b) Modulation of striatal neuronal activity by glutamate and GABA: iontophoresis in awake, unrestrained rats. Brain Res 822:88-106.

Kiyatkin EA, Rebec GV (2000) Dopamine-independent action of cocaine on striatal and accumbal neurons. Eur J Neurosci 12:1789-1800.

Kiyatkin EA, Kiyatkin DE, Rebec GV (2000) Phasic inhibition of dopamine uptake in nucleus accumbens induced by intravenous cocaine in freely behaving rats. Neuroscience 98:729-741.

Krnjevic K, Laverty R, Sharman DF (1963a) Iontophoretic release of adrenaline, noradrenaline and 5-hydroxytryptamine from micropipettes. Br J Pharmacol Chem 20:491-496.

Krnjevic K, Mitchell JF, Szerb JC (1963b) Determination of iontophoretic release of acetylcholine from micropipettes. J Physiol 165:421-436.

Kuhr WG, Wightman RM, Rebec GV (1987) Dopaminergic neurons: simultaneous measurements of dopamine release and single-unit activity during stimulation of the medial forebrain bundle. Brain Res 418:122-128.

Martin GE, Williams M, Haubrich DR (1982) A pharmacological comparison of 6,7-dihydroxy-2-dimethylaminotetralin (TL-99) and N-n-propyl-3-(3-hydroxyphenyl)piperidine with (3-PPP) selected dopamine agonists. J Pharmacol Exp Ther 223:298-304.

Michael D, Travis ER, Wightman RM (1998) Color images for fast-scan CV measurements in biological systems. Anal Chem 70:586A-592A.

Millar J, Stamford JA, Kruk ZL, Wightman RM (1985) Electrochemical, pharmacological and electrophysiological evidence of rapid dopamine release and removal in the rat caudate nucleus following electrical stimulation of the median forebrain bundle. Eur J Pharmacol 109:341-348.

Mirenowicz J, Schultz W (1994) Importance of unpredictability for reward responses in primate dopamine neurons. J Neurophysiol 72:1024-1027.

Montmayeur JP, Guiramand J, Borrelli E (1993) Preferential coupling between dopamine D2 receptors and G-proteins. Mol Endocrinol 7:161-170.

Nastuk WL (1953) Membrane potential changes at a single muscle endplate produced by transitory application of acetylcholine with an electrically controlled microjet. Fed Proc 102.

Olds J, Milner P (1954) Positive reinforcement produced by electrical stimulation of septal area and other regions of rat brain. J Comp Physiol Psychol 47:419-427.

Owesson-White CA, Cheer JF, Beyene M, Carelli RM, Wightman RM (2008) Dynamic changes in accumbens dopamine correlate with learning during intracranial self-stimulation. Proc Natl Acad Sci USA 105:11957-11962.

Owesson-White CA, Ariansen J, Stuber GD, Cleaveland NA, Cheer JF, Wightman RM, Carelli RM (2009) Neural encoding of cocaine-seeking behavior is coincident with phasic dopamine release in the accumbens core and shell. Eur J Neurosci 30:1117-1127.

Phillips PE, Stuber GD, Heien ML, Wightman RM, Carelli RM (2003) Subsecond dopamine release promotes cocaine seeking. Nature 422:614-618.

Pierce RC, Rebec GV (1995) Iontophoresis in the neostriatum of awake, unrestrained rats: differential effects of dopamine, glutamate and ascorbate on motor- and nonmotor-related neurons. Neuroscience 67:313-324.

Purves RD (1977) The release of drugs from iontophoretic pipettes. J Theor Biol 66:789-798.

Purves RD (1979) The physics of iontophoretic pipettes. J Neurosci Methods 1:165-178.

Rebec GV (1998) Real-time assessments of dopamine function during behavior: single-unit recording, iontophoresis, and fast-scan cyclic voltammetry in awake, unrestrained rats. Alcohol Clin Exp Res 22:32-40.

Rebec GV, Christensen JR, Guerra C, Bardo MT (1997) Regional and temporal differences in real-time dopamine efflux in the nucleus accumbens during free-choice novelty. Brain Res 776:61-67.

Robinson DL, Wightman RM (2004) Nomifensine amplifies subsecond dopamine signals in the ventral striatum of freely-moving rats. J Neurochem 90:894-903.

Robinson DL, Wightman RM (2007) Rapid dopamine release in freely moving rats. In: Electrochemical Methods for Neuroscience (Michael AC, Borland LM, eds), pp 17-36. Boca Raton, FL: CRC Press.

Robinson DL, Heien ML, Wightman RM (2002) Frequency of dopamine concentration transients increases in dorsal and ventral striatum of male rats during introduction of conspecifics. J Neurosci 22:10477-10486.

Robinson DL, Hermans A, Seipel AT, Wightman RM (2008) Monitoring rapid chemical communication in the brain. Chem Rev 108:2554-2584.

Robinson DL, Phillips PE, Budygin EA, Trafton BJ, Garris PA, Wightman RM (2001) Sub-second changes in accumbal dopamine during sexual behavior in male rats. Neuroreport 12:2549-2552.

Roitman MF, Stuber GD, Phillips PE, Wightman RM, Carelli RM (2004) Dopamine operates as a subsecond modulator of food seeking. J Neurosci 24:1265-1271.

Roth RH (1979) Dopamine autoreceptors: pharmacology, function and comparison with post-synaptic dopamine receptors. Commun Psychopharmacol 3:429-445.

Saddoris MP, Sugam JA, Cacciapaglia F, Carelli RM (2013) Rapid dopamine dynamics in the accumbens core and shell: learning and action. Front Biosci (Elite Ed) 5:273-288.

Salamone JD, Correa M (2012) The mysterious motivational functions of mesolimbic dopamine. Neuron 76:470-485.

Schultz W (1998) Predictive reward signal of dopamine neurons. J Neurophysiol 80:1-27.

Simmonds MA (1974) Quantitative evaluation of responses to microiontophoretically applied drugs. Neuropharmacol 13:401-406.

Skirboll LR, Grace AA, Bunney BS (1979) Dopamine auto- and postsynaptic receptors. Electrophysiological evidence for differential sensitivity to dopamine agonists. Science 206:80-82.

Stamford JA, Palij P, Davidson C, Jorm CM, Millar J (1993) Simultaneous "real-time" electrochemical and electrophysiological recording in brain slices with a single carbon-fibre microelectrode. J Neurosci Methods 50:279-290.

Stuber GD, Wightman RM, Carelli RM (2005a) Extinction of cocaine self-administration reveals functionally and temporally distinct dopaminergic signals in the nucleus accumbens. Neuron 46:661-669.

Stuber GD, Roitman MF, Phillips PE, Carelli RM, Wightman RM (2005b) Rapid dopamine signaling in the nucleus accumbens during contingent and noncontingent cocaine administration. Neuropsychopharmacol 30:853-863.

Su MT, Dunwiddie TV, Gerhardt GA (1990) Combined electrochemical and electrophysiological studies of monoamine overflow in rat hippocampal slices. Brain Res 518:149-158.

Sugam JA, Day JJ, Wightman RM, Carelli RM (2012) Phasic Nucleus Accumbens Dopamine Encodes Risk-Based Decision-Making Behavior. Biol Psychiatry 71:199-205.

Surmeier DJ, Ding J, Day M, Wang Z, Shen W (2007) D1 and D2 dopamine-receptor modulation of striatal glutamatergic signaling in striatal medium spiny neurons. Trends Neurosci 30:228-235.

Takmakov P, McKinney CJ, Carelli RM, Wightman RM (2011) Instrumentation for fast-scan cyclic voltammetry combined with electrophysiology for behavioral experiments in freely moving animals. Rev Sci Instrum 82:074301-4306.

Valjent E, Bertran-Gonzalez J, Herve D, Fisone G, Girault JA (2009) Looking BAC at striatal signaling: cell-specific analysis in new transgenic mice. Trends Neurosci 32:538-547.

Venance L, Glowinski J (2003) Heterogeneity of spike frequency adaptation among medium spiny neurones from the rat striatum. Neuroscience 122:77-92.

Venton BJ, Michael DJ, Wightman RM (2003) Correlation of local changes in extracellular oxygen and pH that accompany dopaminergic terminal activity in the rat caudate-putamen. J Neurochem 84:373-381.

Wightman RM, Robinson DL (2002) Transient changes in mesolimbic dopamine and their association with 'reward'. J Neurochem 82:721-735.

Yun IA, Wakabayashi KT, Fields HL, Nicola SM (2004) The ventral tegmental area is required for the behavioral and nucleus accumbens neuronal firing responses to incentive cues. J Neurosci 24:2923-2933.

Yung KK, Bolam JP, Smith AD, Hersch SM, Ciliax BJ, Levey AI (1995) Immunocytochemical localization of D1 and D2 dopamine receptors in the basal ganglia of the rat: light and electron microscopy. Neuroscience 65:709-730.

Zimmerman JB, Wightman RM (1991) Simultaneous electrochemical measurements of oxygen and dopamine in vivo. Anal Chem 63:24-28.

Chapter 2

Iontophoresis for quantitative modulation of the D2 autoreceptor

INTRODUCTION

Drug Receptor Theory

Neurons transport information through the brain via the release and detection of neurotransmitters by specific receptors at synaptic junctions. The mechanisms behind the transport of information from neuron to neuron can be investigated with the use of compounds that can block or activate particular receptors. Here, D2 dopamine receptor (D2R) subtype occupancy was modulated with dopamine (DA) and other drugs to determine effects on extracellular DA. D2Rs are found on pre- and post-synaptic terminals. The pre-synaptic D2Rs are commonly referred to as D2-autoreceptors (Roth, 1979) and are found to have an inhibitory effect on DA release. Additionally, there are biochemical (Helmreich et al., 1982; Martin et al., 1982; Claustre et al., 1985), electrophysiological (Skirboll et al., 1979), and behavioral (Bradbury et al., 1984) data that suggest that DA agonists exhibit greater potency at D2 autoreceptors than at post-synaptic D2Rs. Therefore, in the low-dosage range the autoreceptor-mediated effects of DA and other agonists will predominate. D2 autoreceptors have also been linked to short term modulation of DA release (Kita et al., 2007) making them the ideal target when attempting to manipulate evoked DA release quickly.

The negative feedback that these autoreceptors provide on the release of DA at a synapse can also be blocked with the use of antagonists specific for this receptor. Antagonists are drugs that bind a receptor with high affinity but have no intrinsic efficacy to

the receptor, and thus effectively "block" the receptor. Conversely, an agonist interacts with a receptor in a way that mimics the neurotransmitter expected to activate the receptor. This gives the illusion of increased concentration of a neurotransmitter at the synapse and increases the response at the synapse to the neurotransmitter. The illusion of increased DA binding to D2 autoreceptors would signal the decreased release of DA from the pre-synaptic terminal, resulting in a decrease in extracellular DA levels when agonist binds to the receptor.

In pharmacology, dose-response curves serve as a guide to determine relative affinity of drugs for a receptor or efficacy for the onset of a given response. In 1927, A.J. Clark put forth Occupational Theory to explain drug-receptor interactions (Clark, 1926, 1927, 1937). This theory assumes that responses, whether quantified in terms of behavior or evoked release of a given neurotransmitter, are a result of reversible receptor occupation by an agonist and that the magnitude of the response is proportional to the number of receptors occupied by agonist. This theory is particularly useful where the magnitude of response to a drug rather than receptor occupancy from direct binding studies is a more practical piece of information both in terms of results and experimental procedure. Dose response curves are often used to examine this relationship for several reasons including the large range of drug concentrations that can be examined. The relationship between response and the logarithm of drug concentration is almost completely linear between 20% and 80% of the maximum response. On these curves the concentration of a drug that causes 50% of the maximum effect is referred to as the EC_{50}. Potency (but not necessarily affinity) of a drug at a given receptor can be determined from the EC_{50} value.

Competitive antagonism, as modeled here, occurs when both the agonist and antagonist bind to the same site(s) on a receptor and compete for binding at those sites when both are present. While this is a simplified model that does not necessarily hold true for many cases *in vivo*, it is good for initial modeling (Wyllie and Chen, 2007). The binding

of the antagonist can be eliminated by increasing the concentration of the agonist. This is exactly what we observed when a high concentration of the agonist quinelorane was locally ejected into the brain. Then, as quinelorane diffused away from the ejection point, its concentration in the synapses around the electrode decreases and haloperidol, the antagonist, once again dominates the competition for binding to the receptor.

Drug Delivery Methods

Traditional drug delivery tools such as intraperitoneal (i.p.) or intravenous injections affect the system as a whole and potentially activate additional mechanisms on both sides of the blood-brain barrier that can affect the observed results. Systemic drug application also comes with the disadvantages of time delay, potential side effects and toxicity (Hicks, 1984). Localized drug manipulations are therefore necessary to break the system down into individual parts and study each in isolation. With respect to the brain, this leaves researchers with the options of microinjection, pressure ejection and iontophoresis. Microinjection, while more selective than a systemic injection, still provides relatively large injection volumes that can affect multiple, neighboring regions of the brain or specific pathways not under study. Pressure ejection methods are prone to leakage and can disturb tissue at the ejection site.

Fortunately, iontophoresis can deliver incredibly small volumes of concentrated solutions without leakage. Iontophoresis allows for localized drug ejections directly into brain regions of interest by inducing the migration of ions with the application of a current to the solution of interest. Additionally by coupling iontophoresis barrels to a carbon-fiber microelectrode, a novel method by which iontophoresis can be quantified has been developed based on the original design of Armstrong-James and co-workers (Armstrong-James et al., 1981; Herr et al., 2008) and presented in the schematic in Figure 2.1. With this probe, the same microelectrode that is used to sense changes in neurotransmitter

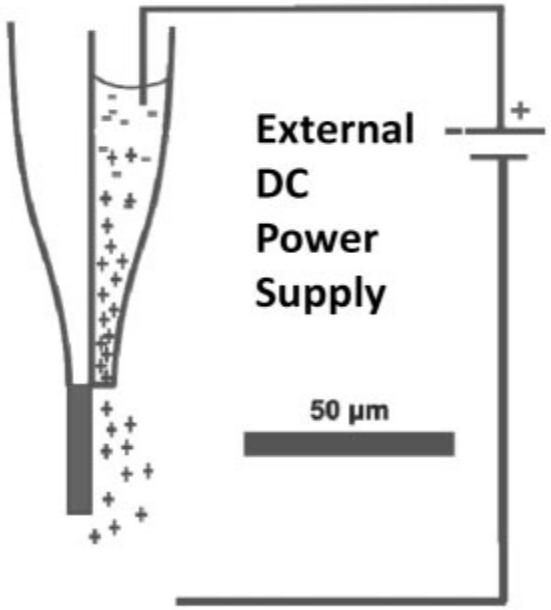

Figure 2.1. Schematic of an iontophoresis probe coupled to a carbon-fiber microelectrode. A positive or negative current is applied to the iontophoresis probe by an external DC power supply. This current causes the migration of the solution within the barrel. From Herr, N.R.; Kile, B.K.; Carelli, R.M.; and Wightman, R.M. (2008) Anal. Chem. 80,8635-8641.

release can also be used to confirm and quantify the iontophoretic ejection with fast-scan cyclic voltammetry (FSCV). This makes iontophoresis an appealing technique for use in pharmacological studies involving specific brain regions.

Iontophoresis

Iontophoresis allows for the ejection of both charged and neutral molecules through a combination of migration and electroosmosis. In glass capillaries pulled to a sharp tip a few microns in diameter, the migration of ions is induced with the application of a current to the solution of interest. The linear velocity of a solution ejected by iontophoresis (υ_{obs}) is defined by

$$\upsilon_{obs} = \upsilon_{eo} + \upsilon_{ep} \tag{2.1}$$

where υ_{eo} is the velocity of electroosmotic flow and υ_{ep} is the rate of migration. These terms are further defined as

$$\upsilon_{eo} = \frac{-\varepsilon\zeta}{\eta} E = \mu_{eo} E \tag{2.2}$$

$$\upsilon_{ep} = \mu_{ep} E \tag{2.3}$$

where μ_{ep} and μ_{eo} are the migration and electroosmotic mobilities respectively. *E* is the applied electric field, ε is the permittivity, ζ is the ζ-potential at the interface of the glass capillary and solution, and η is the viscosity of the solution (Herr et al., 2008).

Classically, the moles of a species ejected with a given current in iontophoresis has been determined by

$$M = n\frac{iT}{zF} \tag{4}$$

where *n* is the transport number, *i* is the applied current, *T* is the ejection time, *z* is the charge, and *F* is Faraday's constant (Stone, 1985). Unfortunately, there is often a huge

difference between the moles predicted by equation 2.4 and the moles in an actual ejection since the equation only takes the electrophoretic mobility of compounds into account. While, iontophoresis has been used in the past as a general approach for localized drug delivery *in vivo*, it has been limited in use as a non-quantitative technique (Curtis, 1964; Bloom, 1974; Purves, 1980) until recently (Herr et al., 2008). The inability of equation 2.4 to accurately predict the concentration of drug delivered means that the only way to account for all forces contributing to an ejection and accurately determine ejection concentrations is through direct measurement of individual ejections.

Radioactive labels (Bevan et al., 1981), fluorescent detection (Purves, 1979) and electrochemical detection (Armstrong-James et al., 1981) have all been used to attempt quantification of iontophoretic ejections. The cumbersome task of radiolabelling compounds or limiting the technique to use only with fluorescent or electroactive molecules made each method too impractical for widespread use however.

Electrochemical techniques allow for the quantitative monitoring of the concentration of an ejection based on the oxidation and reduction of the ejected compound. One major limitation to this method of monitoring ejection molarity is that the drug of interest must be electroactive. So, while the idea of monitoring iontophoretic ejections with electrochemistry was initially proposed in the early 1980's (Armstrong-James et al., 1981) and has been used to examine catecholamine diffusion and rates of DA clearance (Rice and Nicholson, 1989; Kiyatkin et al., 2000) it has until recently (Herr et al., 2008) not been practical to use this technique for localized drug delivery. The ability to only monitor the ejection of electroactive compounds has been overcome with the use of a neutral, electroactive marker molecule that can be co-ejected with nonelectroactive drugs of interest. Using a neutral molecule has further reinforced the long held belief that electroosmosis plays some role in iontophoretic ejections (Curtis, 1964; Bloom, 1974; Purves, 1979; Purves, 1980; Bevan et al., 1981; Pikal and Shah, 1990; Scott et al., 1993; Volpato et al., 1995; Bath et al., 2000; Guy et al., 2000).

By making the neutral marker for electroosmotic flow (EOF) electroactive, the carbon-fiber microelectrode coupled to the iontophoresis probe can be used to quantify directly just how much of the marker is ejected and to indirectly calculate how much of the nonelectroactive drug of interest is concurrently co-ejected. Additionally, the contribution of EOF to iontophoretic ejections allows for the ejection of neutral or even negatively charged compounds with the application of a positive ejection current.

Iontophoresis ejections are controlled by the same combination of migration of charged particles and electroosmotic flow that is seen in capillary electrophoresis. The similarities of these two techniques allows a comparison between retention times for electroactive and nonelectroactive compounds in capillary electrophoresis to serve as an indicator of the iontophoretic flow rate of nonelectroactive compounds in relation to a neutral electroactive marker. The electrophoretic mobilities of AP and other drugs of interest can be used to determine the concentration of other electrochemically inactive charged or neutral drugs co-ejected with AP. A ratio of electrophoretic mobilities of drugs of interest with respect to AP can be determined by capillary electrophoresis where the electrophoretic mobility (μ_{ep}) of each compound is calculated as

$$\mu_{ep} = \left(\frac{L}{t_r}\right)\left(\frac{L_t}{V}\right) \tag{2.5}$$

where L is the distance between the inlet and the detector, t_r is the time required for the analyte to reach the detector, V is the applied voltage, and L_t is the total length of the capillary (Skoog, 1998).

Using electrochemistry to monitor iontophoretic ejections, it has been established that while there is large variability in ejection concentration from barrel to barrel for a given current, there is a direct relationship between ejection current and amount of drug ejected for each individual barrel (Figure 2.2). The reproducibility of a series of ejections from a single barrel is excellent however as shown in Figure 2.3. Additionally, while the quantity of

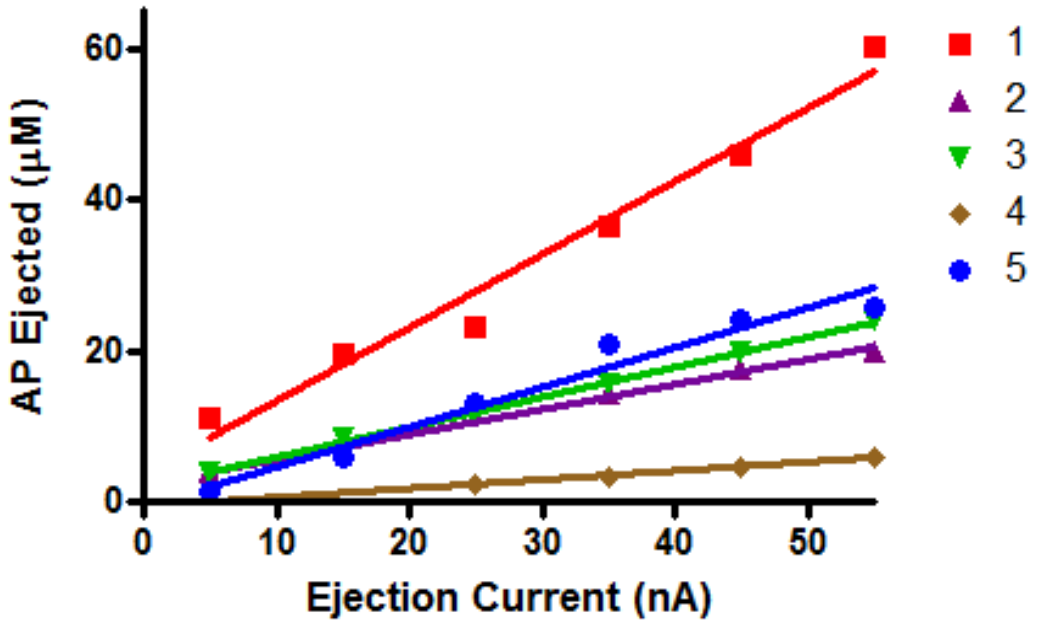

Figure 2.2. The direct relationship between ejection current and amount of drug ejected with iontophoresis. For all barrels, 5 mM AP was ejected for 30 s with the requested current which varied from 5 nA to 55 nA. Barrels 1-3 were attached to different carbon fiber electrodes while barrels 4 & 5 were attached to the same electrode.

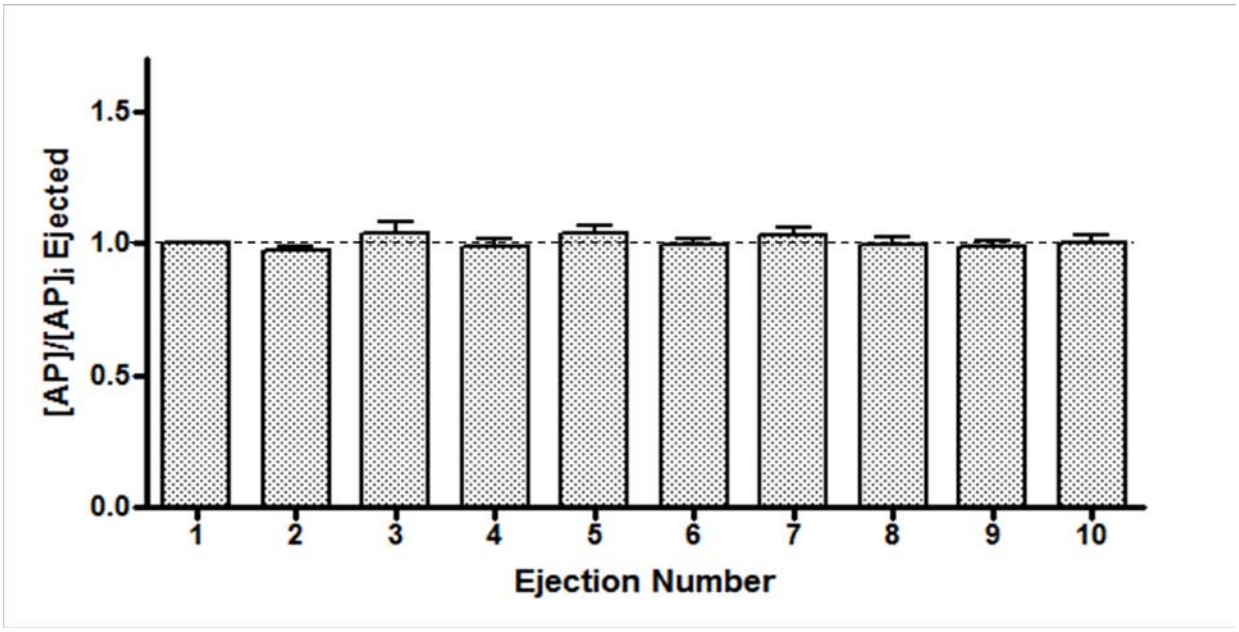

Figure 2.3. The reproducibility of iontophoresis ejections from a single barrel (n=4). All ejections were normalized to the first ejection for that particular barrel ([AP]/[AP]$_i$).

drug ejected for a given current does vary greatly from barrel to barrel the quantity of AP ejected can be monitored and manipulated in real time to reproducibly administer a quantitative amount of drug, regardless of the behavior of a particular barrel.

While the coupled use of electrochemistry and iontophoresis is not common, iontophoresis has been utilized in tandem with electrophysiology to yield important results on the direct effects of small amounts of drug on the firing of single neurons. White and Wang combined single-unit electrophysiology and iontophoresis in anesthetized rats to show that D1R and D2R are found post-synaptically on neurons in the nucleus accumbens, and that these neurons have differential responses to D1R and D2R drugs (White and Wang, 1986). By using iontophoresis for drug delivery, White and Wang were able to monitor similar cells, with the same electrode and in the same animal, unquestionably showing the presence of differentiated D1R and D2Rs. The use of iontophoresis allows for drug ejections so small that they dilute to insignificant quantities as they diffuse away from the ejection point. Additionally, ejections only affect an area a few hundred microns across meaning that relocating the probe gives access to a brain region completely free of previously ejected drugs. If systemic drug delivery were used, only one drug could be used per animal since complete washout from the brain of an anesthetized animal is unlikely. Other groups have used a similar approach in awake animals to show the roles that exogenous glutamate and DA play on dopaminergic cell firing (Rebec, 1998).

The ejection reproducibility of iontophoresis when coupled to the time resolution of FSCV gives us the unique ability to monitor both the drug ejection and its effects on neurotransmitter release quantitatively, in real-time. Dose response curves can be generated relating the concentration of drug iontophoresed to the modulation of extracellular neurotransmitter concentrations *in vivo*. These dose response curves provide researchers with the opportunity to begin linking receptor occupancy and DA release in specific brain regions with behavior in freely-moving animals. Ideally, these dose response curves can be

constructed in freely moving rats to manipulate the concentration of a given neurotransmitter and monitor the affects these changes have on behavior.

General Overview

While our lab has previously adapted a method to quantitatively monitor iontophoretic ejections, the technique had until recently not been applied *in vivo* to modulate electrically evoked release of DA in anesthetized rats. A neutral, electroactive marker molecule that is ejected purely by EOF was used to monitor indirectly the ejection of nonelectroactive dopaminergic drugs (raclopride, quinpirole, quinelorane, and nomifensine). The modulation of stimulated release in an anesthetized animal using a 30 s ejection of quinelorane is demonstrated and changes in evoked DA release are seen 30 s from the conclusion of the ejection. Presented here are the first attempts at creating dose-response curves that monitor changes in electrically evoked DA due to the introduction of DA agonists and antagonists. Coupling iontophoresis and FSCV allows quantitative relationships between receptor occupancy to be linked with millisecond temporal resolution for the first time. This technique allows for more reproducible ejections from barrel to barrel and with these more accurate measurements of drug ejections, more precise dose response curves were constructed.

Presented here are the first attempts at creating dose-response curves monitoring changes in electrically evoked DA due to the introduction of DA agonists and antagonists. Coupling iontophoresis and FSCV allows quantitative relationships between receptor occupancy to be linked with millisecond temporal resolution for the first time. Here dose-response curves were created as quinelorane replaces haloperidol at the D2 autoreceptors. Quinelorane has a higher affinity for the D2R than DA (Bates et al., 1991; Mercier et al., 2001) making it an excellent drug with which to begin this modeling. The high brain concentration of haloperidol after i.p. administration and its high affinity for the D2

autoreceptor ensures that after an ejection haloperidol will once again occupy the autoreceptors when quinelorane diffuses away. Haloperidol has been found to accumulate 22 times more in the brain compared to serum (Tsuneizumi et al., 1992) and to have an affinity 20 times greater for the D2R over the D3 (Sokoloff et al., 1990). So administration of haloperidol by i.p. injection before other drugs are locally injected into the brain ensures that all receptors are occupied and allows for the use of the model of competitive antagonism to be used when constructing dose response curves. This is important because changes in tonic DA concentration are not accounted for in the current model and cannot be monitored or quantified using FSCV (Wightman et al., 2007).

Recently, the Wightman lab (Herr et al., 2010) presented the first use of quantitative iontophoresis for modulation of DA release in the striatum of anesthetized rats. Results presented here indicate that pharmacologically active cations such as nomifensine, quinpirole and raclopride are ejected at approximately twice the rate of AP, the neutral EOF marker. We also established that the applied current and the EOF marker did not affect evoked DA release or uptake, validating the method's assumption that only the drug of interest is responsible for any change in evoked DA concentration after an ejection. Here the D2 autoreceptor agonist quinelorane is iontophoretically ejected to modulate extracellular DA levels in the striatum of anesthetized rats that have received systemic ejections of haloperidol. Results show that modulation is rapid, with the onset of the drug effect occurring in less than 30 s.

Going even further, the extent to which the DA signal is modified can be quantified and used to create dose-response curves that show just how much quinelorane is required to cause a given percent decrease in electrically evoked DA release. Initial results show this technique allows the construction of sigmoidal dose response curves that are reproducible at multiple locations along the dorsal ventral axis in the striatum of a single animal. However, variations in sensitivity to drug dosage are seen from animal to animal lending

credence to the theory of biological variation from animal to animal both in terms of drug sensitivity and DA receptor density (Mandt et al., 2008; Mandt et al., 2009; Mandt and Zahniser, 2010). This work lays the foundation for future experiments in freely-moving animals where localized drug ejections can be associated with the study of reward-seeking behaviors.

MATERIALS & METHODS

Chemicals

Unless otherwise noted, all chemicals were purchased from Sigma-Aldrich (St. Louis, MO) and used as received. Solutions were prepared using doubly distilled deionized water (Megapure system, Corning, NY). A physiological buffer solution, pH 7.4, (15 mM TRIS, 126 mM NaCl, 2.5 mM KCl, 25 mM $NaHCO_3$, 2.4 mM $CaCl_2$, 1.2 mM NaH_2PO4, 1.2 mM $MgCl_2$, 2.0 mM Na_2SO_4) was used in all electrochemical experiments.

Construction of Iontophoresis Probes

Iontophoresis probes were constructed by filling one barrel of multibarrel (three or four) fused glass capillaries (Stoelting Co., Wood Dale, IL) with a single glass barrel (A-M Systems, Carlsborg, WA) already containing a single carbon fiber (Thornel T-650, Amoco Corp., Greenville, SC). The filaments aid in the filling of the iontophoresis barrels with solution while the addition of the extra, filament free single glass barrel around the carbon fiber (CF) helps eliminate cross-talk between barrels and ensures the filament of the outer barrel does not interfere with the quality of the carbon fiber-glass seal. Heat shrink was then applied to the ends of each multibarrel glass capillary before being pulled on a vertical micropipette puller (Narashige, Tokyo, Japan) in a two step process. The electrode was then

cut so the length of exposed carbon fiber was 20-50 µm and the barrel backfilled with an electrolyte solution (4 M $KC_2H_3O_2$, 150 M KCl). A three barrel probe is seen in Figure 2.4.

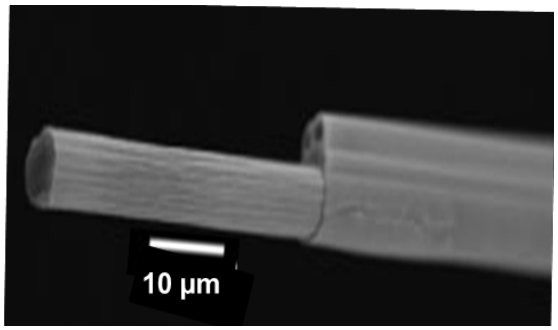

Figure 2.4. Scanning electron microscopy image of a carbon-fiber iontophoresis probe. Carbon-fiber iontophoresis probes are made starting with three barrel glass. The carbon fiber is in one of the barrels leaving two empty barrels for iontophoresis. Modified from Herr, N.R.; Kile, B.K.; Carelli, R.M.; and Wightman, R.M. (2008) Anal Chem 80, 8635-8641.

Electrochemistry

FSCV was performed using locally constructed hardware and software (Michael *et al.*, 1999). A triangle waveform (-0.4 V to 1.3 V) was applied to the carbon fiber at a scan rate of 400 V/s at a frequency of 60 Hz for pre-conditioning and 10 Hz for data acquisition. The potential was held at -0.4 V between scans. The generated current was filtered at a frequency of 2 kHz.

Iontophoresis Ejections

Ejections were carried out via a 30 s application of a positive current (1 nA to 250 nA) to the iontophoresis barrel containing the solution to be ejected. All currents were generated using a NeuroPhore BH-2 (Harvard Apparatus, Medical Systems Research Products, Holliston, MA).

Ejected solutions were composed of 0 mM to 20 mM quinelorane and 5 mM AP dissolved in a 5 mM NaCl solution, pH 5.5, to help promote electroosmotic flow. For all quantitative ejection experiments, a current of 0 nA was applied to barrels between ejections.

Anesthetized Rat Surgery

In vivo experiments were carried out using male Sprague-Dawley Rats (300-500 g, Charles River Laboratories, Wilmington, MA) anesthetized with 1.5 g/kg urethane (50% urethane/50% saline, w/w). Urethane has been established, with respect to other anesthetics, to minimally inhibit brain metabolism, neuronal activity, and response to stimuli (Buzsaki et al., 1983). Using bregma as a reference, holes were drilled through the skull for placement of the working electrode in the striatum (AP +1.2 mm, ML +2.0 mm, DV -4.0 to -6.0 mm) and bipolar stimulating electrode in the medial forebrain bundle (MFB) (AP -2.8 mm, ML +1.7 mm, DV -7.0 to -9.0 mm). A reference electrode (Ag/AgCl) was implanted in

the posterior half of the contralateral hemisphere. Biphasic stimulation of the MFB was performed with an analog stimulus isolator (A-M Systems, Sequim, WA) and in house software (Tarheel CV). All experiments were performed with a 60 Hz, 40 pulse, 300 µA biphasic stimulation. Stimulations were applied between potential scans to avoid electrical interference in the cyclic voltammograms (CVs).

Calibration Procedure

At the conclusion of each experiment, electrodes were calibrated *in vitro* for sensitivity to both DA and AP using a four point calibration procedure over the range of 0.5 µM to 4000 µM. Calibrations were carried out using a flow injection apparatus as previously described by Kristensen (Kristensen et al., 1986) and the same calibration method used with iontophoresis probes by Herr *et al*. (Herr et al., 2008). Here, a loop injector was mounted on an actuator (Rheodyne model 7010 valve and 5701 actuator) that was used with a 12 V DC solenoid valve kit (Rheodyne, Rohnert Park, CA) to introduce either DA or AP to the outlet of a six-port rotary valve where is the electrode is positioned (Kristensen et al., 1986). The linear flow velocity (1.0 cm s^{-1}) was controlled with a syringe infusion pump (Harvard Apparatus model 940, Holliston, MA).

Capillary Electrophoresis

Capillary electrophoresis experiments were carried out on a custom built system constructed in-house that consisted of a 30 kV power supply (Spellman CZE 1000R, East Tambaram, Chennai, India) and an absorbance detector (Linear UVIS 200, Hauppauge, NY). Absorbance was measured at 193 nm in all experiments. All separations were performed on a 50 µm (inner diameter) fused silica capillary with a total length (L_t) of 96.0 cm and a distance of 87.5 cm between the inlet and the UV detector (L). All experiments were carried out in cationic mode with the outlet acting as the cathode. Data

was collected and analyzed using a custom LabVIEW program (courtesy of Dr. James Jorgensen, UNC-CH) and IGOR Pro (WaveMetrics, Inc., Lake Oswego, OR). Samples contained approximately 100 µM of each compound in 5 mM phosphate buffered saline (PBS), pH 5.5. This was consistent with the pH and buffer composition of the drug solutions ejected in the iontophoresis experiments.

Very similar to iontophoretic ejections (equation 2.1) the electrophoretic mobility (μ_{ep}) of each compound in the capillary electrophoresis experiments was calculated using:

$$\mu_{ep} = \mu_{app} - \mu_{eo} \tag{2.6}$$

Where the mobility due to the applied current (μ_{app}) and the mobility due to electroosmosis (μ_{eo}) were determined from capillary electrophoresis specific variations on equation 2.5 and calculated as:

$$\mu_{app} = \left(\frac{L}{t_r}\right)\left(\frac{L_t}{V}\right) \tag{2.7}$$

and

$$\mu_{eo} = \left(\frac{L}{t_{neutral}}\right)\left(\frac{L_t}{V}\right) \tag{2.8}$$

L is the distance from the inlet to the detection point, t_r is the time required for the analyte to reach the detection point, $t_{neutral}$ is the time required for the neutral species (AP) to reach the detection point, V is the applied voltage, and L_t is the total length of the capillary.

In Vivo **Protocol**

In each animal, a “hot-spot” for the stimulated release of DA (Moquin and Michael, 2009) was found within the previously listed range of dorsal-ventral surgical coordinates and then stimulated every 120 s. When a stable level of stimulated DA release was seen for 10 consecutive stimulations, haloperidol (0.5 mg/kg rat unless otherwise noted) was administered i.p. Haloperidol was dissolved in bacteriostatic water with citric acid at pH ~2

and then brought back up to a pH of 5.5 to 6.0 with 0.1 M NaOH. The DA signal was then recorded every 120 s until the signal stabilized for 5 consecutive stimulations (normally 9-15 stimulations or 18 to 30 min). At this point, manipulation of the DA signal with 30 s ejections of quinelorane was initiated. Stimulations were carried out every 120 s to ensure that a depletion of intracellular DA was in no way affecting the observed stimulated release. The 30 s drug ejections were timed to occur in the 120 s interval between stimulations, so the timing of the stimulations was not interrupted. Additionally, the first post-ejection stimulation took place about 30 s after the cessation of the ejection. While quinpirole is more often used in experiments that involve modulation of the D2 autoreceptors and as such is better characterized, quinelorane was used in these experiments due to its greater binding affinity and specificity for the receptor (Foreman et al., 1989; Storey et al., 1995). Finally, the probe was lowered 400 µm further into the brain to a region unaffected by previous ejections where the protocol could be repeated (Herr et al., 2010).

Construction of Dose Response Curves

Dose response curves were generated using the variable slope sigmoidal dose response curve and single site binding hyperbola regressions in GraphPad Prism 4.02 (GraphPad Software, Inc., San Diego, CA). The variable slope sigmoid equation was used:

$$y = b + \frac{t - b}{\left(1 + \frac{10^{\log EC_{50}}}{10^{x}}\right)^{H}} \tag{2.9}$$

where *y* is the percent change in DA response, *x* is the logarithm of the quantity of quinelorane administered, *t* is the maximal response (set to 0% in this case), and *b* is the response seen in the absence of the drug (always set to 100%). The program then determines logEC_{50}, the drug dose that would give a 50% change in DA release and *H* is a

measure of the slope of the linear region of the curve. For dose response curves with an arithmetic dosage scale the following one site binding hyperbola equation was used:

$$y = \frac{xB_{\max}}{K_d + x} \tag{2.10}$$

where *x* and *y* are quantity of drug administered and resulting percent change in DA release respectively, B_{max} is the drug concentration at maximal binding and K_d is the drug concentration required for half of maximal binding.

RESULTS & DISCUSSION

Determination of relative iontophoretic mobility

Relative iontophoretic mobilities, normalized to the mobility of a neutral molecule have been reported previously for DA, uric acid, and AP using electrochemical detection in co-ejection experiments and used to establish both the role of electroosmosis in iontophoresis and the similarities in ejection forces in iontophoresis and CE (Herr et al., 2008). In those experiments, mobilities were determined electrochemically as the relative ejection amounts in a series of experiments where DA, uric acid and AP were co-ejected with 2-(4-nitrophenoxy) ethanol (NPE). Unfortunately the use of electrochemical detection with this coejection technique limits its use to electroactive compounds, so an indirect method must be used to determine the relative iontophoretic mobility with respect to a neutral marker of nonelectroactive compounds of interest. Overall, iontophoretic mobility at a capillary tip and electrophoretic mobility through a capillary column are both governed by a combination of migration of charged ions and electroosmosis so capillary electrophoresis can be used to calculate electrophoretic mobilities. Evidence of a linear correlation between iontophoretic and electrophoretic mobilities in capillary electrophoresis experiments has previously been established (Herr et al., 2008) and here will be used to indirectly determine the iontophoretic mobilities of nonelectroactive compounds.

Use of UV-VIS detection instead of electrochemical in the capillary electrophoresis experiments allowed the retention times of both electroactive and nonelectroactive compounds to be determined. A representative electropherogram measured for DA, nomifensine, quinelorane, quinpirole, raclopride, AP, and uric acid is shown in Figure 2.5. The relative retention time of each compound with respect to AP was then used to determine the contribution of electrophoretic mobility to the migration of each compound through the CE.

These mobilities were then used along with relative co-ejection rates to create the coordinates to graph uric acid, AP and DA in Figure 2.6. These three points were then used create the linear regression that was used to determine the iontophoretic ejection rates relative to EOF based on the electrophoretic mobilities of the nonelectroactive compounds from the CE experiments. The relative iontophoretic ejection rates extrapolated from Figure 2.6 are summarized in Table 2.1. Data from a previous version of this experiment (Herr et al., 2010) indicated that raclopride will be ejected at a rate 1.75 times as fast as AP and quinpirole ejected at a rate 2.18 times as fast as AP, lending credence to the reproducibility of both the ratio of iontophoretic to electroosmotic flow and our laboratory's method to determine this ratio.

With the relative iontophoretic mobilities in hand, electrochemical techniques can be utilized to quantitatively monitor the ejection of nonelectroactive compounds. In this procedure, a known concentration of AP was coejected with a known concentration of a neuroactive, but not electroactive, drug of interest, here quinelorane. During the iontophoretic ejection, the oxidation and reduction current from AP was monitored. The voltammetric signal measured for AP was then directly related to the amount of drug ejected via the relative iontophoretic mobilities with respect to a neutral species and the relative concentration of the drugs in the solution.

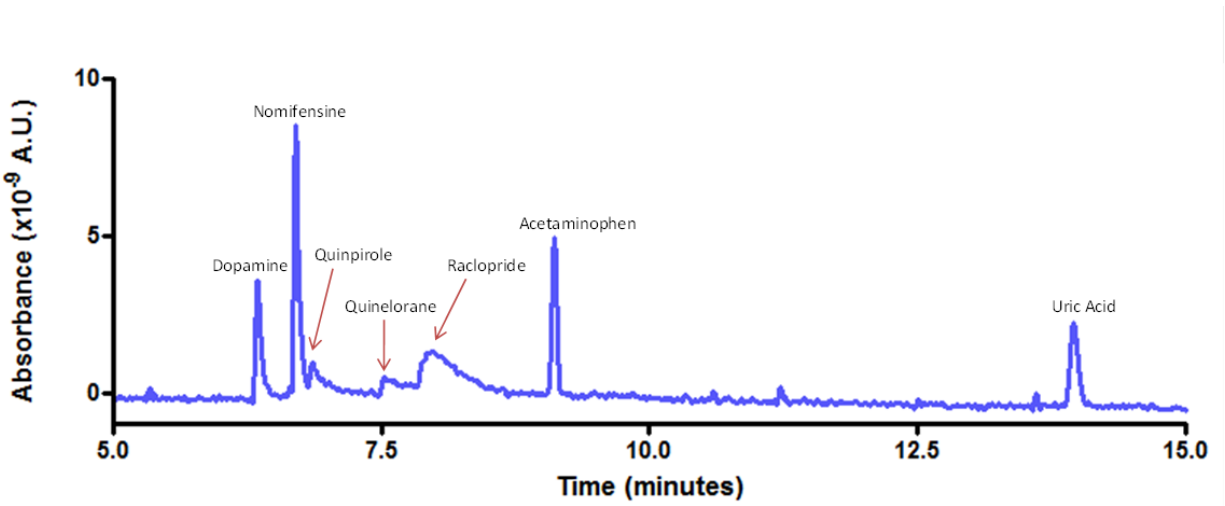

Figure 2.5. Representative electropherogram from the capillary electrophoresis experiment used to determine contribution of EOF and relative electrophoretic mobility of compounds.

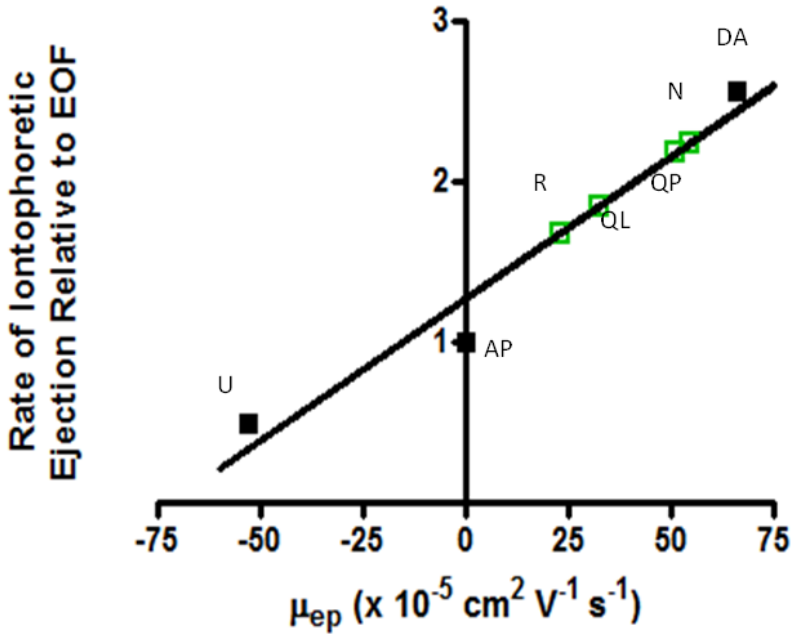

Figure 2.6. Relationship between iontophoretic and electrophoretic mobility. Black squares (■) represent the electroactive compounds uric acid (U), AP, and DA plotted using previously reported iontophoretic ejection rates relative to EOF (taken to correspond to the amount of the neutral ejected) and electrophoretic mobilities determined here with CE. These points were then used to construct the linear regression seen. The open green squares (□) represent raclopride (R), quinelorane (QL) , quinpirole (QP), and nomifensine (N) which were then plotted along the linear regression based on their electrophoretic mobilities calculated from the capillary electrophoresis experiments to determined the relative iontophoretic ejection rate relative to EOF.

Table 2.1. Rate of iontophoretic delivery relative to electroosmotic mobility of acetaminophen (AP)

Compound	**Concentration Ejected Relative to AP**
Nomifensine	2.24
Quinpirole	2.18
Quinelorane	1.85
Raclopride	1.68

Localization of iontophoretic ejections

Substances dilute into the surrounding environment primarily by diffusion when ejected from the iontophoretic barrel (Rice and Nicholson, 1989). Taking this diffusion into account helps to better estimate the concentration of drug at receptors responsible for the change in evoked release of DA in response to a drug ejection. Figure 2.7A shows a schematic of an iontophoresis barrel with an attached carbon fiber electrode along with circles modeling the diffusion sphere of compounds from the point at which they are ejected. For a substance nondestructively monitored by voltammetry at the carbon fiber, the amplitude of the voltammetric current is expected to increase as the ejected substance diffuses from the ejection point down the length of the fiber, and to remain constant once the diffusion distance exceeds the electrode length. As such, the rise time of the voltammetric current should be related to the length of the electrode, with longer electrodes having longer rise times because of the greater time required for the diffusion sphere to fully encompass the electrode. Additionally, diffusion can be considered not only the when looking at how long it takes for a particular carbon fiber to sense a constant concentration of drug but also to look at how long a compound stays in the vicinity of the carbon fiber at the cessation of the ejection. Figure 2.7B shows a representative color plot collected during a 30 s iontophoretic delivery of AP into agarose gel and for 120 s after the ejection. Figure 2.7C shows examples of the current traces for two different 30 s ejections of AP into agarose gel along with the decay of the current monitored for an additional 120 s at the conclusion of the ejection. These particular ejections put out such a large concentration of AP that adsorption to the electrode may also be playing a role in the lingering AP current, but the larger ejections clearly illustrate the diffusion of drug away from the ejection point. While the ejection of additional material from the iontophoretic barrel stopped as soon as a current was no longer applied to the barrel, the ejected material did not suddenly disappear but

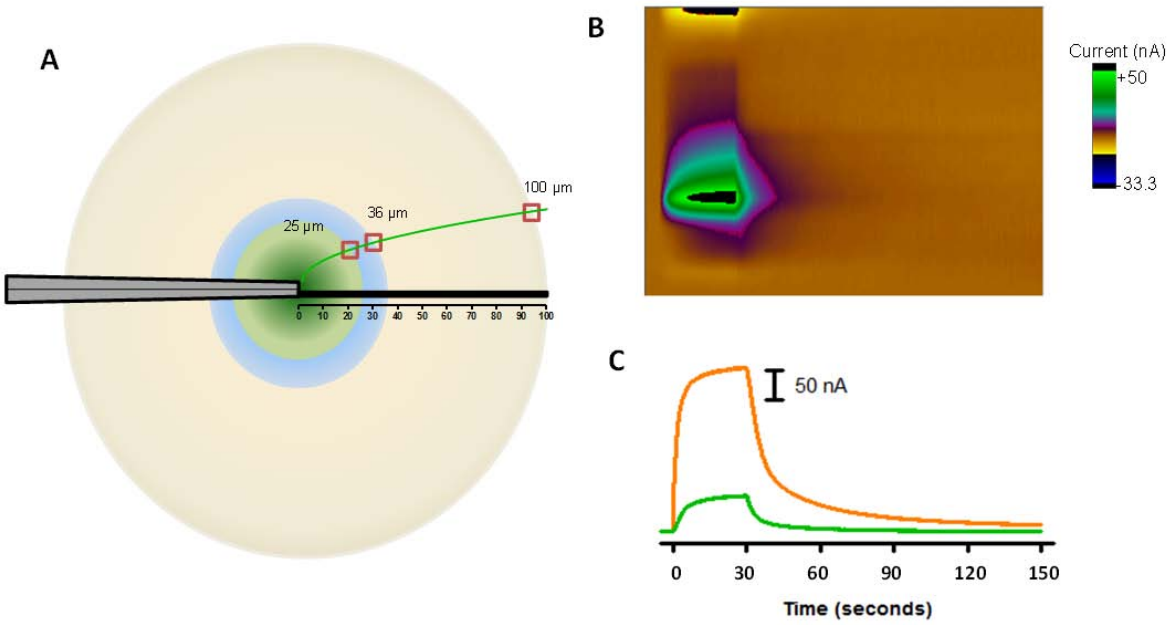

Figure 2.7. Spatial distribution of an iontophoretic ejection. (A) Tip of iontophoresis probe and attached exposed carbon fiber superimposed on two-dimensional representation of ejection spheres 25 µm (green), 36 µm (blue), and 100 µm (tan) to illustrate the sphere size for a carbon fiber of that length to experience a constant concentration. The green line shows the time required for an ejection sphere of a given size to develop as a function of diameter. (B) Representative color plot for a 30 s iontophoretic ejection that reaches steady state at 56 nA AP. At the conclusion of the ejection, CVs were collected for an additional 120 s to demonstrate the diffusion of AP away from the carbon fiber after an ejection. (C) Current traces for two different 30 s ejections of AP into agarose gel along with the decay of the current monitored for an additional 120 s at the conclusion of the ejection.

instead diffused away from the ejection point. This can help to tell us approximately how much of our drug of interest, here quinelorane, was present 30, 60, 90, or 120 s after the ejection giving an idea of how much of the drug is actually working on receptors around the carbon fiber at these later times when the release of DA was once again evoked.

The average concentration of AP still present at the carbon fiber after the cessation of the iontophoretic ejection is listed in Table 2.2 as a percentage of the concentration of the AP delivered during the ejection (n=7). In our calculations, the percent of drug detected 60 s after the ejection was used to determine the concentration of quinelorane causing the observed decrease in DA stimulated release. While Table 2.2 shows the combined averages for diffusion of an ejection into agarose gel and into the brains of anesthetized animals, this same experiment can be carried out in the brain of an anesthetized animal at the start of an experiment to account for the diffusion characteristics of the ejection point source, the specific carbon fiber, and the brain of the animal. Experiments carried out *in vivo* showed similar diffusion times and have been factored into the averages in Table 2.2.

Effects of iontophoresed reagents on dopamine sensitivity

The concentration of AP sensed by the carbon fiber is in fact an average concentration of AP present along the length of the carbon fiber. The drug concentration at the portion of the carbon fiber closest to the iontophoresis tip is orders of magnitude greater than this average concentration and presumed to be very near the drug concentration inside the barrel (5 mM). Exposure of the carbon fiber microelectrode to high drug concentrations during iontophoretic ejections could potentially alter the sensitivity of the electrode to DA as reported for nomifensine in similar experiments and GBR 12909 (Davidson et al., 2000). A series of carbon-fiber iontophoresis probes were calibrated before and after iontophoretic ejections to determine if any loss in DA sensitivity occurs. One of the iontophoresis barrels was loaded with 10 mM of AP or 10 mM AP plus 10 mM of the drug of interest. While

Table 2.2. Concentration of acetaminophen at the carbon fiber after ejection current is turned off.

Time after ejection (seconds)	10	30	60	90	120
Drug present (% of ejection concentration)	19.94 ± 4.55	7.43 ± 2.05	3.26 ± 1.32	1.95 ± 1.04	1.34 ± 0.83

electrochemically monitoring the response of AP, the loaded solution was ejected into buffer for 40 min at a current sufficient to continuously deliver approximately 10 µM of AP (generally between 10-15 nA). The results from these experiments are presented in Table 2.3 as the average and standard deviation of three separate experiments. The neutral EOF markers AP and NPE did not significantly alter DA sensitivity. Pharmacological agents, such as nomifensine, quinpirole, and raclopride, have slight effects on the electrodes' response to DA, but the ejection times and concentrations used during these sensitivity experiments were considerably longer than would be used in most *in vivo* experiments. Given the small effect observed even with these prolonged iontophoresis conditions, the iontophoresis of these drugs during *in vivo* experiments should not significantly affect the DA sensitivity of the carbon fiber.

Effects of large ejection currents on stimulated dopamine release in anesthetized animals

Iontophoretic literature has discussed that current artifacts can be seen neurophysiologically due to the introduction of Na^+ and Cl^- that are present in a drug solution (Curtis, 1964; Stone, 1985). While cell firing was not monitored in these experiments it was still important to determine if currents applied by the iontophoresis pump for an ejection altered the stimulated release of DA. The stimulated release of DA was monitored before and after the ejection of NaCl with currents up to +505 nA, double the maximum currents used even in very large ejections in *in vivo* experiments. An example of this experiment can be seen in Figure 2.8. A representative baseline trace is shown in Figure 2.8A. To test the effects of large currents on DA release, NaCl was iontophoresed for 30 s using large pump currents following stimulation. This current trace cannot be quantitatively linked to a concentration of saline ejected, but it does serve to confirm the occurrence of an ejection. Stimulation was repeated after the ejection of saline with excessive current, and the maximum amplitude of released DA and its time course remained the same. Measurements were repeated every

Table 2.3. Effect of Drugs on Carbon Fiber Sensitivity for Dopamine

Compound(s) Ejected	**Post Ionto/Pre Ionto Sensitivity (nA/nM)**
AP	1.00 ± 0.10
AP + NPE	1.01 ± 0.07
AP + Nomifensine	0.86 ± 0.08
AP + Quinpirole	0.91 ± 0.08
AP+ Raclopride	0.87 ± 0.07
AP+ Quinelorane	0.94 ± 0.07

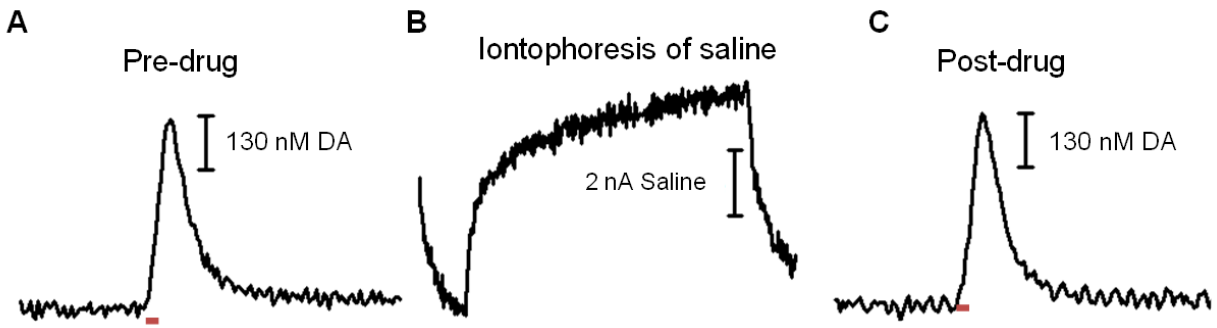

Figure 2.8. Effect of current on stimulated dopamine release. The panels show current as a function of time. (A) A representative baseline current trace for the stimulated release of dopamine. (B) Representation of iontophoretic ejection of 2 nA saline. (C) Current trace for stimulated release after ejection seen in B. There is no change in the extracellular concentrations of dopamine seen in A and C elicited with a stimulation indicated by the red bar at t=0 for each trace.

120 s for a total of 30 min with no significant change in the amount of DA released or rate of uptake observed as shown in Fig 2.8C (n=4 animals with three release sites tested in each animal for 12 total locations). The ejection of NaCl was confirmed electrochemically as the combination of an acidic pH shift and increased capacitance in the double layer at the electrode's surface. As Figure 2.9 illustrates, increased capacitance was also seen in a NaCl injection in the flow cell, but as the trace in Figure 2.9B shows, this is not the only factor contributing to the *in vivo* saline CV. The NaCl ejected with large currents does alter the double layer of the carbon fiber, although this is not seen with the lower ejection currents typically used.

Effects of EOF marker on stimulated dopamine release

Before this technique was used to investigate the effect of DA agonists at autoreceptors on electrically stimulated DA release, it was important to ensure that AP did not affect stimulated DA release. Figure 2.10 shows the results of a representative experiment in an anesthetized rat. A carbon-fiber iontophoresis probe was lowered into the striatum and a 'hot-spot' for the stimulated release of DA found. A representative baseline trace and color plot are shown in Figure 2.10A. To test the effects of the EOF marker on DA release, AP was iontophoresed for 30 s following stimulation. The amount of AP delivered was monitored electrochemically, and the concentration vs. time trace and color plot are shown in Figure 2.10B. The stimulation was repeated after AP delivery. The maximum amplitude of released DA and its time course remained the same. Measurements were repeated every 2 min for a total of 30 min, and no significant change in the amount of DA released or rate of uptake was observed as shown in Fig 2.10C ($n = 9$, $p > 0.01$). The same experiment was performed for NPE, with no measurable difference observed from control (Herr et al., 2010). The experiment was also carried out in anesthetized rats after the i.p. administration of haloperidol with no significant change in electrically evoked DA release

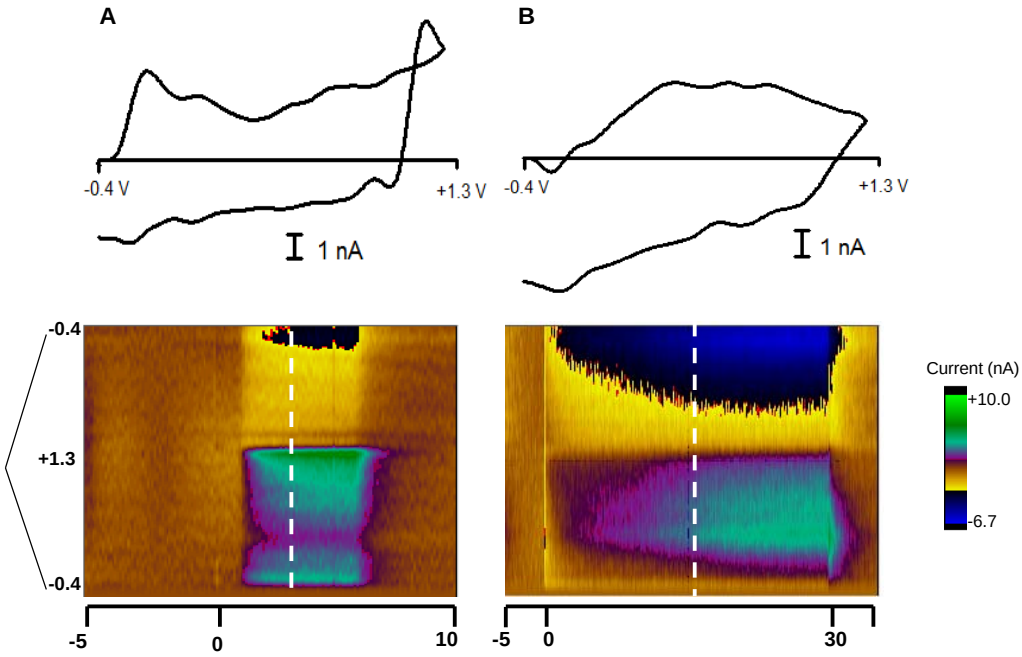

Figure 2.9. Comparison of NaCl CVs *in vitro* and *in vivo*. (A) The CV and colorplot for an *in vitro* injection of NaCl. The colorplot shows a 5 s injection of 27 mM NaCl into Tris buffer at pH 7.4. CVs were taken at the times indicated with a white dashed line in the colorplots. The rectangular shape of the CV, while still keeping sharp features, indicates an increase in capacitance at the surface of the electrode. (B) Representative CV and color plot for an *in vivo* ejection of NaCl. The color plot is a 30 s ejection of 5 mM NaCl at pH 5.8 into the brain of an anesthetized animal and the CV was taken at the time indicated with a white dashed line in the colorplot. While this CV also shows the broadening characteristic of increased capacitance, there is also a shape change in part associated with acidic pH.

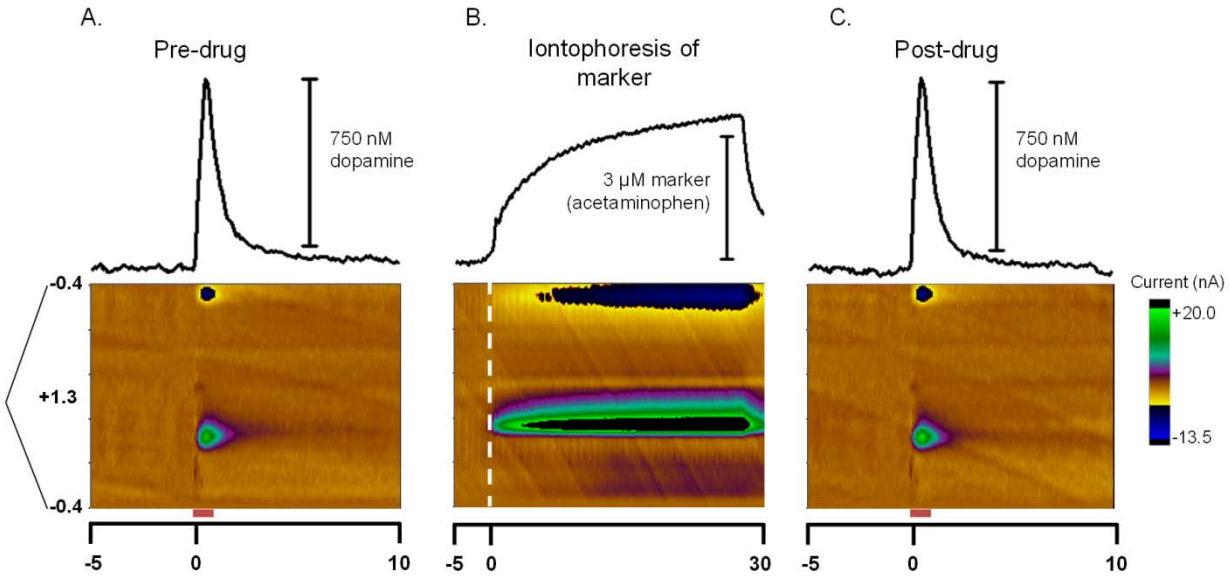

Figure 2.10. Effect of AP on stimulated dopamine release. The top panels show current as a function of time while the lower panels are two-dimensional colorplots where current is shown in false color on the potential vs. time axes. (A) A representative baseline current trace and colorplot for the stimulated release of DA. (B) Representation of iontophoretic ejection of 3 µM AP. The white dashed line (t=0) indicates application of a positive current to the barrel. (C) Current trace and colorplot for stimulated release immediately after ejection seen in B. There is no change in the extracellular concentrations of DA seen in A and C elicited with a stimulation indicated by the red bar and t=0 for each trace.

observed. This ensured that AP did not interact with haloperidol or the D2 autoreceptor in a way that altered electrically evoked DA release in the striatum.

Effect of systemic administration of haloperidol on the stimulated dopamine release

In vivo the amount of DA released per stimulation remains fairly constant during the stimulation of the MFB (May et al., 1988). Additionally, the increase in stimulated DA release stays more or less constant with haloperidol administered i.p. (Wiedemann et al., 1992). A 0.5 mg/kg challenge of haloperidol given i.p. was previously established to increase stimulated extracellular DA levels four-fold in approximately 40 min and from there slowly decay to half of the pre-challenge levels over the course of nine hours (Wiedemann et al., 1992). In this study, a similar dose of haloperidol caused approximately a 2.5-fold increase in extracellular DA and remained at this elevated level for at least an hour (though usually much longer) in all cases before slowly decaying back down to below the initial DA concentration in the same manner described previously. Figure 2.11 shows the electrically evoked DA release recorded at 120 s intervals over the course of four hours both with and without the i.p. administration of haloperidol at 20 min (indicated by the arrow). Without the administration of haloperidol, the signal decays 10% over the first 2 to 2.5 hours with about a 30% decrease seen after 4 hours and a 50% decay in signal after 5 hours of stimulations. In the presence of haloperidol, stimulated release reaches a maximum level one hour into recording (40 minutes after i.p. injection) at 2.3-times the initial baseline concentration. The signal then decreases 33% over the next four hours, showing a decay trend consistent with evoked release in the absence of haloperidol.

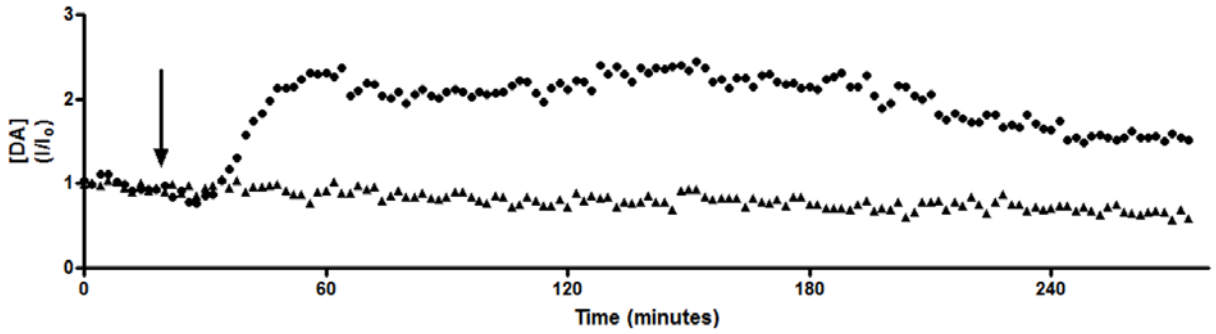

Figure 2.11. Temporal response (•) of extracellular DA concentration induced by electrical stimulation of the medial forebrain bundle of a rat given haloperidol (0.5 mg/kg, i.p.) at 20 min (arrow). DA response to repeated stimulations in rat without haloperidol on board is represented with ▲. Stimulations were repeated every 2 min.

Modulation of stimulated release of dopamine with quinelorane can be monitored over several hours for multiple ejections

It was previously established that localized ejections of drugs that interact with D2 autoreceptors affect stimulated DA release in the same manner as systemic ejections but on a much faster timescale (Herr et al., 2010). The timecourse for the effects of localized drug ejections on stimulated DA release had not yet been explored however. Here, quinelorane was used to decrease the stimulated release of DA. Figure 2.12 shows the current versus time traces and color plots for the stimulated release of DA before and after the quinelorane ejection (Figure 2.12B). In the example shown in Figure 2.12A, there was approximately 1.03 µM DA released in response to the stimulus indicated by the dashed white line. After a 6.5 µM quinelorane ejection (Figure 2.12), 0.754 µM DA was detected at the electrode in response to the stimulus (Figure 2.12C), a 22.7% decrease in the electrically evoked release of DA after the local ejection. The time course of both the onset and recovery of the drugs affects was then monitored for trends between the concentration of drug administered and duration and extent of modulation to the DA signal.

In Figure 2.12, and in all other experiments, the concentration of quinelorane during the time of the ejection was determined from the plateau current for AP seen during the ejection. This current was converted into an AP concentration using the data from post-experiment calibration of the carbon fiber for AP sensitivity. Finally, using the relative iontophoretic mobility from Table 2.1 along with a ratio of the relative concentrations of AP and quinelorane in the ejection solution, the concentration of quinelorane during the ejection was indirectly determined. Again, this reported quinelorane concentration at the time of the ejection measured the maximum output of drug during the ejection. As the data in Table 2.2 reports, this concentration quickly decays away at the cessation of an ejection. In order to account for this rapid decay of drug that occurs before DA is once again electrically evoked, the percentage of the ejection concentration of the drug remaining at 60 s after the ejection

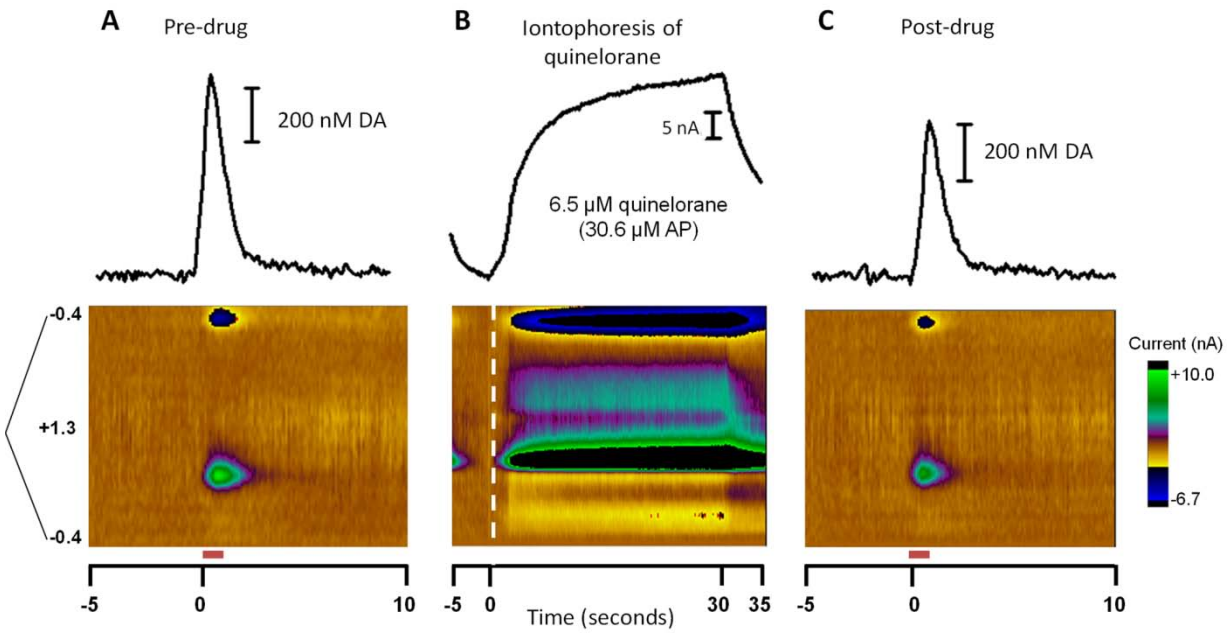

Figure 2.12. Stimulated dopamine release in an anesthetized animal before and after a localized ejection of solution containing both AP and quinelorane. The top panels show current as a function of time while the lower panels are two dimensional colorplots where current is shown in false color on the potential vs. time axes. (A) A representative baseline current trace and colorplot for the stimulated release of dopamine. (B) Representation of iontophoretic ejection of 30.6 µM AP and 6.5 µM quinelorane. The white dashed line (t=0) indicates the onset of current application to the barrel. Note that quinelorane cannot be seen in the color plots or current as a function of time traces. (C) Current trace and colorplot for stimulated release after ejection seen in B. The extracellular concentration of DA seen in C less than 50% of that evoked in A. In both A and C the time of stimulation is indicated by the white dashed line at t=0.

was reported as the concentration of quinelorane present at the first post-ejection electrical stimulation of DA.

Figure 2.13 shows the typical time course for the repeated iontophoretic ejection of quinelorane into the striatum of an anesthetized rat after the systemic i.p. administration of haloperidol. Again, each point represents the release of DA in response to an electrical stimulation. Stimulation events occurred every 120 s. An increase in the concentration of quinelorane administered resulted in further depression of the stimulated release of DA. Regardless of quinelorane concentration, depression of the DA signal occurred during the stimulation immediately following the iontophoretic ejection, which occurred less than 30 s after the conclusion of the ejection. However, the greater the concentration of quinelorane administered, the longer it took for the maximum depression in stimulated release to occur.

In Figure 2.13, the 45.8 nM ejection of quinelorane causes a 21.0% decrease in the DA signal within the first 30 s but over the course of the next 8 min the DA signal continues to decrease to 59% of the pre-ejection DA signal. Recovery times varied from animal to animal, but consistently increased with increasing drug concentration. There was also consistently a recovery of the DA signal to the concentrations seen before the quinelorane ejection, at which point drug was again iontophoresed and modulation of the signal monitored. These repeated ejections showed a reproducible time course and magnitude for similar concentrations of quinelorane indicating that recovery of the signal can also be used to tease out diffusion rates and relative drug affinities for the D2 autoreceptor. The timecourse seen in Figure 2.13 also establishes that repeated ejections can be carried out in the same location in an animal over the course of 3 hours with the decay in baseline DA signal following the same trend seen in Figure 2.11. This means that the same location can be stimulated for several hours and repeatedly modulated as long as the signal is allowed to recover back to the original baseline concentration before the next ejection, an act not possible with systemic injections. The duration of DA modulation after a quinelorane

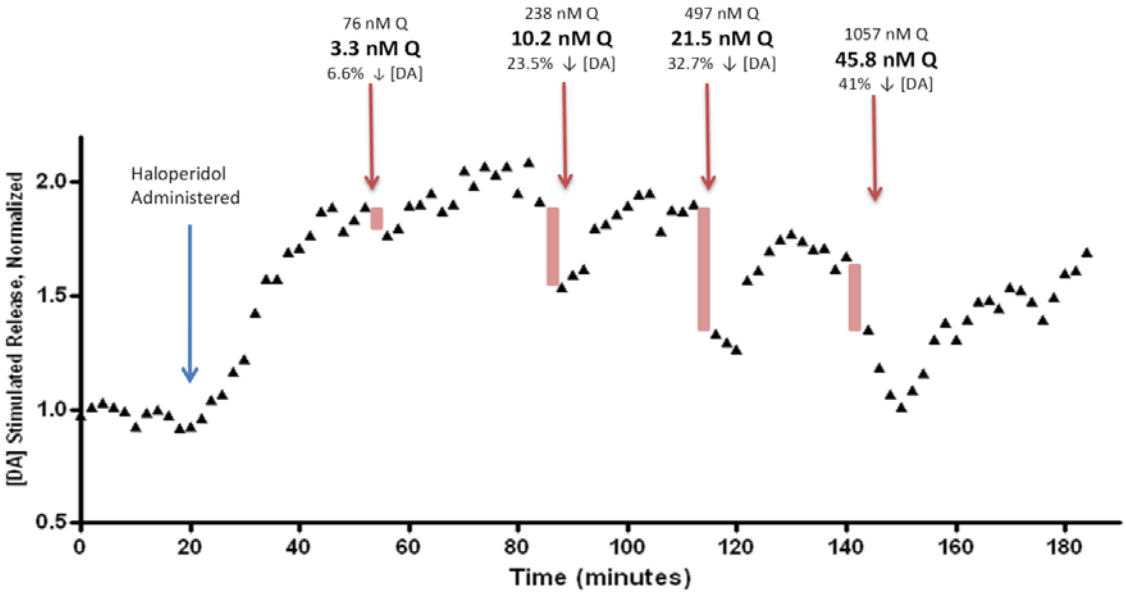

Figure 2.13. Time course for changes in stimulated dopamine release with ejections of quinelorane. Modulation of stimulated release of dopamine with quinelorane can be monitored over several hours for multiple ejections.

ejection was typically 20 min or less for changes of less than 50% to the DA signal (but never more than 30 min).

Dose response curves built using the neutral marker technique instead of pump current as an indicator of ejected drug concentration

Iontophoretic drug ejections are typically monitored and reported as a function of the current applied to a barrel. The complaints that iontophoresis is unpredictable and irreproducible can be traced to the use of this method to monitor ejections. While pump current may serve as a decent indicator of relative ejection amounts from a single barrel, Figure 2.2 demonstrates that there was a large variation in the ejection from barrel to barrel for a given current and no way to account for this variation without actually monitoring ejections.

Here, an iontophoresis probe consisting of a single carbon fiber coupled to three iontophoresis barrels all containing the same drug solution (0.5 mM quinelorane and 5 mM AP) was inserted into the striatum of an anesthetized rat. After a stable baseline of stimulated release was established, a 10 nA current was applied to one of the iontophoresis barrels. When the stimulated DA signal had recovered to the pre-ejection baseline, a 10 nA current was then applied to a different iontophoresis barrel. This was carried out with 10, 30 and 90 nA on all three barrels, as well as with 145 nA and 234 nA currents on the first barrel. The ejection currents as well as the subsequent percent decrease in stimulated DA release were then plotted regardless of barrel number and a linear dose response curve (linear scale on both the x- and y-axes) fitted to the data (Figure 2.14A). The three very different responses to the same current seen at 10 nA, 30 nA and 90 nA in Figure 2.14A clearly illustrate the complaint about the perceived irreproducibility of iontophoresis. The variation in the changes in signal for the three points at each current once again confirms the claim that barrels do have individual slopes (Figure 2.2).

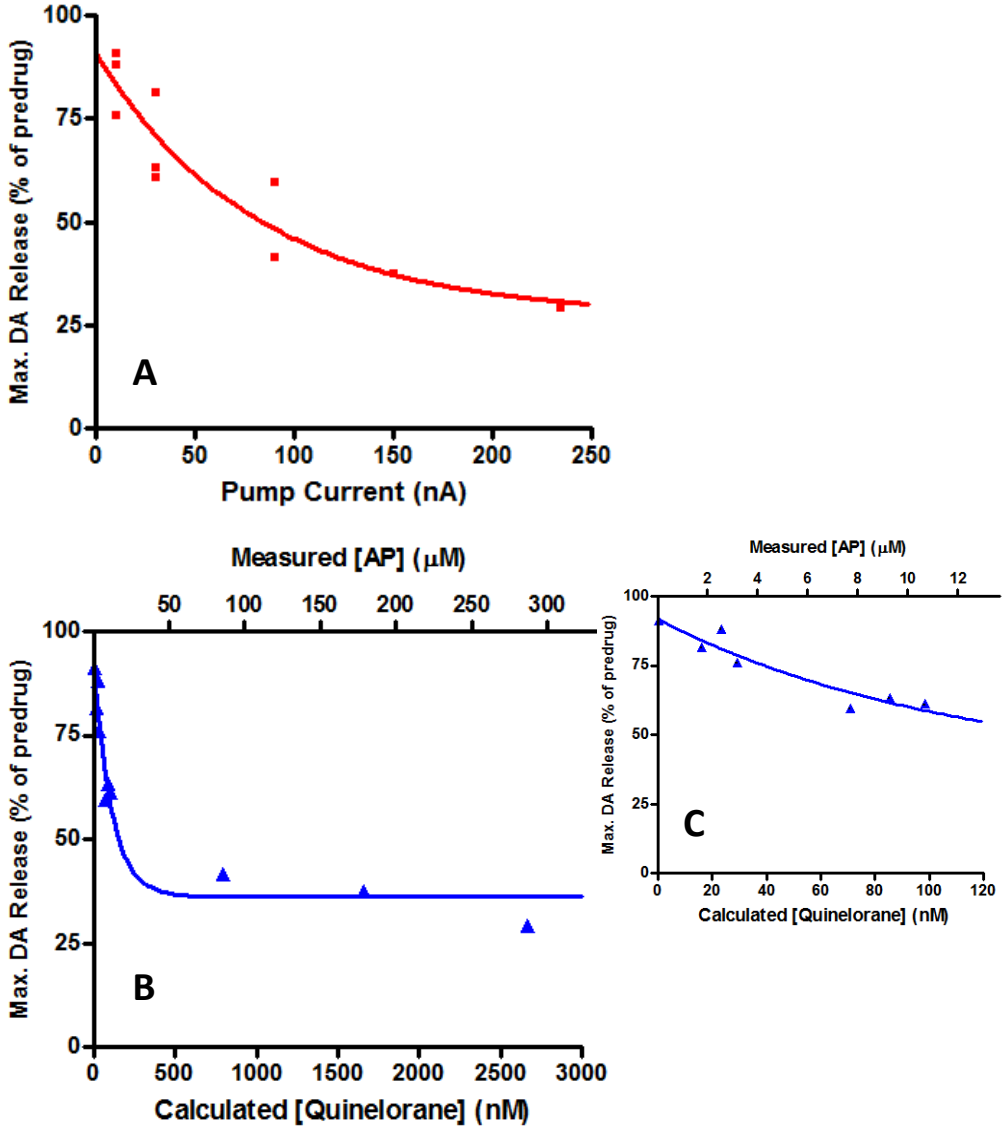

Figure 2.14. Linear dose-response curves constructed where ejected (dose) is recorded as the pump current compared to our technique where concentration of AP is monitored and used to calculate the concentration of the drug of interest. (A) Dose response curve for the change in extracellular dopamine for a given current (nA) requested on the iontophoresis pump for three different iontophoresis barrels in the same animal. (B) Dose response curve for the change in extracellular dopamine concentration for a given current (nA) of AP measured in real time during the ejection with FSCV in the same experiment displayed in A. The measured [AP] is shown in the top x-axis while the concentration of quinelorane calculated from this measured concentration is seen in the bottom x-axis. (C) Zoomed in view of the ≤50% of predrug region of the graph seen in B. Here, the measured concentration of AP is once again on the top x-axis while the calculated concentrations of quinelorane responsible for these changes are listed on the lower x-axis.

Figure 2.14B then shows the subsequent dose response curve created from the same experiment if the calculated concentration of quinelorane ejected, instead of ejection current was used. The concentration of quinelorane was determined for each individual ejection on all three barrels by monitoring of the oxidation and reduction of the neutral marker, AP, the measured concentration of which is seen on the upper x-axis. Using the concentration of quinelorane instead of the ejection current as the measure of dosage allowed for excellent agreement between the data points acquired and a regression that fits the behavior of a linear dose response curve. Additionally, using the calculated concentration of quinelorane instead of ejection current, nanomolar concentrations of quinelorane can be linked to reductions in the electrically evoked DA release seen within the caudate of an anesthetized animal (Figure 2.14C).

Since quinelorane is the compound responsible for the decrease in stimulated DA release, the goal was to determine a method that allows quantitative ejection of this nonelectroactive drug. For the curve in Figure 2.14B, quinelorane's EC_{50} (which again gives potency but not necessarily affinity for a receptor) was 62 nM. While a larger value than the EC_{50} value of 5.3 ± 11 nM determined for quinelorane in brain slices our calculated values still come within an order of magnitude of reported values (unpublished, Dissertation of C. Miller, 2008). Additionally, according to tritium radiolabel binding studies *in vitro* on brain slices quinelorane bound with an incredibly high affinity (K_D=1.8 nM) with very low non-specific binding (Gackenheimer et al., 1995). The systemic administration of haloperidol does have an effect on the K_D of quinelorane however and the same study also confirmed that D2 antagonists inhibited the binding of quinelorane and specifically that haloperidol had a K_i of 3.1 nM for this inhibition (Gackenheimer et al., 1995). The order of magnitude discrepancy between the EC_{50} reported here and that determined *in vitro* in slices in our lab can be attributed to two factors: the competitive antagonism of haloperidol at the receptors of interest and potentially inflated calculated quinelorane concentrations at the synapses of

interest during stimulations. While the presence of haloperidol at the receptors definitely decreased the potency of quinelorane, there most likely still remains a discrepancy between the maximum concentration of quinelorane during the ejection and the concentration of quinelorane actually interacting with D2 autoreceptors at the time of evoked release that still needs further investigation beyond the diffusion studies carried out thus far. But, this affects only the potential accuracy of the EC_{50} values seen on our dose response curves not the validity of the method for monitoring the ejection. Finally, while the presence of haloperidol at receptors was needed to ensure that variations in tonic DA do not affect quinelorane potency at receptors, an estimated EC_{50} in the absence of haloperidol could potentially be obtained through the construction of a series of competitive antagonist dose response curves at various haloperidol concentrations.

Construction of an intra-animal dose response curve

While the heterogeneity of receptors from region to region and even with a single region in the brain has long been debated it was established to not be an issue over the length of a carbon fiber (Venton et al., 2003) but is still potentially an issue as the electrode is moved further down into the brain. This is theorized to be a result of changes in tonic DA levels within a region, which unfortunately cannot be monitored over time using background-subtracted FSCV. The application of a D2 antagonist has been shown to eliminate or greatly reduce this heterogeneity in the rat striatum however (Moquin and Michael, 2009). This behavior supports the theory that tonic extracellular DA levels cause any differences in electrically evoked release from location to location or for a given dosage of drug. With haloperidol occupying many of the DA autoreceptors we want to manipulate, any changes in tonic DA should not affect stimulated release or recovery time of the DA signal after a drug ejection. Additionally, quinelorane has a higher affinity for the D2 autoreceptor than DA

itself (Storey et al., 1995) so the relationship explored was only competitive antagonism of the D2 autoreceptor between haloperidol and quinelorane.

After stabilization of DA stimulated release with haloperidol on board, quinelorane (0.5 mM) and AP were co-ejected for 30 seconds as the stimulated release of DA was continually monitored every 120 seconds until the signal recovered to pre-drug levels. When stimulated release re-stabilized post-ejection, drug was once again iontophoresed using a larger positive ejection current. Ejections were repeated for 5 different AP currents over 3 orders of magnitude had been collected in a single location in the animal's brain. These drug ejections and the subsequent reductions in stimulated release of DA were then used to construct the sigmoidal dose response curve seen in Figure 2.15. The probe was then moved a minimum of 400 µm further down into the brain until another DA hotspot was located. At this new location, drug was once again iontophoresed using different positive currents while monitoring the ejection via AP current. The drug ejection concentrations and the changes in DA stimulated release they induced were then plotted on the dose response curve made higher up in the brain. This process was then repeated at 400 µm intervals further down into the striatum. As Figure 2.15 shows, the dose response curve created at the initial location in the brain also described the dose-response relationship seen further down in the caudate and nucleus accumbens. This gives credence to the homogeneity of the D2 autoreceptor density in the with regards to the area over which the carbon fiber measures average responses.

CONCLUSIONS

Here controlled iontophoresis was used to not only modulate the stimulated release of DA *in vivo* but to create dose response curves modeling the role of the agonist quinelorane at the D2 autoreceptor with stimulated release of DA. First the relative iontophoretic mobilities of nonelectroactive compounds with respect to a neutral marker

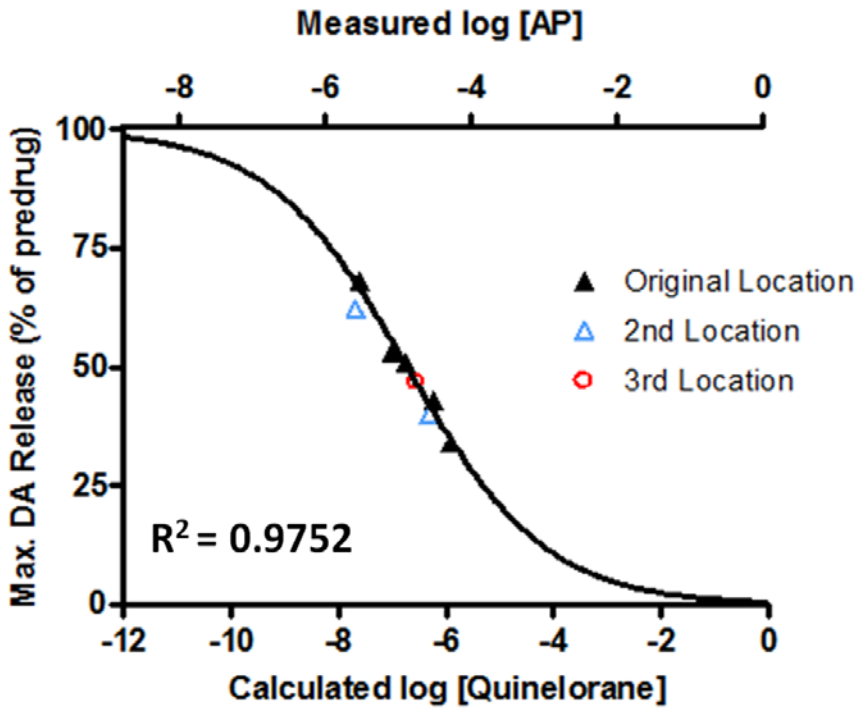

Figure 2.15. Sigmoidal dose response curve for quinelorane in an anesthetized animal with quinelorane concentrations on a logarithmic scale. Curve was constructed using the points collected at the original location (▲) and the data collected at the two deeper locations (**Δ** and ○) plotted on the same graph. R-squared value is for data points from all three locations in comparison to the curve created using the original location however.

molecule were determined using CE and UV-VIS detection. The diffusion from the point of an iontophoretic ejection was then examined to better give an idea of the dose of drug present when “responses” were measured. The neutral marker molecules of choice and large ejection currents were established to have no effect on the stimulated release of DA in the striatum and AP, NPE, nomefensine, raclopride, quinpirole and quinelorane were determined to have no significant effect on the DA sensitivity of a carbon-fiber microelectrode.

After establishing that the technique itself did not modify the stimulated release of DA, the modulation of stimulated release in an anesthetized animal using quinelorane was demonstrated and carried out over several hours both in the same location in the rat brain and at 400 µm intervals more ventral in the brain with consistent responses to drug dosages. This technique also allowed for more reproducible ejections from barrel to barrel and with these more accurate measurements of drug ejections, more precise dose response curves were constructed.

Future works includes determining the range of magnitudes over which the sigmoidal dose response curves modeled here hold true and to determine the extremes to which the DA signal can be modulated with this technique. Finally, while the presence of haloperidol at receptors was needed ensure that variations in tonic DA do not affect quinelorane potency at receptors, an estimated EC_{50} in the absence of haloperidol could potentially be obtained through the construction of a series of competitive antagonist dose response curves at various haloperidol concentrations.

REFERENCES

Armstrong-James M, Fox K, Kruk ZL, Millar J (1981) Electrochemical detection of dopamine agonists. Br J Pharmacol 74:224P-224P.

Bates MD, Senogles SE, Bunzow JR, Liggett SB, Civelli O, Caron MG (1991) Regulation of responsiveness at D2 dopamine receptors by receptor desensitization and adenylyl cyclase sensitization. Mol Pharmacol 39:55-63.

Bath BD, Scott ER, Phipps JB, White HS (2000) Scanning electrochemical microscopy of iontophoretic transport in hairless mouse skin. Analysis of the relative contributions of diffusion, migration, and electroosmosis to transport in hair follicles. J Pharm Sci 89:1537-1549.

Bevan P, Bradshaw CM, Pun RY, Slater NT, Szabadi E (1981) Electro-osmotic and iontophoretic release of noradrenaline from micropipettes. Experientia 37:296-297.

Bloom FE (1974) To spritz or not to spritz: the doubtful value of aimless iontophoresis. Life Sci 14:1819-1834.

Bradbury AJ, Cannon JG, Costall B, Naylor RJ (1984) A comparison of dopamine agonist action to inhibit locomotor activity and to induce stereotyped behaviour in the mouse. Eur J Pharmacol 105:33-47.

Buzsaki G, Leung LW, Vanderwolf CH (1983) Cellular bases of hippocampal EEG in the behaving rat. Brain Res 287:139-171.

Clark AJ (1926) The reaction between acetyl choline and muscle cells. J Physiol 61:530-546.

Clark AJ (1927) The reaction between acetyl choline and muscle cells: Part II. J Physiol 64:123-143.

Clark AJ, Raventos, J. (1937) The antagonism of acetylcholine and of quaternary ammonium salts. Exp Physiol 26:375-392.

Claustre Y, Fage D, Zivkovic B, Scatton B (1985) Relative selectivity of 6,7-dihydroxy-2-dimethylaminotetralin, N-n-propyl-3-(3-hydroxyphenyl)piperidine, N-n-propylnorapomorphine and pergolide as agonists at striatal dopamine autoreceptors and postsynaptic dopamine receptors. J Pharmacol Exp Ther 232:519-525.

Curtis D (1964) Micro-electrophoresis. In: Physical Techniques in Biological Research (WL N, ed), pp 144-190. New York: Academic Press.

Davidson C, Ellinwood EH, Douglas SB, Lee TH (2000) Effect of cocaine, nomifensine, GBR 12909 and WIN 35428 on carbon fiber microelectrode sensitivity for voltammetric recording of dopamine. J Neurosci Methods 101:75-83.

Foreman MM, Fuller RW, Hynes MD, Gidda JS, Nichols CL, Schaus JM, Kornfeld EC, Clemens JA (1989) Preclinical studies on quinelorane, a potent and highly selective D2-dopaminergic agonist. J Pharmacol Exp Ther 250:227-235.

Gackenheimer SL, Schaus JM, Gehlert DR (1995) [3H]-quinelorane binds to D2 and D3 dopamine receptors in the rat brain. J Pharmacol Exp Ther 274:1558-1565.

Guy RH, Kalia YN, Delgado-Charro MB, Merino V, Lopez A, Marro D (2000) Iontophoresis: electrorepulsion and electroosmosis. J Control Release 64:129-132.

Helmreich I, Reimann W, Hertting G, Starke K (1982) Are presynaptic dopamine autoreceptors and postsynaptic dopamine receptors in the rabbit caudate nucleus pharmacologically different? Neurosci 7:1559-1566.

Herr NR, Kile BM, Carelli RM, Wightman RM (2008) Electroosmotic flow and its contribution to iontophoretic delivery. Anal Chem 80:8635-8641.

Herr NR, Daniel KB, Belle AM, Carelli RM, Wightman RM (2010) Probing presynaptic regulation of extracellular dopamine with iontophoresis. ACS Chem Neurosci 1:627-638.

Hicks TP (1984) The history and development of microiontophoresis in experimental neurobiology. Prog Neurobiol 22:185-240.

Kita JM, Parker LE, Phillips PE, Garris PA, Wightman RM (2007) Paradoxical modulation of short-term facilitation of dopamine release by dopamine autoreceptors. J Neurochem 102:1115-1124.

Kiyatkin EA, Kiyatkin DE, Rebec GV (2000) Phasic inhibition of dopamine uptake in nucleus accumbens induced by intravenous cocaine in freely behaving rats. Neuroscience 98:729-741.

Kristensen EW, Wilson RL, Wightman RM (1986) Dispersion in flow injection analysis measured with microvoltammetric electrodes. Anal Chem 54:986-988.

Mandt BH, Zahniser NR (2010) Low and high cocaine locomotor responding male Sprague-Dawley rats differ in rapid cocaine-induced regulation of striatal dopamine transporter function. Neuropharmacol 58:605-612.

Mandt BH, Allen RM, Zahniser NR (2009) Individual differences in initial low-dose cocaine-induced locomotor activity and locomotor sensitization in adult outbred female Sprague-Dawley rats. Pharmacol Biochem Behav 91:511-516.

Mandt BH, Schenk S, Zahniser NR, Allen RM (2008) Individual differences in cocaine-induced locomotor activity in male Sprague-Dawley rats and their acquisition of and motivation to self-administer cocaine. Psychopharmacology (Berl) 201:195-202.

Martin GE, Williams M, Haubrich DR (1982) A pharmacological comparison of 6,7-dihydroxy-2-dimethylaminotetralin (TL-99) and N-n-propyl-3-(3-hydroxyphenyl)piperidine with (3-PPP) selected dopamine agonists. J Pharmacol Exp Ther 223:298-304.

May LJ, Kuhr WG, Wightman RM (1988) Differentiation of dopamine overflow and uptake processes in the extracellular fluid of the rat caudate nucleus with fast-scan in vivo voltammetry. J Neurochem 51:1060-1069.

Mercier D, Falardeau P, Levesque D (2001) Autoreceptor preference of dopamine D2 receptor agonists correlates with preferential coupling to cyclic AMP. Neuroreport 12:1473-1479.

Moquin KF, Michael AC (2009) Tonic autoinhibition contributes to the heterogeneity of evoked dopamine release in the rat striatum. J Neurochem 110:1491-1501.

Pikal MJ, Shah S (1990) Transport mechanisms in iontophoresis. II. Electroosmotic flow and transference number measurements for hairless mouse skin. Pharm Res 7:213-221.

Purves R (1980) Ionophoresis - progress and pitfalls. Trends Neurosci 3:245-247.

Purves RD (1979) The physics of iontophoretic pipettes. J Neurosci Methods 1:165-178.

Rebec GV (1998) Real-time assessments of dopamine function during behavior: single-unit recording, iontophoresis, and fast-scan cyclic voltammetry in awake, unrestrained rats. Alcohol ClinExpRes 22:32-40.

Rice ME, Nicholson C (1989) Measurement of nanomolar dopamine diffusion using low-noise perfluorinated ionomer coated carbon fiber microelectrodes and high-speed cyclic voltammetry. Anal Chem 61:1805-1810.

Roth RH (1979) Dopamine autoreceptors: pharmacology, function and comparison with post-synaptic dopamine receptors. Commun Psychopharmacol 3:429-445.

Scott ER, White HS, Phipps JB (1993) Iontophoretic transport through porous membranes using scanning electrochemical microscopy: application to in vitro studies of ion fluxes through skin. Anal Chem 65:1537-1545.

Skirboll LR, Grace AA, Bunney BS (1979) Dopamine auto- and postsynaptic receptors. Electrophysiological evidence for differential sensitivity to dopamine agonists. Science 206:80-82.

Skoog D, Holler, FJ, Nieman, TA (1998) Principles of instrumental analysis. Philadelphia, PA: Saunders College Pub, Harcourt Brace College Publishers.

Sokoloff P, Giros B, Martres MP, Bouthenet ML, Schwartz JC (1990) Molecular cloning and characterization of a novel dopamine receptor (D3) as a target for neuroleptics. Nature 347:146-151.

Stone TW (1985) Microionotphoresis and Pressure Ejection. London: John Wiley and Sons.

Storey VJ, Middlemiss DN, Reavill C (1995) Effect of haloperidol and (-)-sulpiride on dopamine agonist-induced hypoactivity. Neuropharmacol 34:449-455.

Tsuneizumi T, Babb SM, Cohen BM (1992) Drug distribution between blood and brain as a determinant of antipsychotic drug effects. Biol Psychiatry 32:817-824.

Venton BJ, Zhang H, Garris PA, Phillips PE, Sulzer D, Wightman RM (2003) Real-time decoding of dopamine concentration changes in the caudate-putamen during tonic and phasic firing. J Neurochem 87:1284-1295.

Volpato NM, Santi P, Colombo P (1995) Iontophoresis enhances the transport of acyclovir through nude mouse skin by electrorepulsion and electroosmosis. Pharm Res 12:1623-1627.

White FJ, Wang RY (1986) Electrophysiological evidence for the existence of both D-1 and D-2 dopamine receptors in the rat nucleus accumbens. J Neurosci 6:274-280.

Wiedemann DJ, Garris PA, Near JA, Wightman RM (1992) Effect of chronic haloperidol treatment on stimulated synaptic overflow of dopamine in the rat striatum. J Pharmacol Exp Ther 261:574-579.

Wightman RM, Heien ML, Wassum KM, Sombers LA, Aragona BJ, Khan AS, Ariansen JL, Cheer JF, Phillips PE, Carelli RM (2007) Dopamine release is heterogeneous within microenvironments of the rat nucleus accumbens. Eur J Neurosci 26:2046-2054.

Wyllie DJ, Chen PE (2007) Taking the time to study competitive antagonism. Br J Pharmacol 150:541-551.

Chapter 3

Iontophoretic modulation of neuronal transmission and cerebral oxygen: Proof of principle and word of warning

INTRODUCTION

The brain is composed of a complex neuronal network where neurons synapse onto one another to transmit information via chemical signaling. Glucose, the raw material to fuel this energy intensive process, is delivered with molecular oxygen (O_2) to this network via blood. As Figure 3.1 shows, astrocytes serve as the intermediary between neurons and blood vessels of all sizes (Attwell and Laughlin 2001). Astrocytes play a central role in neurometabolic coupling and cerebral blood flow (CBF) by producing lactate and ATP from glucose provided by blood vessels. Lactate then fuels synaptic transmission. The tight coupling between CBF and neural activity is referred to as functional hyperemia and has been established in studies that monitor both events simultaneously (Thompson, Peterson et al. 2003).

Increased CBF delivers glucose and Ca^{2+} to a region and removes CO_2 and H_2O from that same region (Figure 3.1B). While CBF can be measured directly with optical methods (Lauritzen 2001; Harrison, Sigler et al. 2009) or by measuring the rate at which H_2 is removed from a region (Young 1980), changes in O_2 concentration also serve as an indicator of changes in CBF (Boutelle, Zetterstrom et al. 1990; Lowry, Boutelle et al. 1997). Consumption of glucose by metabolic processes in the brain is the prime reason increases

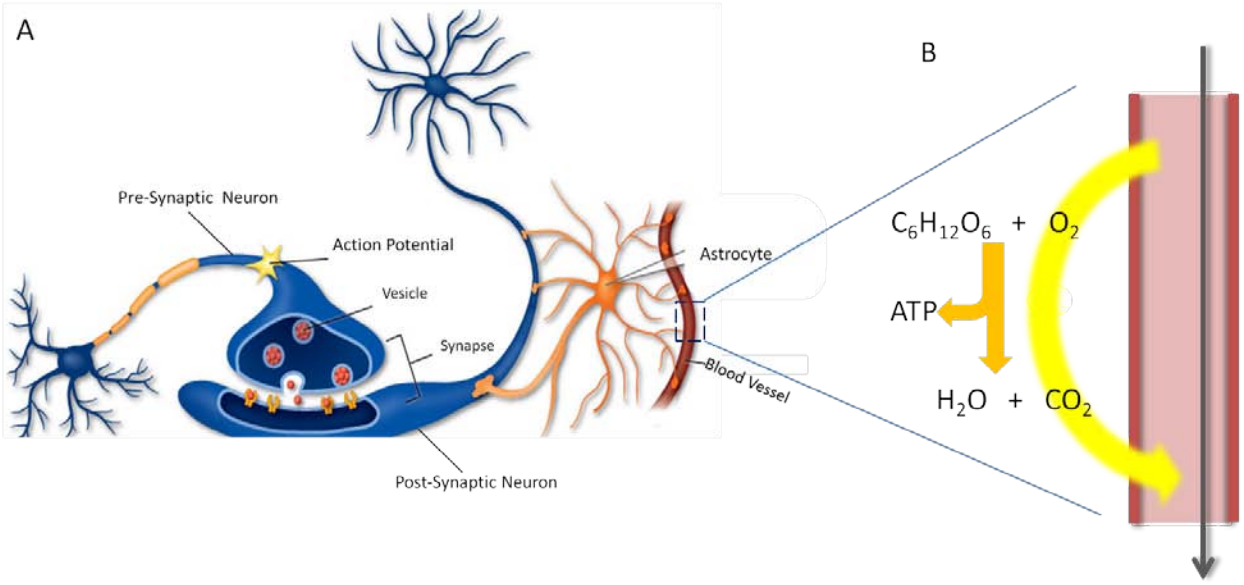

Figure 3.1. How cerebral blood flow fuels neuronal signaling. A) The neuro-vascular unit consists of pre- and post-synaptic neurons that synapse onto one another to transmit chemical signals. Blood vessels and microcapillaries provide the raw materials to fuel this energy demanding neurotransmission. The activities of vessels and neurons are mediated by astrocytes and glia that synapse onto both. B) Blood vessels deliver O_2 and glucose to astrocytes where they are used to create the fuel for neural processes (ATP) and carry away the byproducts of this reaction, CO_2 and H_2O.

in CBF are seen to coincide with neuronal activity. The simultaneously delivered O_2 is not consumed as rapidly by the brain and thus increases in CBF are accompanied by a large overshoot in O_2 concentration in a region (Fox, Raichle et al. 1988).

Complex signaling cascades, involving many different chemical messengers, regulate all steps in functional hyperemia. Individual chemical messengers can be monitored and manipulated to understand the relationship between neuronal transmission and CBF. The association between local O_2 and neuronal activity has primarily been evaluated for glutamatergic neurotransmission and is relatively well understood (Zonta, Angulo et al. 2003; Attwell, Buchan et al. 2010). Glutamate stimulates aerobic glycolysis which results in the release of lactate from astrocytes. Lactate then contributes to the activity-dependent fuelling of the neuronal energy demands associated with synaptic transmission. Additionally, glutamate and Ca^{2+} intake by astrocytes can trigger a cascade of events that increases CBF at capillaries (Attwell, Buchan et al. 2010).

Glutamate is involved in many neuronal pathways in the nucleus accumbens (NAc) (Iadecola and Nedergaard 2007) and thus its neurotransmission in this region is also well studied. Because of its established ability to increase cell firing in a region, glutamate is commonly introduced directly into the brain with iontophoresis to modulate cell firing (White and Wang 1986; Kiyatkin and Rebec 1996; Kiyatkin and Rebec 1999; Kiyatkin and Rebec 1999). Here we use the technique of controlled iontophoresis (Belle, Owesson-White et al. 2013) to electrochemically monitor the direct application of exogenous glutamate to the NAc. During this application we simultaneously monitor O_2 changes electrochemically (Zimmerman and Wightman 1991; Zimmerman, Kennedy et al. 1992; Venton, Michael et al. 2003) and cell firing with electrophysiology (Cheer, Heien et al. 2005) to better understand the relationship between glutamate release, postsynaptic signaling cascades, and functional hyperemia. Finally, using this well understood relationship between glutamatergic signaling

and functional hyperemia we confirm the utility of this combined electrochemical technique to understand the role of neuroactive substances in functional hyperemia.

METHODS

Chemicals

All chemicals were purchased from Sigma-Aldrich (St. Louis, MO) and used as received. Solutions were prepared using deionized water. Phosphate buffered saline (PBS) (0.010 M), pH 7.4, was used in all calibration experiments.

Surgeries

Male Sprague-Dawley rats (350-500 g; Charles River, Wilmington, MA) were anesthetized with urethane (1.5 mg/kg) and placed in a stereotaxic frame (Kopf, Tujunga, CA). Surgeries were performed as previously described (Herr, Daniel et al. 2010). The working electrode was placed in the NAc (2.2 AP, 1.7 ML, DV 7.0-8.0) (Paxinos and Watson 2007) and a bipolar stimulating electrode (Plastics One, Roanoke, VA) was lowered into the MFB (-2.8 AP, 1.7 ML, 7.8-8.6 DV). The carbon-fiber and stimulating electrodes were individually adjusted in the dorsal−ventral coordinate to optimize O_2 release. A Ag/AgCl electrode was placed in the contralateral hemisphere and secured with a stainless steel screw to act as both reference for the carbon-fiber electrode and a ground for the iontophoresis barrels. All procedures were approved by the Institutional Animal Care and Use Committee of the University of North Carolina.

Electrochemical Data Acquisition and Presentation

Electrochemical data were acquired using data-acquisition hardware and local software (HDCV) written in LabVIEW (National Instruments, Austin, TX). The cyclic voltammetry waveform was generated and the voltammetric signal acquired with a computer interface board, the PCIe-6363 X Series (National Instruments). The voltammetric

waveform was input into a custom-built instrument for application to the electrochemical cell (University of North Carolina at Chapel Hill, Department of Chemistry Electronics Facility). Background subtraction, signal averaging, and digital filtering (low-pass filtered at 2 kHz) were under software control. To avoid distortion caused by background drift, scans used for background subtraction were recorded within 2 minutes of the subtracted data.

The waveform was applied at a scan rate of 400 V/s with a rest potential of 0.0 V versus the Ag/AgCl reference electrode between scans. The voltage was scanned linearly from the rest potential to +0.8 V, followed by a scan to -1.4 V and back to the rest potential. Before measurements were recorded, the carbon fiber surface was conditioned with this waveform repeated at 60 Hz. After conditioning, scans were repeated every 100 ms.

Iontophoresis Probe Preparation

Three barrel iontophoresis probes with an attached carbon-fiber electrode were constructed as described previously (Belle, Owesson-White et al. 2013). For application of glutamate, a barrel contained 200 mM L-glutamic acid, 5 mM of the electroactive marker, 4-methylcatechol (4-MC), and 5 mM NaCl and another barrel contained just 5 mM 4-MC in 5 mM NaCl. The exact electrophoretic mobility of glutamate with respect to 4-MC was not determined due to equipment malfunctions. Instead, the electrophoretic mobility of glutamate was estimated based on the experimental mobility of uric acid, an anion of similar charge and mass. Uric acid has a relative electrophoretic mobility of 0.49 with respect to a neutral species (Herr et al., 2008) and here we use this same value to calculate glutamate concentrations. For barrels containing ethylene glycol tetraacetic acid (EGTA) or calcium (Ca^{2+}) bromide hydrate, 20 mM was dissolved in 5 mM NaCl. Because EGTA adsorbs to the electrode surface, its signal prevented quantization. Ejection currents were delivered by a constant current source designed for iontophoresis (Neurophore, Harvard Apparatus, Holliston, MA). Positive current was used to eject all drugs.

Experimental Protocol

The probe was slowly lowered to 1.0 mm above the NAc where the electrode was conditioned for 15 min before application of the waveform every 100 ms. The iontophoresis barrels were primed as described previously (Herr, Daniel et al. 2010) and pump currents to deliver desired amounts of each drug were determined at this depth. Between probes and from barrel to barrel, the amount of current required to achieve a desired concentration varied from 10 nA to 400 nA with 0 nA applied between ejections.

The electrode was then lowered into the NAc (7.0 mm DV). For experiments where chemical information and cell-firing were monitoring simultaneously the waveform was altered to concurrently allow FSCV and electrophysiological recordings (Owesson-White, Cheer et al. 2008). A solid-state relay in the headstage alternated between the current amplifier for voltammetric scans and a voltage follower for unit-recording. The unit-recording interval had a 20 ms gap every 180 ms when voltammograms were collected. In the first 5 ms of this interval, a potential of -0.4 V was applied. The potential sweep for voltammetry remained the same as during the initial cycling.

Once in the NAc, data collection occurred at sites where a single unit was isolated. A single unit was classified as an MSN if baseline firing frequency was below 15 Hz and the waveform duration was less than 1.2 ms (Kish, Palmer et al. 1999; Carelli and Ijames 2001). After unit activity was monitored for 20 min to ensure a constant firing rate, drug was applied to the unit. Units recorded at carbon-fiber electrodes were amplified (x 1,000) and band-pass filtered (300–3,000 Hz). All signals were digitized with commercially available software (DIGITIZER, Plexon, Dallas, TX) and isolation of a unit was accomplished with principal component analysis in commercially available software (OFFLINE SORTER, Plexon, Dallas, TX). Digital outputs synchronized HDCV (FSCV) and Plexon (electrophysiology) records to iontophoretic ejections or electrical stimulations.

Data was displayed as a colorplot with the applied voltage plotted on the ordinate, time on the abscissa, and resulting current changes in false color. Colorplots allow examination of multiple cyclic voltammograms (CVs) recorded over several seconds simultaneously. O_2 is reduced at -1.3 V and 4-MC is oxidized at 0.7 V.

Flow Injection Apparatus

In vitro experiments and calibration of carbon-fiber microelectrodes occurred in a flow injection analysis system (Kristensen, Wilson et al. 1986). The linear flow velocity (2.0 mL/min) was controlled with a syringe infusion pump (Harvard Apparatus model 940, Holliston, MA). An injection valve, controlled by a 12 V DC solenoid, introduced analyte from an injection loop (volume of 0.7 mL) into an electrochemical cell. The carbon-fiber microelectrode was lowered through the electrochemical cell into the opening of the attached PEEK tubing. Five concentrations between 500 nM to 1 µM were used to construct the 4-MC calibration curve. O_2 calibrations were carried out on an O_2 impermeable system using air (~21% O_2), an O_2 saturated solution and nitrogen saturated solution with the exact concentration of O_2 in each solution calculated as described previously (Zimmerman and Wightman 1991).

RESULTS & DISCUSSION

Increased medium spiny neuron activity with local glutamate application

Here we demonstrate that extracellular glutamate concentrations influence the firing rate of medium spiny neurons (MSNs), neurons found post-synaptically in the NAc. To examine prolonged (60 s) effects of glutamate on MSN firing, the firing rate of an isolated MSN was monitored for 30 minutes in an awake or urethane anesthetized animal. This same MSN was then monitored for 30 minutes during which 30 15 s iontophoretic

applications of glutamate occurred at equally spaced intervals. Figure 3.2A shows the firing rates during these two periods for a single MSN in a single awake animal. As Figure 3.2B shows, MSNs fire more frequently in an awake animal. Awake rats have more extracellular glutamate than those under urethane anesthesia (Windels and Kiyatkin 2006). We also confirm that local application of additional glutamate increased cell firing in both basal glutamate conditions. This implies that in an awake but quiescent animal, glutamatergic receptors are not yet saturated and demonstrates the utility of our drug delivery technique to apply small (but not saturating) drug concentrations to a region.

O_2 changes with local glutamate application

In addition to increasing the firing rate of MSNs, local glutamatergic activity has been shown to increase CBF (Lauritzen 2001; Vlassenko, Rundle et al. 2006). CBF and O_2 changes are also directly related to one another (Boutelle et al., 1990), but the direct confirmation that glutamate can induce local changes in O_2 has not been reported. Here, we show that glutamate does induced changes in O_2 and demonstrate the utility of using controlled iontophoresis coupled to electrochemical detection of O_2 to monitor functional hyperemia. Application of less than 50 µM of glutamate along with 4-MC caused an increase in O_2 (Figure 3.3B) while ejection of 4-MC alone did not (Figure 3.3A) (n=5). This result demonstrates controlled iontophoresis' ability to monitor and modulate O_2 dynamics in the intact brain. While glutamate's role in functional hyperemia has been studied extensively using methods that monitor CBF (Lauritzen 2001; Vlassenko, Rundle et al. 2006), or optical techniques that monitor blood-oxygen level-dependent (BOLD) responses

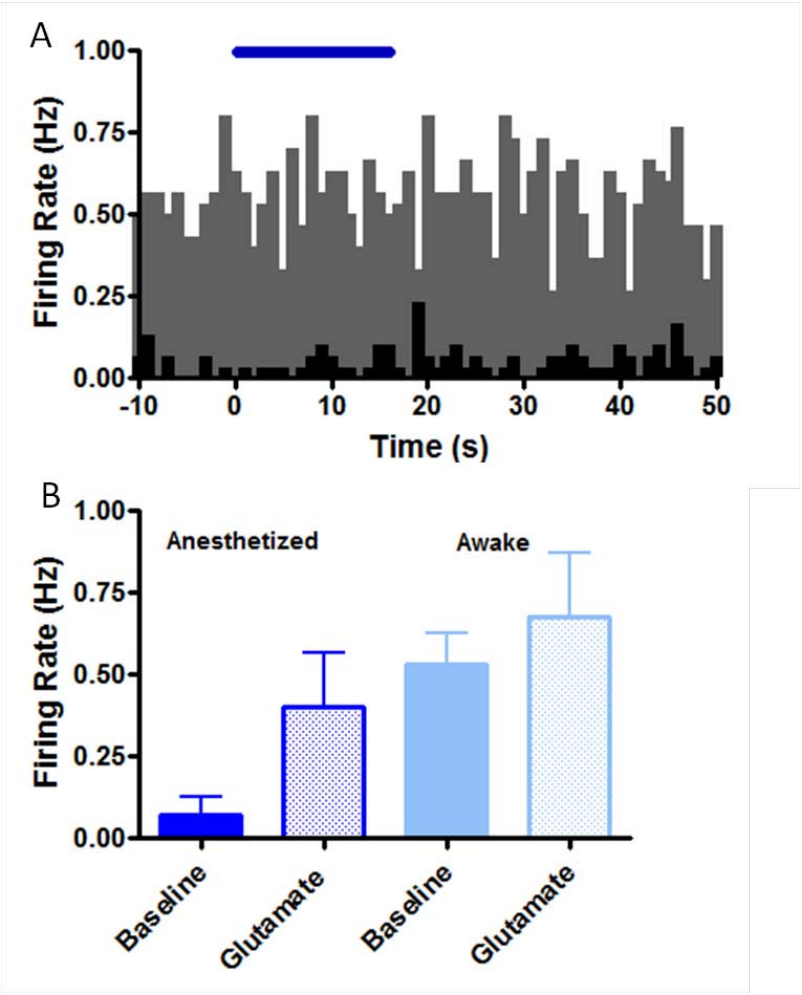

Figure 3.2. Glutamatergic modulation of MSN firing. (A) Histogram of average firing rate for a single MSN in an awake rat in baseline conditions (black) and with glutamate application (grey). The blue bar indicates the onset and duration of glutamate application that began at t=0s. (B) The average baseline firing rate for MSNs (n=4) in animals under urethane anesthesia (left, dark blue) or awake (right, light blue) are shown in addition to the average firing rate of these same MSNs with exogenous glutamate application. All firing rates are significantly different from one another ($p<0.0001$, 1-way ANOVA with Tukey's post-test).

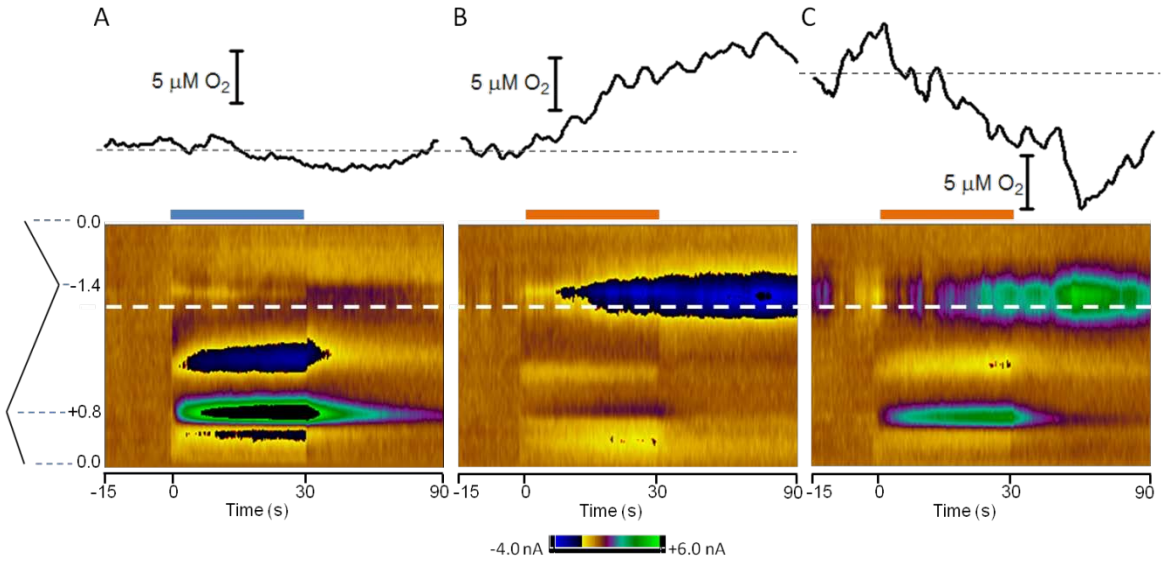

Figure 3.3. Glutamate evoked changes in O_2. Colorplots show FSCV data collected around 30 s ejections of 4-MC (A, light blue) or 4-MC & glutamate (B & C, orange) with time on the x-axis and potential sweep on the y-axis as labeled. Oxidation of 4-MC occurs at 0.7 V and O_2 changes are monitored just before -1.3 V. Above each colorplot is a trace showing changes in O_2 concentration with time extracted from the current at the potential marked with a white dashed line in each colorplot. (A) ejection of 10 µM 4-MC alone, (B) ejection of 1.5 µM 4-MC & 40 µM glutamate, (C) ejection of 5 µM 4-MC & 100 µM glutamate.

(Enzi et al., 2012; Falkenberg et al., 2012), this is the first demonstration of glutamate's ability to induce local changes in O_2.

Interestingly, when ten times more glutamate was applied to the same location in the NAc, the expected increase in O_2 no longer occurs. Instead, decreases in [O_2] of up to 20 µM occurred a few seconds into the application of this higher concentration of glutamate (Figure 3.3C) (n=5). These large decreases are of the same magnitude as the increases in O_2 seen with electrical stimulation (Venton, Michael et al. 2003). The decreases are likely due to increased metabolic activity in response to excessive glutamate application that is known to cause neuronal damage (Shimada, Graf et al. 1989). Such neuronal damage has been shown to cause a burst in MSN firing followed by a cessation in firing activity (Paschen 1996; Schousboe, Sonnewald et al. 1997; Mehta, Prabhakar et al. 2013). Figure 3.3C displays the O_2 changes that accompany this toxic overstimulation of MSNs and demonstrate the danger of applying too much glutamate into the brain as can happen when techniques other than controlled iontophoresis.

At many locations in the NAc there are regular, ongoing fluctuations in O_2 concentration (discussed in Chapter 4) occurring in the environment around the electrode that can be identified as such by their CVs (Figure 3.4A). As Figure 3.4B shows, these O_2 fluctuations look electrochemically distinct from the oscillations seen after application of glutamate concentrations (> 1 mM) known to cause the O_2 decrease seen in Figure 3.3C. These oscillations appear to be ionic changes in the charging current of the electrode because they exhibit current spikes at the voltages where the direction of the voltage scan is switched. Such behavior can occur when electrochemically inert cations can adsorb to functional groups on the surface of the carbon fiber changing the double-layer

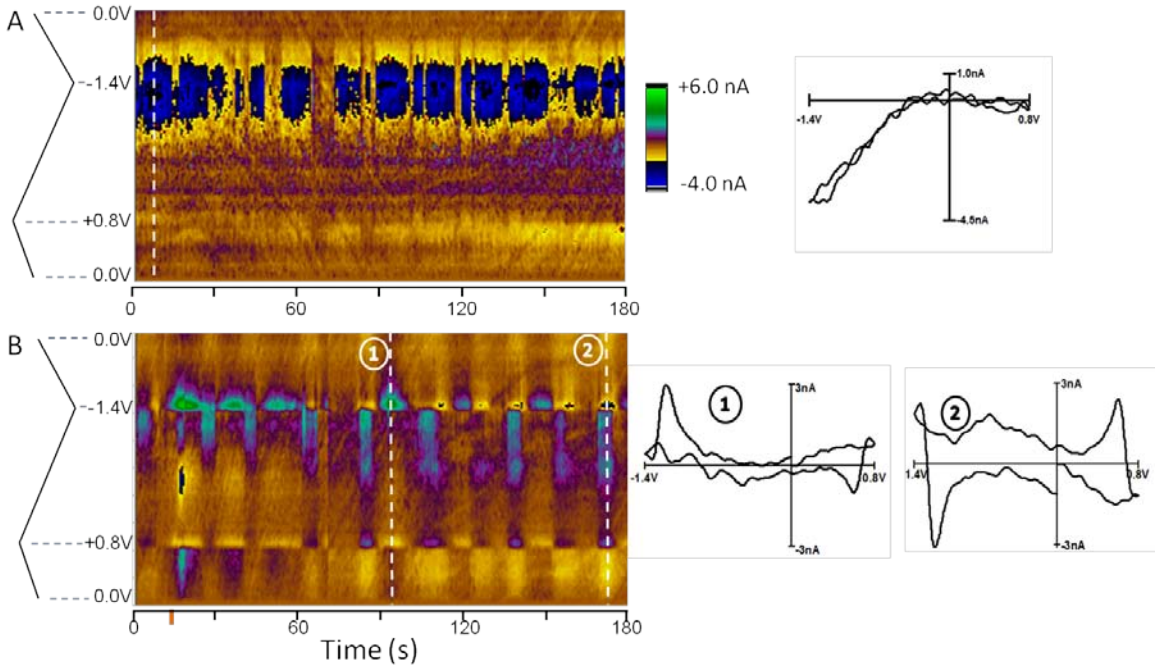

Figure 3.4. Changes in the environment around the carbon-fiber electrode *in vivo*. (A) Natural O_2 fluctuations and (B) ionic oscillations induced with 2 s ejection of glutamate at the orange bar. CVs to the right of each colorplot are from the time(s) indicated with a vertical dashed white line.

capacitance of the electrode and thus the charging of the double layer (Bath, Michael et al. 2000; Bard and Faulkner 2001). This adsorption of cations results in distinct background subtracted CVs unique from those seen for faradaic processes.

Several cations including Ca^{2+}, Mg^{2+}, K^{+}, H^{+} and Na^{+} maintain constant extracellular concentrations in the brain to support ionic gradients across cell membranes. With excessive metabolic activity or an occlusion of CBF, these gradients are disturbed however (Dreier 2011), leading to large ionic changes that may appear in CVs. Increased glutamate concentrations are shown to coincide with disruption of these gradients and inducing large Ca^{2+} 'waves' (Butcher et al., 1990; Wahl et al., 1994). These 'waves' may then alter the ionic gradients of other neurons as well, an event referred to as spreading depression.

In Figure 3.4B, a decrease in current is apparent a few millivolts after the -1.4 V switching potential. The presence of this current decrease at the onset of a positive scan, regardless of initial potential, indicates that the current arises from capacitive changes. Ca^{2+} and Mg^{2+} have been characterized previously (Takmakov, Zachek et al. 2010, Jones et al., 1994; Kume-Kick and Rice, 1998) and were shown to cause shifts in the charging current of the carbon-fiber electrode that appeared as unique CVs after background subtraction. Physiologically relevant changes (~100 µM) in both Ca^{2+} and Mg^{2+} were not detectable *in vivo* in these studies. But, Ca^{2+} changes seen in response to glutamate induced excitotoxicity may be much larger like the Ca^{2+} changes seen with occlusion of blood flow (Pluta et al., 1988; Dohmen et al., 2005) and thus apparent in these experiments. Here, ionic fluctuations induced by glutamate are in fact creating unique CVs that serve as an indication of neuronal damage. The fact that these oscillations are usually not seen *in vivo* with carbon-fiber electrodes provides evidence that they do not cause spreading depression by causing damage to tissue. The appearance of these oscillations in background subtracted electrochemical experiments, however, can serve as an indicator of potential neuronal dysregulation in a region.

CONCLUSIONS

With this combined electrochemical/electrophysiological/iontophoretic method we monitored the effects of exogenous glutamate on cell firing, CBF (via O_2), and local ionic gradients. Here we presented for the first time the O_2 component of glutamatergic signaling and excitotoxicity in the NAc. This work shows very clearly the potential negative consequences of blind glutamate application on ionic gradients, cell firing, and functional hyperemia. The use of controlled iontophoresis to prevent *in vivo* neurotoxicity of exogenous glutamate application was also presented. We also discuss the likelihood that Ca^{2+} fluctuations are responsible for the ionic shifts at the electrode and that these fluctuations likely indicate local neuronal damage, an important thing to recognize during experiments.

REFERENCES

Attwell D, Laughlin SB (2001) An energy budget for signaling in the grey matter of the brain. J Cereb Blood Flow Metab 21:1133-1145.

Attwell D, Buchan AM, Charpak S, Lauritzen M, Macvicar BA, Newman EA (2010) Glial and neuronal control of brain blood flow. Nature 468:232-243.

Bard AJ, Faulkner LR (2001) Electrochemical Methods, Fundamentals and Applications, 2nd Edition. New York: John Wiley.

Bath BD, Michael DJ, Trafton BJ, Joseph JD, Runnels PL, Wightman RM (2000) Subsecond adsorption and desorption of dopamine at carbon-fiber microelectrodes. Anal Chem 72:5994-6002.

Belle AM, Owesson-White C, Herr NR, Carelli RM, Wightman RM (2013) Controlled Iontophoresis Coupled with Fast-Scan Cyclic Voltammetry/Electrophysiology in Awake, Freely Moving Animals. ACS Chem Neurosci.

Boutelle MG, Zetterstrom T, Pei Q, Svensson L, Fillenz M (1990) In vivo neurochemical effects of tail pinch. J Neurosci Methods 34:151-157.

Butcher SP, Bullock R, Graham DI, McCulloch J (1990) Correlation between amino acid release and neuropathologic outcome in rat brain following middle cerebral artery occlusion. Stroke 21:1727-1733.

Carelli RM, Ijames SG (2001) Selective activation of accumbens neurons by cocaine-associated stimuli during a water/cocaine multiple schedule. Brain Res 907:156-161.

Cheer JF, Heien ML, Garris PA, Carelli RM, Wightman RM (2005) Simultaneous dopamine and single-unit recordings reveal accumbens GABAergic responses: implications for intracranial self-stimulation. Proc Natl Acad Sci USA 102:19150-19155.

Dreier JP (2011) The role of spreading depression, spreading depolarization and spreading ischemia in neurological disease. Nat Med 17:439-447.

Dohmen C, Kumura E, Rosner G, Heiss W-D, Graf R (2005) Extracellular correlates of glutamate toxicity in short-term cerebral ischemia and reperfusion: A direct in vivo comparison between white and gray matter. Brain Research 1037:43-51.

Enzi B, Duncan NW, Kaufmann J, Tempelmann C, Wiebking C, Northoff G (2012) Glutamate modulates resting state activity in the perigenual anterior cingulate cortex - a combined fMRI-MRS study. Neuroscience 227:102-109.

Falkenberg LE, Westerhausen R, Specht K, Hugdahl K (2012) Resting-state glutamate level in the anterior cingulate predicts blood-oxygen level-dependent response to cognitive control. Proc Natl Acad Sci U S A 109:5069-5073.

Fergus A, Lee KS (1997) Regulation of cerebral microvessels by glutamatergic mechanisms. Brain Res 754:35-45.

Fox PT, Raichle ME, Mintun MA, Dence C (1988) Nonoxidative glucose consumption during focal physiologic neural activity. Science 241:462-464.

Harrison TC, Sigler A, Murphy TH (2009) Simple and cost-effective hardware and software for functional brain mapping using intrinsic optical signal imaging. J Neurosci Methods 182:211-218.

Herr NR, Daniel KB, Belle AM, Carelli RM, Wightman RM (2010) Probing presynaptic regulation of extracellular dopamine with iontophoresis. ACS Chem Neurosci 1:627-638.

Herr NR, Kile BM, Carelli RM, Wightman RM (2008) Electroosmotic flow and its contribution to iontophoretic delivery. Anal Chem 80:8635-8641.

Iadecola C, Nedergaard M (2007) Glial regulation of the cerebral microvasculature. Nat Neurosci 10:1369-1376.

Kish LJ, Palmer MR, Gerhardt GA (1999) Multiple single-unit recordings in the striatum of freely moving animals: effects of apomorphine and D-amphetamine in normal and unilateral 6-hydroxydopamine-lesioned rats. Brain Res 833:58-70.

Kiyatkin EA, Rebec GV (1996) Dopaminergic modulation of glutamate-induced excitations of neurons in the neostriatum and nucleus accumbens of awake, unrestrained rats. J Neurophysiol 75:142-153.

Kiyatkin EA, Rebec GV (1999a) Striatal neuronal activity and responsiveness to dopamine and glutamate after selective blockade of D1 and d2 dopamine receptors in freely moving rats. J Neurosci 19:3594-3609.

Kiyatkin EA, Rebec GV (1999b) Modulation of striatal neuronal activity by glutamate and GABA: iontophoresis in awake, unrestrained rats. Brain Res 822:88-106.

Kristensen EW, Wilson RL, Wightman RM (1986) Dispersion in flow injection analysis measured with microvoltammetric electrodes. Anal Chem 54:986-988.

Kume-Kick J, Rice ME (1998) Dependence of dopamine calibration factors on media Ca^{2+} and Mg^{2+} at carbon-fiber microelectrodes used with fast-scan cyclic voltammetry. J Neurosci Methods 84:55-62.

Lauritzen M (2001) Relationship of spikes, synaptic activity, and local changes of cerebral blood flow. J Cereb Blood Flow Metab 21:1367-1383.

LeMaistre JL, Sanders SA, Stobart MJ, Lu L, Knox JD, Anderson HD, Anderson CM (2012) Coactivation of NMDA receptors by glutamate and D-serine induces dilation of isolated middle cerebral arteries. J Cereb Blood Flow Metab 32:537-547.

Lowry JP, Boutelle MG, Fillenz M (1997) Measurement of brain tissue oxygen at a carbon past electrode can serve as an index of increases in regional cerebral blood flow. J Neurosci Methods 71:177-182.

Mehta A, Prabhakar M, Kumar P, Deshmukh R, Sharma PL (2013) Excitotoxicity: bridge to various triggers in neurodegenerative disorders. Eur J Pharmacol 698:6-18.

Owesson-White CA, Cheer JF, Beyene M, Carelli RM, Wightman RM (2008) Dynamic changes in accumbens dopamine correlate with learning during intracranial self-stimulation. Proc Natl Acad Sci USA 105:11957-11962.

Parfenova H, Tcheranova D, Basuroy S, Fedinec AL, Liu J, Leffler CW (2012) Functional role of astrocyte glutamate receptors and carbon monoxide in cerebral vasodilation response to glutamate. Am J Physiol Heart Circ Physiol 302:H2257-2266.

Paschen W (1996) Glutamate excitotoxicity in transient global cerebral ischemia. Acta Neurobiol Exp (Wars) 56:313-322.

Paxinos G, Watson C (2007) The Rat Brain in Stereotaxic Coordinates, 6 Edition. Amsterdam: Elsevier.

Pluta R, Salinska E, Puka M, Stafiej A, Lazarewicz JW (1988) Early changes in extracellular amino acids and calcium concentrations in rabbit hippocampus following complete 15-min cerebral ischemia. Resuscitation 16:193-210.

Schousboe A, Sonnewald U, Civenni G, Gegelashvili G (1997) Role of astrocytes in glutamate homeostasis. Implications for excitotoxicity. Adv Exp Med Biol 429:195-206.

Shimada N, Graf R, Rosner G, Wakayama A, George CP, Heiss WD (1989) Ischemic flow threshold for extracellular glutamate increase in cat cortex. J Cereb Blood Flow Metab 9:603-606.

Takmakov P, Zachek MK, Keithley RB, Bucher ES, McCarty GS, Wightman RM (2010) Characterization of local pH changes in brain using fast-scan cyclic voltammetry with carbon microelectrodes. Anal Chem 82:9892-9900.

Thompson JK, Peterson MR, Freeman RD (2003) Single-neuron activity and tissue oxygenation in the cerebral cortex. Science 299:1070-1072.

Venton BJ, Michael DJ, Wightman RM (2003) Correlation of local changes in extracellular oxygen and pH that accompany dopaminergic terminal activity in the rat caudate-putamen. J Neurochem 84:373-381.

Vlassenko AG, Rundle MM, Raichle ME, Mintun MA (2006) Regulation of blood flow in activated human brain by cytosolic NADH/NAD^+ ratio. Proc Natl Acad Sci U S A 103:1964-1969.

Wahl F, Obrenovitch TP, Hardy AM, Plotkine M, Boulu R, Symon L (1994) Extracellular glutamate during focal cerebral ischaemia in rats: time course and calcium dependency. J Neurochem 63:1003-1011.

White FJ, Wang RY (1986) Electrophysiological evidence for the existence of both D-1 and D-2 dopamine receptors in the rat nucleus accumbens. J Neurosci 6:274-280.

Windels F, Kiyatkin EA (2006) General anesthesia as a factor affecting impulse activity and neuronal responses to putative neurotransmitters. Brain Res 1086:104-116.

Young W (1980) H2 clearance measurement of blood flow: a review of technique and polarographic principles. Stroke 11:552-564.

Zimmerman JB, Wightman RM (1991) Simultaneous electrochemical measurements of oxygen and dopamine in vivo. Anal Chem 63:24-28.

Zimmerman JB, Kennedy RT, Wightman RM (1992) Evoked neuronal activity accompanied by transmitter release increases oxygen concentration in rat striatum in vivo but not in vitro. J Cereb Blood Flow Metab 12:629-637.

Zonta M, Angulo MC, Gobbo S, Rosengarten B, Hossmann KA, Pozzan T, Carmignoto G (2003) Neuron-to-astrocyte signaling is central to the dynamic control of brain microcirculation. Nat Neurosci 6:43-50.

Chapter 4

Serotonergic modulation of oxygen in two distinct brain regions

INTRODUCTION

Despite occupying a relatively small volume, the mammalian brain demands disproportionately high amounts of O_2 and glucose (Armstrong, 1982; Attwell et al., 2010). This high energy demand requires a tightly regulated vascular network to control cerebral blood flow (CBF) that operates independently of systemic or arterial blood pressure (Paulson et al., 1995). Astrocytes, whose end-feet encapsulate the brain's microcapillaries, are the gatekeepers for O_2 and glucose exchange between the capillaries and neurons. Neuronal activation results in extra-cellular neurochemical cascades that allow astrocytes to sense and therefore balance supply and demand for energy (Iadecola et al., 2007). Additionally, serotoninergic terminals innervate the peri-vesicular space and its receptors are located directly on the blood vessels (Cohen et al., 1995).

Local increases in O_2 concentration result from increases in CBF (Lauritzen et al., 2001), whereas decreases can be a result of increased metabolism and/or decreases in CBF. Thus, local O_2 changes are a good indicator of dynamic metabolic events. Local *in vivo* O_2 concentrations can be monitored noninvasively with a number of techniques. Positron emission tomography (PET) and functional magnetic resonance imaging (fMRI) with blood-O_2-level-dependent (BOLD) contrast (Samanez-Larkin et al., 2010) allow imaging of O_2 changes within the intact brain of immobile subjects. Intrinsic optical spectroscopy (Harrison et al., 2009) and laser doppler flowmetry (Lauritzen et al., 2001) are used extensively to characterize dynamic events associated with CBF. Laser methods, unless

coupled with fiber optics that can damage tissue, are restricted to cortical regions. To study intact deeper brain structures, smaller and less invasive probes are required. Electrochemistry has previously been explored as a successful option (Clark et al., 1958; Bartlett et al., 2008; Bolger et al., 2011; Thompson et al., 2003). In this study, we apply fast-scan cyclic voltammetry (FSCV) at carbon-fiber electrodes, to simultaneously monitor electroactive neurotransmitters and O_2 fluctuations in deep brain structures in real time (Venton et al., 2003; Zimmerman et al., 1991) with minimal tissue damage (Peters, 2004).

The association between local O_2 and neuronal activity has primarily been evaluated for glutamatergic neurotransmission (Attwell et al., 2010). However, other neurotransmitters such as norepinephrine (Bekar et al., 2012), GABA, acetylcholine (Hamel et al., 2006), and histamine (Haas et al., 2008) also regulate CBF. Our own studies showed a role for nitric oxide and adenosine in the rat striatum (Venton et al., 2003). Serotonin plays an important role for systemic blood regulation (Cohen et al., 1996) and there are several reports implicating its roles in modulating CBF. For example, serotonin neurons increase their firing rates in response to acidic pH shifts and increases in CO_2 (Richerson et al., 2004) and greatly affect cerebral glucose utilization (Bonvento et al., 1991). Furthermore, serotonin terminals directly contact arterioles, capillaries, and astrocytes (Cohen et al., 1995). Finally, astrocytes contain membrane-bound serotonin transporters (Inazu et al., 2001) and serotonin receptors (Hosli et al., 1993) implicating their role as an intermediary for serotoninergic regulation of neurovascular coupling (Cohen, 1996).

Here, we more fully explore serotonin's role in regulating CBF in deep structures of the rat brain by monitoring O_2. We targeted two brain regions with differing serotoninergic anatomy; the nucleus accumbens (NAc), a region primarily composed of dopaminergic terminals but with 10% serotonergic innervation, and the substantia nigra pars reticulata (SNr), a region primarily composed of serotonin terminals (Moukhles et al., 1997). We show endogenous O_2 fluctuations in both regions and we utilized three strategies to examine

serotonin's role in modulating this O_2. First, electrical stimulation was used to release serotonin throughout the NAc and SNr. Then, pharmacology was employed to modulate serotonin dynamics while changes in O_2 were monitored. Finally, serotonin was directly introduced in discrete locations within the SNr or the NAc. The results of these investigations present a compelling set of evidence that serotonin plays an important role in modulating O_2 availability in select areas of the brain.

METHODS

Chemicals

All chemicals were purchased from Sigma-Aldrich (St. Louis, MO) and used as received. Solutions were prepared using deionized water. Brains for slice experiments were stored and sliced in a sucrose slice buffer consisting of 87 mM NaCl, 2.5 mM KCl, 1.2 mM NaH_2PO_4, 0.5 mM $CaCl_2$, 7 mM $MgCl_2$, 25 mM $NaHCO_3$, and 75 mM sucrose, pH 7.4**.** Artificial cerebral spinal fluid (aCSF) consisting of 126 mM NaCl, 2.5 mM KCl, 1.0 mM NaH_2PO_4, 2.4 mM $CaCl_2$, 1.2 mM $MgCl_2$, 25 mM $NaHCO_3$, and 11 mM D-glucose, pH 7.4 was used in slice experiments. A physiological buffer solution (15 mM TRIS, 126 mM NaCl, 2.5 mM KCl, 25 mM $NaHCO_3$, 2.4 mM $CaCl_2$, 1.2 mM NaH_2PO_4, 1.2 mM $MgCl_2$, 2.0 mM Na_2SO_4), pH 7.4, was used in all calibration experiments.

Surgeries

Male Sprague-Dawley rats (350-500g; Charles River, Wilmington, MA) were anesthetized with urethane (1.5 mg/kg) and placed in a stereotaxic frame (Kopf, Tujunga, CA). Surgeries were performed as previously described (Herr, 2010). The working electrode was placed in the NAc (2.2 AP, 1.7 ML, DV 7.0-8.0) or SNr (-5.2 AP, 2.5 ML, DV 8.0-8.6) (Paxinos & Watson, 2007) and a bipolar stimulating electrode (Plastics One, Roanoke, VA) was lowered into the medial forebrain bundle (MFB) (-2.8 AP, 1.7 ML, 7.8-

8.6 DV). Coordinates for the bipolar stimulating electrode ensure activation of the dopaminergic neurons projecting to the NAc and the serotoninergic neurons projecting to the SNr and NAc (Hashemi et al., 2011). The carbon-fiber and stimulating electrodes were individually adjusted in the dorsal−ventral coordinate to optimize O_2 release. A Ag/AgCl electrode was placed in the contralateral hemisphere and secured with a stainless steel screw to act as both reference for the carbon-fiber electrode and a ground for the iontophoresis barrels. All procedures were approved by the Institutional Animal Care and Use Committee of the University of North Carolina.

Slice Preparation

Male Sprague-Dawley rats (350-500g; Charles River, Wilmington, MA) were anesthetized with urethane (1.5 mg/kg), decapitated, and brains immediately removed and placed in chilled sucrose buffer solution. The aCSF was continuously saturated with 95% O_2/5% CO_2. The brain was then mounted on a Teflon block with Krazy Glue® and sliced on a NVSL vibratome (World Precision Instruments, Sarasota, FL). Slices were 300 µm thick and stored at 37 ºC in sucrose slicing buffer. A single slice was then submerged under 37ºC aCSF in a superfusion chamber (Warner Instruments, Hamden, CT) and aCSF continuously replaced in the chamber at a rate of 2 mL/min. Each slice was allowd to equilibrate for 30 min in the chamber before the electrode was lower with the aid of a microscope into the region of interest in the slice.

Electrochemical Data Acquisition and Presentation

Electrochemical data were acquired using data-acquisition hardware and local software (HDCV) written in LabVIEW (National Instruments, Austin, TX). The cyclic voltammetry waveform was generated and the voltammetric signal was acquired with a computer interface board, the PCIe-6363 X Series (National Instruments). The voltammetric

waveform was input into a custom-built instrument for application to the electrochemical cell (University of North Carolina at Chapel Hill, Department of Chemistry Electronics Facility). Background subtraction, signal averaging, and digital filtering (low-pass filtered at 2 kHz) were under software control. To avoid distortion caused by background drift, scans used for background subtraction were recorded within 2 minutes of the subtracted data.

The waveform was applied at a scan rate of 400 V/s with a rest potential of 0.0 V versus a Ag/AgCl reference electrode between scans. The voltage was scanned linearly from the rest potential to +0.8 V, followed by a scan to -1.4 V and back to the rest potential. Before measurements were recorded, the carbon fiber surface was conditioned with this waveform repeated at 60 Hz. After conditioning, scans were repeated every 100 ms.

Iontophoresis Probe Preparation

Three barrel iontophoresis probes attached to a carbon fiber electrode were constructed as described previously (Belle et al., 2013). For application of antagonists, one barrel contained 5 mM methiothepin and the other barrel contained 5 mM raclopride and 5 mM SCH 23390. All barrels contained 5 mM 4-methylcatechol that was used as an electroactive marker (Herr et al., 2010) and 5 mM NaCl. The relative electrophoretic mobility of ralcopride (1.68) and SCH 23390 (1.90) with respect to 4-methylcatechol was used to calculate the concentration of each drug ejected (Belle et al., 2013; Herr et al., 2010). Because methiothepin strongly adsorbs to the electrode surface, its signal prevented quantification as reported for other substances (Herr et al., 2010). When directly applying neurotransmitters, two of the iontophoresis barrels were filled with 5 mM dopamine and 0.6 mM serotonin, both dissolved in 5 mM NaCl. The third barrel contained 5 mM 4-methlcatechol in 5 mM NaCl or NaCl alone. Ejection currents were delivered by a constant current source designed for iontophoresis (Neurophore, Harvard Apparatus, Holliston, MA). Positive current was used to eject all drugs.

Experimental Protocol

The probe was slowly lowered to 1.0 mm above the region of interest (6.0 mm for the NAc and 7.0 mm for the SNr) where the electrode was conditioned for 15 min before application of the waveform every 100 ms. The iontophoresis barrels were primed as described previously (Herr et al., 2010) and pump currents to deliver desired amounts of each drug were determined at this depth. Between probes and from barrel to barrel, the amount of current required to achieve a desired concentration varied from 10 nA to 400 nA. A current of 0 nA was applied between ejections. To ensure a barrel was not leaking solution, a negative current was applied to the barrel while electrochemical information about the area directly around the carbon-fiber was recorded. If there was a change in the background of the electrode or if any compound was ejected when the current was increased from its negative value to 0 nA the barrel was not used and a negative retaining current was applied to the barrel for the duration of the experiment. The electrode was then lowered into the NAc (7.0 mm DV) or SNr (8.0 mm DV). In experiments involving electrical stimulation of the MFB, recordings were made at sites with optimized neurotransmitter and O_2 signals (Zimmerman et al., 1991).

An example set of optimized voltammetric recordings in the NAc are shown in Figure 4.1 in which chemical events were evoked with a 2 s, 60 Hz electrical stimulation of the (MFB). Each cyclic voltammogram took approximately 10 ms to record and was background subtracted (Figure 4.1, left panel, the background was normally taken 1 s before the event of interest). Data were displayed as a color plot (Figure 4.1, middle panel), with the applied voltage plotted on the ordinate, time on the abscissa, and measured current in false color. Color plots allow examination of multiple cyclic voltammograms recorded over several seconds simultaneously. Dopamine, with an oxidation peak at 0.6 V, is released during the electrical stimulation. The time course of this release can be followed by

examining its oxidation current in successive cyclic voltammograms (Figure 4.1, green trace). O_2 is reduced at -1.3 V. It too increases in concentration after the stimulation as shown by the changes in its reduction current in successive voltamograms (Figure 4.1, black trace).

Calibrations

The response of the carbon-fiber electrode was calibrated in a flow injection analysis system. The linear flow velocity (2.0 mL/min) was controlled with a syringe infusion pump (Harvard Apparatus model 940, Holliston, MA). O_2 calibrations were carried out on an O_2 impermeable system using air (~21% O_2), an O_2 saturated solution and nitrogen saturated solution with the exact concentration of O_2 in each solution calculated as described previously (Zimmerman et al., 1991). The voltammetric current was measured at the peak potential for each analyte at four concentrations for serotonin and dopamine.

Histology

After animal experiments were complete, 15 V (vs Ag/AgCl) was applied to the electrode to lesion the region around the carbon fiber. The animals were euthanized, and brains were removed from the skull and stored in 10% formaldehyde for at least 3 days. Brains were coronally sectioned into 40−50 μm thick slices with a cryostat and the lesion identified visually under a stereoscope equipped with a camera. Data were discarded if the histology showed the lesion was not in the desired region.

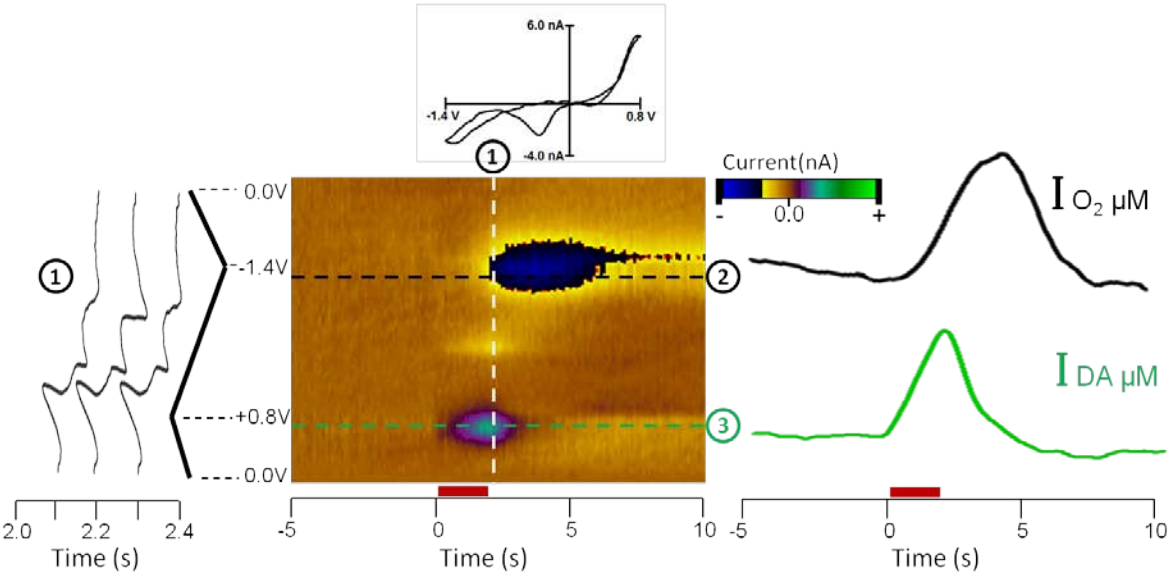

Figure 4.1. Voltammetric response of dopamine (DA) and O_2 in the NAc evoked by a 2 s electrical stimulation (red bar) of the MFB. Every 100 ms a cyclic voltammogram was collected showing changes in current for the potential scan (left). (middle) This color plot contains 150 cyclic voltammograms placed sequentially with current changes encoded by color. The vertical white dashed line (1) indicates a time for which a single cyclic voltammogram can be isolated and graphed with current changes as a function of potential (above) or time (far left). The horizontal black dashed line (2) indicates the potential where O_2 reduction is monitored and the horizontal green dashed line (3) represents the potential where DA oxidation is monitored with concentration traces (right) showing concentration changes for O_2 (2) and DA (3).

RESULTS

Naturally occurring changes in the brain.

While an electrical or pharmacological stimulus is generally used to evoke changes in monoamines and O_2, here background-subtracted cyclic voltammograms reveal spontaneous O_2 oscillations in 90 % of the locations probed in the NAc and the SNr of the anesthetized rat. Examples are shown in Figure 4.2 in which fluctuations in the measured current reveal O_2 concentration changes. The oscillations were observed spontaneously in the absence of pharmacological or electrical stimulations. In some locations, large infrequent O_2 fluctuations (Figure 4.2A) were recorded whereas in other regions more frequent O_2 changes (Figure 4.2B) were observed. In 18% of locations in the SNr, signals in addition to the O_2 oscillations were observed (Figure 4.2C). Individual cyclic voltammograms recorded at such locations showed current surges at the switching apices of the cyclic voltammograms. Current surges at the switching apices can arise in the presence of cations such as Ca^{2+}. Cations adsorb to the electrode's surface altering the surface capacitance and generating non-oxygen or neurotransmitter signals (Takmakov et al., 2010). Locations with ionic fluctuations were not used for O_2 measurements because of the overlap in signals.

When the electrode was lowered in 200 µm intervals through a brain region, different oscillatory patterns were observed at each location. This suggests that local O_2 changes depend on the relative proximity of the electrode to blood vessels, capillaries, astrocytes, and neurons.

Effect of electrical stimulation parameters on O_2 release in the SNr and NAc.

MFB stimulations cause dopamine and serotonin release in the NAc and the SNr (Hashemi et al., 2011). We previously showed that dopamine release in the striatum was accompanied by a biphasic O_2 change (Venton et al., 2003). The first phase of this increase

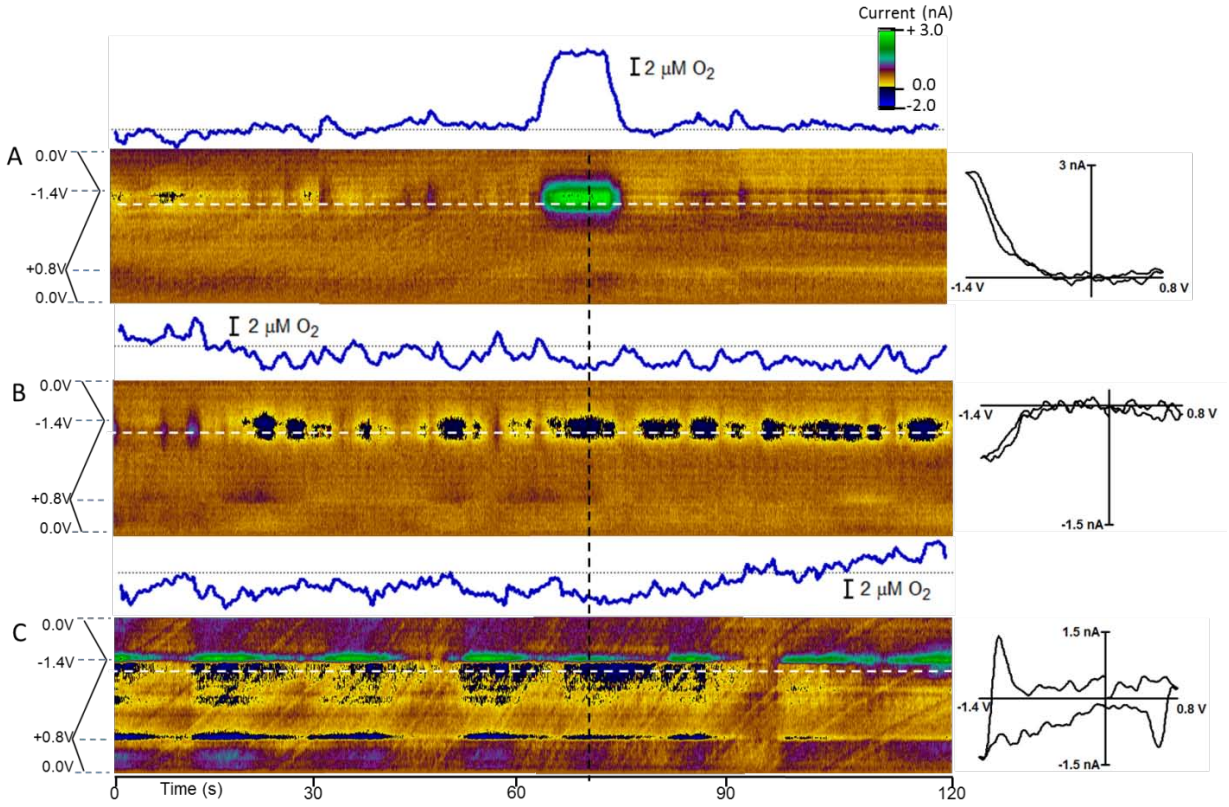

Figure 4.2. Naturally occurring O_2 changes. For all panels, the potential scan applied to the electrode is shown on the vertical axis of the color plot and time on the horizontal axis. The white dashed line indicates the potential at which the concentration changes in O_2 (blue line, above each color plot) were monitored. The vertical dashed line indicates where the cyclic voltammograms to the right of each colorplot was taken. A) Representative color plot of naturally occurring, large, infrequent O_2 changes in the brain, collected in the NAc, 5 cyclic voltammograms collected at 52 s were averaged and used for background subtraction. B) Representative color plot of frequent changes in O_2 in the SNr. Background was taken as the average of 5 cyclic voltammograms collected at 55 s. C) Representative color plot of ionic changes in the SNr. Background was taken as the average of 5 cyclic voltammograms collected at 95 s.

occurred with the onset of electrical stimulation and then dissipated; the second, slower increase in O_2 occurred many seconds after the electrical stimulation concluded and lasted at least 30 s. In this work we replicated this finding in the NAc (Figure 4.3A) and also showed a similar biphasic O_2 response in the SNr (Figure 4.3B). In the NAc, we measured dopamine and O_2 simultaneously (Figure 4.3A), and the cyclic voltammograms allowed each to be identified. In the SNr, serotonin and O_2 responses were collected in separate experiments.

To determine how maximal evoked O_2 concentration ($[O_2]_{max}$) varied with stimulus frequency, we examined both peaks during stimulations at 20, 40, and 60 Hz. At each frequency, 120 biphasic pulses of 350 µA were applied. In general, neurotransmitters reach higher concentrations during high frequency stimulations because there is less time for uptake to clear neurotransmitter in the time between stimulus pulses. The insets in Figure 4.3 show the results of these stimulations on $[O_2]_{max}$ for each peak in both the NAc and SNr. A slight decrease was seen for the $[O_2]_{max}$ of Peak 1 with increasing stimulation frequency in the NAc (slope of -0.92 ± 0.11 µM O_2 per 20 Hz, r^2=0.9417). Peak 2 showed the opposite trend in the same region, with $[O_2]_{max}$ decreasing with stimulation frequency at a rate of 0.80 ± 0.01 µM O_2 per 20 Hz (r^2=0.9991). In the SNr both O_2 peaks decreased with stimulation frequency. In the SNr, $[O_2]_{max}$ for Peak 1 decreased with stimulation frequency at a rate of 3.10 ± 0.19 µM O_2 per 20 Hz (r^2=0.9851) and $[O_2]_{max}$ for Peak 2 decreased with stimulation frequency at a rate of 1.52 ± 0.42 µM O_2 per 20 Hz (r^2=0.7661).

Attenuation of stimulated O_2 changes with methiothepin

In the striatum, adenosine is the chemical messenger that evokes Peak 2 (Venton et al., 2003; Zimmerman et al., 1992) therefore the following examines Peak 1. Stimulations were repeated every 4 minutes until 5 consecutive stimulations showed similar responses. We systemically administered selective dopamine and serotonin antagonists. For

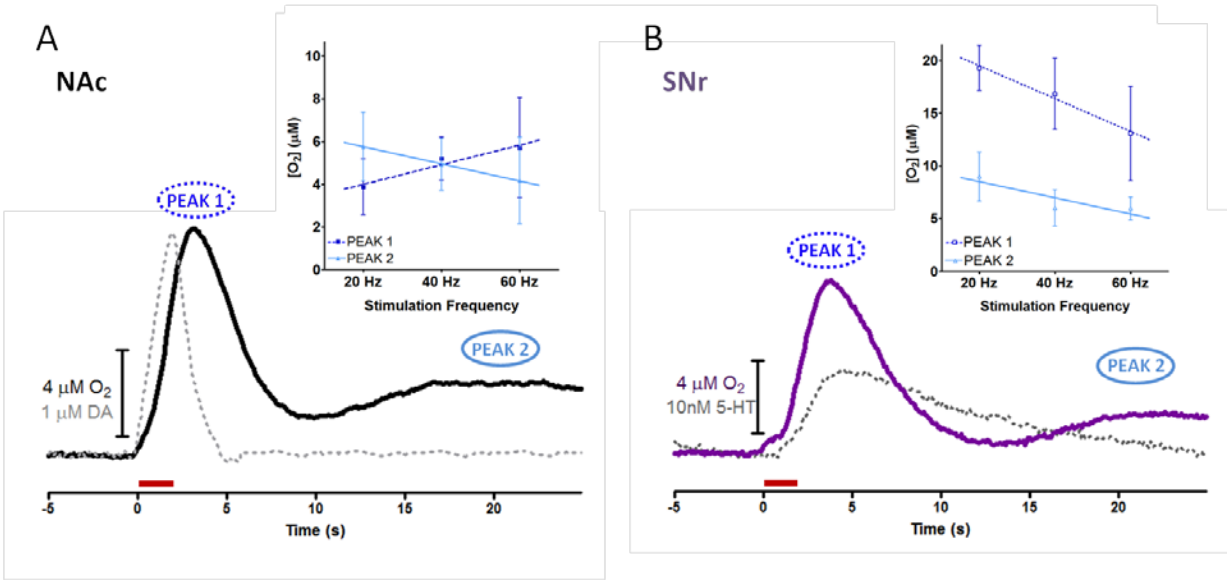

Figure 4.3. Effect of electrical stimulation parameters on subsequent O_2 release in the SNr and NAc. A) Average O_2 and dopamine (DA) concentration traces in the NAc (n = 6 rats). B) Average O_2 and serotonin (5-HT) concentration traces in the SNr (n = 6 rats). In both panels, the red bar at 0 s indicates the onset of the 2 s electrical stimulation. The circled labels designate Peak 1 and Peak 2 of the O_2 response. Inset graphs show the amplitude of change in $[O_2]_{max}$ as a function of the frequency at which 120 350 µA pulses were applied to the MFB (n = 5 rats).

measurements in the NAc, raclopride (2 mg/kg), a D2 receptor antagonist, and SCH 23390 (1 mg/kg), a D1 receptor antagonist, were first administered simultaneously via intraperitoneal (i.p.) injection. This combined treatment decreased $[O_2]_{max}$ slightly ($n = 6$ rats, $p < 0.001$) in the NAc from a maximal value of 11.6 ± 3.0 µM to 9.0 ± 2.6 µM (Figure 4.4A). The nonspecific serotonin receptor antagonist methiothepin (20 mg/kg) was then administered i.p. 2 hours after injection of the dopamine antagonists. As shown in Figure 4.4A, methiothepin caused $[O_2]_{max}$ to decrease to 28% of the original signal, 3.2 ± 1.0 µM ($n = 6$ rats, $p < 0.0001$). Figure 4.4C shows averaged concentration traces taken for O_2 in the SNr ($n = 6$, $\pm$ SEM) before and after methiothepin. Methiothepin caused a significant decrease in $[O_2]_{max}$ from 10.6 ± 4.6 µM to 1.7 ± 2.3 µM ($p < 0.0001$). There was also a significant increase in serotonin, ($n = 5$, $p < 0.0001$) from 5.2 ± 1.4 nM to 7.6 ± 0.2 nM.

To confirm that O_2 attenuation was due to local antagonism in the region adjacent to the electrodes, similar experiments were repeated using iontophoretic delivery of the antagonists. Iontophoresis uses a current to induce the migration of these antagonists through a glass capillary into the brain with negligible tissue perturbation (Rebec, 1998). Electrical stimulation was again applied every 4 minutes for the duration of the experiment. After priming, the electrode was lowered to the region of interest. After five consecutive stimulations showed a constant O_2 response, 14.2 ± 7.3 µM raclopride and 22.6 ± 10.7 µM SCH 23390 were ejected for 30 s approximately 90 s before the next stimulation. Alterations in electrically evoked O_2 were seen immediately following drug ejection. Ejections were repeated until responses to stimulations returned to pre-drug values. A minimum of three stimulations were applied between drug ejections even if changes were not observed. The same procedure was repeated for three 30 s ejections of methiothepin.

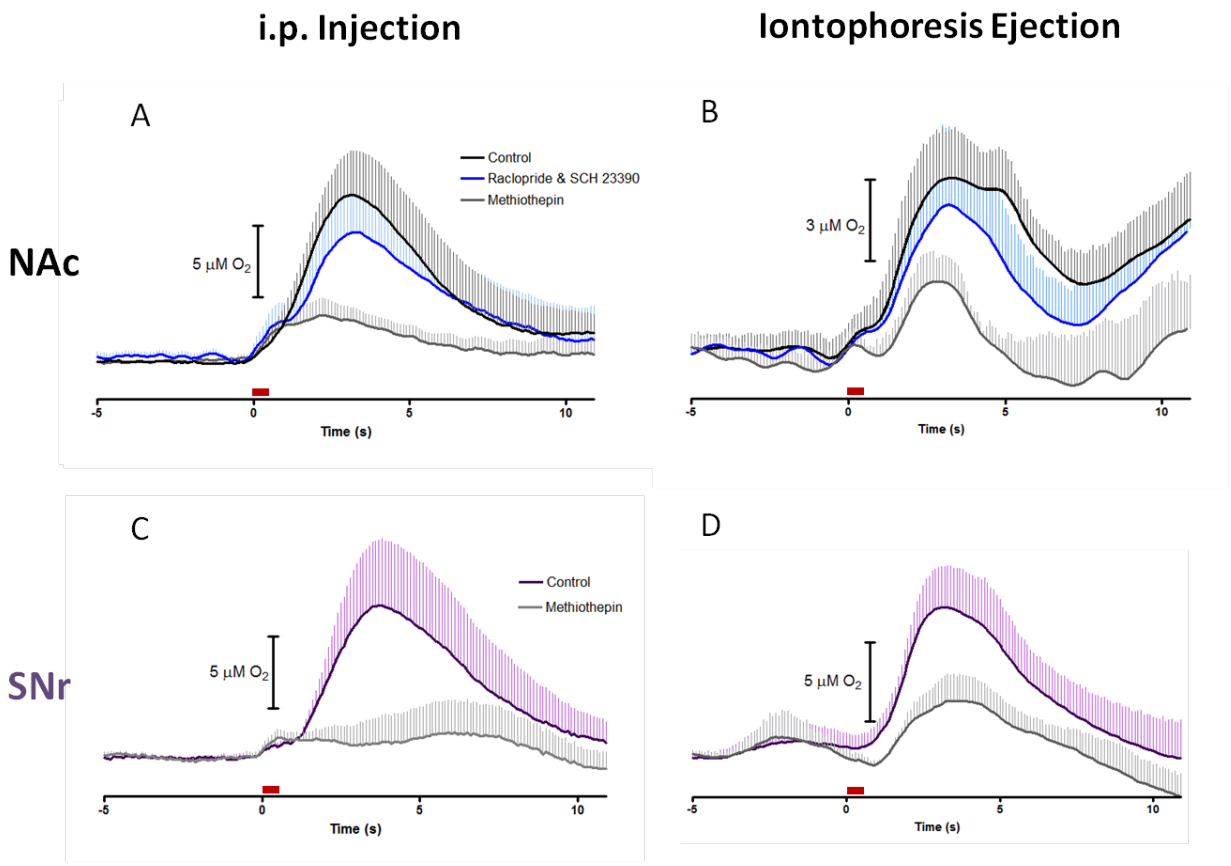

Figure 4.4. Antagonism of dopamine receptors with raclopride and SCH 23390 and serotonin receptors with methiothepin. A) Average concentration changes for O_2 in the NAc before (black) and 1 hour after i.p. administration of both SCH 23390 (1 mg/kg) and raclopride (2 mg/kg) (blue) and 1 hour after i.p. administration of methiothepin (20 mg/kg) (grey) (n = 6 rats). B) Average concentration changes for O_2 in the NAc 60 s after iontophoretic application of antagonists (n = 5 rats). C) Average concentration over time for electrically stimulated O_2 in the SNr before (purple) and 1 hour after i.p. administration of methiothepin (20 mg/kg) (grey) (n = 6 rats). D) Average concentration changes for O_2 in the SNr 60 s after iontophoretic application of antagonists (n = 5 rats). In both panels, red bar at 0 s indicates the onset and duration of stimulation.

The averaged O_2 responses before and after iontophoretic drug application are shown in Figure 4.4 in the NAc and SNr. In the NAc (Figure 4.4B), raclopride and SCH 23390 did not significantly alter the concentration of electrically evoked O_2 ($p > 0.05$) while methiothepin significantly attenuated $[O_2]_{max}$ from 6.2 ± 1.9 µM to 2.4 ± 1.1 µM ($n = 5$, $p < 0.01$), to 35% of the pre-drug response. In the SNr, methiothepin significantly attenuated the $[O_2]_{max}$ ($n = 5$, $p < 0.0001$) to 38% of pre-drug, from 18.9 ± 5.1 µM to 7.1 ± 3.3 µM.

Direct application of serotonin into the NAc via iontophoresis.

To further investigate the roles of serotonin and dopamine in the regulation of local O_2, they were directly applied to each region. Prior work has shown that dopaminergic drugs do not affect O_2 changes (Zimmerman et al., 1991; Venton et al., 2003) and thus its ejection ensures there are no O_2 changes or other artifacts caused by iontophoretic ejections. Here, a primed iontophoresis probe was lowered into either the SNr or NAc and the endogenous chemical environment recorded (Figure 4.5A). Then dopamine was iontophoresed for 2 s, the same duration as electrical stimulation, at increasing concentrations from 500 nM to 5 µM with 5 minutes between drug applications (example trace shown in Figure 4.5B). Into the same location, 20 nM serotonin was subsequently iontophoresed (Figure 4.5C). The time course and relative concentrations for the ejections of dopamine and serotonin are compared in Figure 4.5D and the resulting O_2 changes were compared to traces recorded before any application (Figure 4.5E). This experiment was repeated at 200 µm intervals along the dorsal-ventral tract through each brain region. At all locations, dopamine ejections did not affect O_2 in the SNr ($n = 5$ rats, $n = 7$ locations) and NAc ($n = 5$ rats, $n=6$ locations).

To confirm that the O_2 changes seen with iontophoresis were correlated to changes in CBF the above experiment was repeated in a slice preparation. Brain slices lack blood

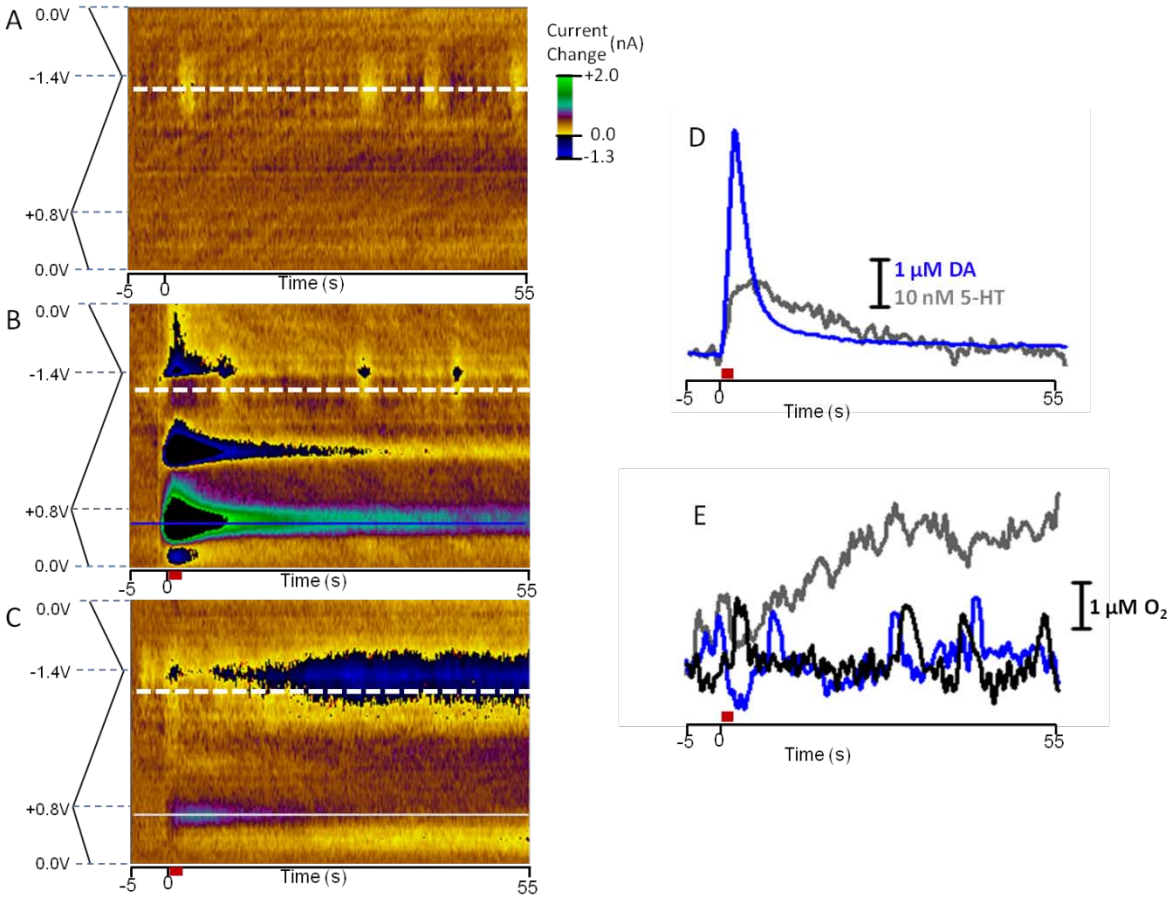

Figure 4.5. Ejection of dopamine and serotonin into the NAc in an anesthetized animal. Color plots showing 3 averaged 60 s files for each of the following at t = 0 s: A) no event B) 2 s ejection of 5 µM dopamine and C) 2 s ejection of 20 nM serotonin. The dashed line in each color plot indicates the potential at which O_2 changes were monitored and the solid lines in B and C show the potential at which dopamine and serotonin changes respectively were monitored. D) Applied concentration over time traces for the average concentration of dopamine (blue) and serotonin (grey) taken the potential indicated by the similarly colored solid lines in panels B and C respectively. E) O_2 responses occurring naturally (black), or induced by iontophoretic delivery of dopamine (blue) or serotonin (grey). Traces obtained at the potential for O_2 reduction (white dashed line in A-C). The red bars indicate the onset and duration of drug delivery.

flow (Iadecola et al., 2007) so any O_2 changes seen in the slice experiment could not be attributed to CBF. As Figure 4.6 shows, both dopamine and serotonin application caused no changes in O_2 in the SNr (n = 4 rats, n = 8 locations, 2 slices/rat) or NAc (n = 4 rats, n=8 locations, 2 slices/rat).

A 2 s application of serotonin at concentrations from 10 nM to 250 nM caused O_2 changes in 77% of locations in the NAc (n = 6 rats, n = 17 locations) and 87% of locations in the SNr (n = 10 rats, n = 38). While the majority of serotonin applications in the NAc (61%) and SNr (55%) increased O_2, the responses were critically dependent on serotonin concentration, and did not show monotonic responses at a single location. As the concentration of serotonin was increased, the response of O_2 abruptly changed (examples in Figure 4.7A recorded in the SNr). For measurements, in the NAc, there was no statistically significant correlation between the concentration of serotonin and resulting O_2 changes. In the SNr, 20% of locations evoked O_2 correlated with increasing serotonin (Figure 4.7B). In these locations, O_2 change varied from 11.5 ± 4.8 to 48.8 ± 20.8 nM O_2 per nanomolar serotonin for individual locations with an average rate of 21.9 ± 8.7 nM O_2 per nanomolar serotonin.

To ensure that all recorded O_2 changes were evoked by serotonin application; ejections were repeated at least twice at each location for each serotonin concentration. Replicate ejections caused the same O_2 change. These sites were also probed with dopamine ejections and had no effect as described above. Serotonin responses were not examined at sites with large, frequent endogenously occurring O_2.

DISCUSSION

These experiments reveal that FSCV at microelectrodes can provide recordings of local O_2 fluctuations and serotonin release. The recordings provide information from a

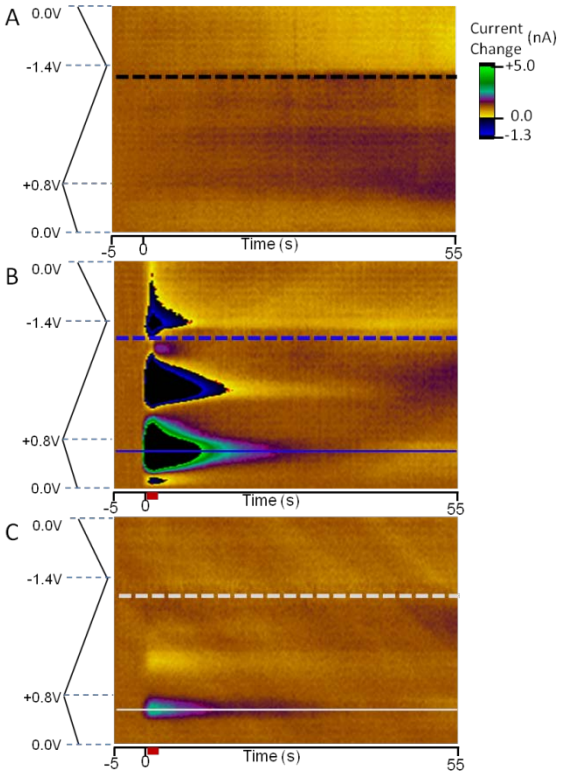

Figure 4.6. Ejection of dopamine and serotonin into the NAc in a slice preparation. Color plots showing 3 averaged 60 s files for each of the following at t = 0 s: A) no event B) 2 s ejection of 10 µM dopamine and C) 2 s ejection of 70 nM serotonin. The dashed line in each color plot indicates the potential at which O_2 changes were monitored and the solid lines in B and C show the potential at which dopamine (solid blue) and serotonin (solid grey) changes were monitored. The red bars indicate the onset and duration of drug delivery. No significant changes in O_2 were observed.

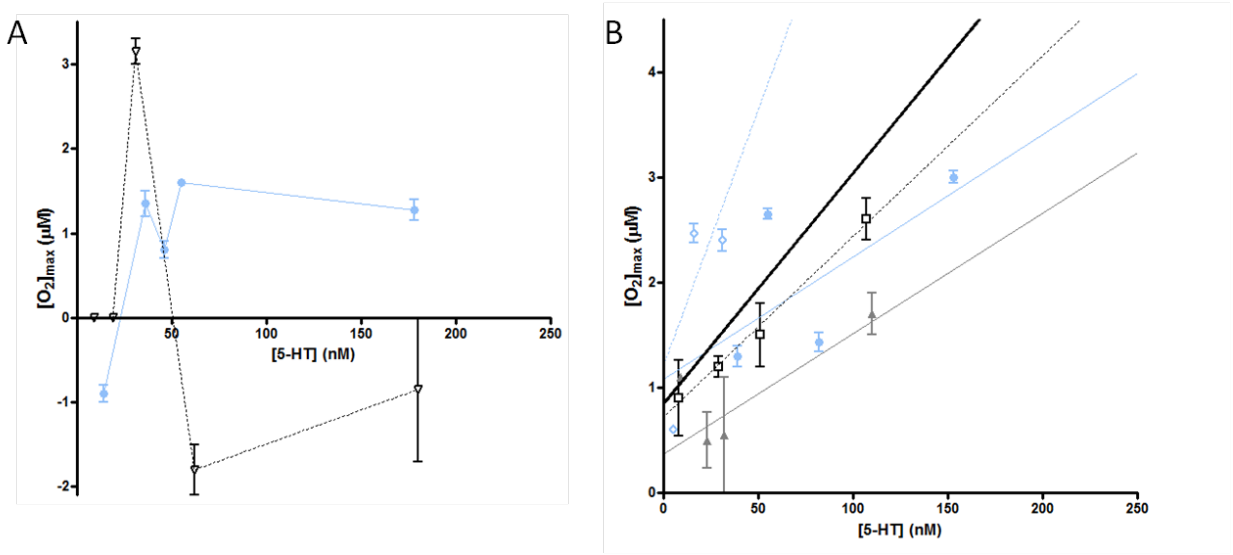

Figure 4.7. O_2 changes with local application of serotonin (5-HT) in the SNr. Two different response behaviors were seen in a single location to application of increasing concentrations of 5-HT: B) 80% of locations showed mixed changes in $[O_2]_{max}$ (increases and decreases) after iontophoretic application of 5-HT. Two example locations are shown, one trending positive (light blue, closed circles) and one negative (black line, open triangles). Lines are drawn through responses from each location (each in a separate animal) to demonstrate fluctuations. B) 20 % of locations showed only increases in $[O_2]_{max}$ in response to iontophoretic application of 5-HT. Each shape represents averaged ejections in a different animal and location. These increases happened at an average rate of 21.9 ± 8.7 nM O_2 per 1 nM serotonin applied (solid black line).

relatively small population of neurons deep within the brain and show that serotonin plays a dual vasoactive role in the brain. Through interaction with receptor and transporter proteins, serotonin released from nerve terminals causes increases in local O_2 in the SNr and NAc. Local application of exogenous serotonin predominantly increased O_2, but decreases or no change were also seen at the same location. This variability in O_2 responses is not a property of the measurements because the measurements are reproducible with the same dose at a common location. In the following sections, we postulate the physiological origins that underlie our observations.

Naturally occurring O_2 fluctuations in the brain

We have previously voltammetrically characterized electrically stimulated O_2 in the brain (Venton et al., 2003). Here, for the first time, we show that our method can detect rapid, naturally occurring O_2 fluctuations. It has previously been difficult to detect ambient O_2 perturbations because O_2 supply and demand is so closely maintained. However, our ultra-fast, sensitive FSCV method allows tiny homeostatic adjustments of O_2 to be captured. Recent results have revealed that natural changes in glucose occur on this time scale (Kiyatkin et al., 2012). This is important because FSCV can routinely be applied in freely moving, behaving animals (Cheer et al., 2006; Ariansen et al., 2012). Therefore future studies can probe behaviorally activated O_2.

Electrically induced O_2 increases

Biphasic O_2 responses induced by electrical stimulation were previously investigated in the dorsal striatum where we applied an increasing number of pulses to the MFB over 2 s and reported a linear increase in $[O_2]_{max}$ of Peak 1 and no change in $[O_2]_{max}$ of Peak 2 (Zimmerman et al., 1991). Here, we instead varied the duration over which 120 pulses were applied by increasing frequency. Increased frequencies result higher concentrations of

extracellular neurotransmitter. Consistent with this principle, as stimulation frequency increased, the maximum concentration of dopamine increased (Park et al., 2011), and this was accompanied by an increase in $[O_2]_{max}$ of Peak 1 in the NAc. Surprisingly, in the SNr, $[O_2]_{max}$ of Peak 1 decreases with stimulation frequency suggesting different regulatory mechanisms. Our own previous data showed that the primary a serotonin effect because MFB stimulation causes its release in the SNr with non-detectable contributions from dopamine (Hashemi et al., 2011). Additionally, we previously showed that dopamine release does not correspond to O_2 changes in the NAc (Venton et al., 2003), a finding confirmed here with dopamine receptor antagonists both in the NAc and in the SNr. Peak 2, an event previously shown to be adenosine mediated, was relatively insensitive to changing stimulus parameters.

Serotonin contributes to O_2 changes in both the NAc and SNr

While we cannot monitor serotonin in the NAc due to the overwhelming concentration of dopamine region, it is present in the NAc and could contribute to O_2 effects (Kuczenski et al., 1995). Instead of monitoring stimulated serotonin release in the NAc, we established with pharmacology that serotonin plays a role in Peak 1 in both the NAc and SNr. Methiothepin increased stimulated release of serotonin in the SNr and attenuated $[O_2]_{max}$ of Peak 1 in both the NAc and SNr when applied systemically. The local effects of iontophoretic application of methiothepin confirmed that the O_2 changes were mediated locally. Methiothepin, while a potent inhibitor of the serotonin autoreceptor (Martin et al., 1982) also antagonizes all serotonin receptor subtypes and has also been shown to antagonize α_1-adrengeric receptors (Wikberg-Matsson et al., 1998). Adrenergic receptors could play a role in the measured O_2 changes because norepinephrine is released by MFB stimulation (Park et al., 2011), and its receptors are located on large vessels and capillaries

on the surface of the brain and play a role in controlling vasoconstriction on large vessels on the surface of the brain (Hamel et al., 2006).

Iontophoretic application of serotonin directly into the SNr and NAc showed that serotonin has potent effects on local O_2, a distinction not possible with systemic administration of drugs. Dopamine altering agents produce no effects on O_2 when introduced iontophoretically. Similarly, iontophoresis of another electroactive molecule, 4-methylcatechol, did not change O_2 changes (data not shown). These findings show that the variation in O_2 following serotonin ejection is not an iontophoretic artifact.

Variability in O_2 with direct application of serotonin

O_2 responses to the regional release of neurotransmitters evoked by electrical stimulation of the MFB were consistent in both locations. However, local application of serotonin elicited a variety of O_2 changes in both the NAc and SNr. A dual response profile evoked with local serotonin application is not surprising given the spatially heterogeneous distribution of its receptors and transporters throughout the brain. While serotonin is known to constrict blood vessels directly via receptors (Monassier et al., 2010), a contrasting dilatory role has also been reported, mediated by β-receptors (Edvinsson et al., 1977). Additionally, serotonin receptors and transporters are found on astrocytes implying a role of serotonin in the indirect modulation of O_2 (Cohen et al., 1996).

Previous experiments used high concentrations of serotonin to consistently constrict large cerebral arteries (Lincoln, 1995). Here local application of low concentrations (<250 nM) of serotonin induce a variety of O_2 changes in all locations in the NAc and 80% of locations in the SNr. Generally, serotonin terminals do not form synapses and rely on volume transmission to allow serotonin to diffuse through the extracellular space to receptors on astrocytes and blood vessels (Fuxe et al., 2010; Cohen et al., 1995). When released globally with MFB stimulation serotonin activates a consistent receptor population.

In contrast, iontophoresis applies a concentrated local serotonin bolus that indiscriminately diffuses to the nearest receptors regardless of their proximity to serotonin terminals. As the concentration of ejected serotonin is increased, the size of the bolus is also increased, resulting in an increased number, type, and location of activated receptors (Belle et al., 2013). In the NAc O_2 responses are highly variable, however in the SNr, a large (20%) fraction of locations studied exhibited monotonic increases in O_2 with increasing serotonin concentration. Monotonic O_2 increases correlate with the greater percentage of serotonergic synapses in the SNr.

CONCLUSIONS

FSCV at carbon fiber microelectrodes provides a unique opportunity to monitor local functional O_2 changes that arise from changes in CBF in the brain. We show there are differences in O_2 induced systemically with electrical stimulation, or locally with iontophoresis. While the majority of direct serotonin applications resulted in increased O_2, variability in the O_2 response was also observed. This suggests that local application affects a subset of receptors whose spatial sphere increases with the increased serotonin concentration. This work demonstrates that serotonin plays a complex and multifaceted role in the functional regulation of O_2 in the brain. Serotonin is tightly regulated by efficient transport and metabolic processes. Its dual role as a neurotransmitter and vasoactive agent are consistent with tight synaptic regulation. Dysregulation of serotonin transmission is fatal, as demonstrated by serotonin syndrome.

REFERENCES

Ariansen JL, Heien ML, Hermans A, Phillips PE, Hernadi I, Bermudez MA, Schultz W, Wightman RM (2012) Monitoring extracellular pH, oxygen, and dopamine during reward delivery in the striatum of primates. Front Behav Neurosci 6:36.

Armstrong E (1982) A look at relative brain size in mammals. Neurosci Lett 34:101-104.

Attwell D, Buchan AM, Charpak S, Lauritzen M, Macvicar BA, Newman EA (2010) Glial and neuronal control of brain blood flow. Nature 468:232-243.

Bartlett K, Saka M, Jones M (2008) Polarograghic electrode measures of cerebral tissue oxygenation: implications for functional brain imaging. Sensors 8:7649-7670.

Bekar LK, Wei HS, Nedergaard M (2012) The locus coeruleus-norepinephrine network optimizes coupling of cerebral blood volume with oxygen demand. JCBFM 32:2135-2145.

Belle AM, Owesson-White C, Herr NR, Carelli RM, Wightman RM (2013) Controlled Iontophoresis Coupled with Fast-Scan Cyclic Voltammetry/Electrophysiology in Awake, Freely Moving Animals. ACS Chem Neurosci.

Bolger FB, McHugh SB, Bennett R, Li J, Ishiwari K, Francois J, Conway MW, Gilmour G, Bannerman DM, Fillenz M, Tricklebank M, Lowry JP (2011) Characterisation of carbon paste electrodes for real-time amperometric monitoring of brain tissue oxygen. J Neurosci Methods 195:135-142.

Bonvento G, Lacombe P, MacKenzie ET, Seylaz J (1991) Effects of dorsal raphe stimulation on cerebral glucose utilization in the anaesthetized rat. Brain Res 567:325-327.

Cheer JF, Wassum KM, Wightman RM (2006) Cannabinoid modulation of electrically evoked pH and oxygen transients in the nucleus accumbens of awake rats. J Neurochem 97:1145-1154.

Clark LC, Jr., Misrahy G, Fox RP (1958) Chronically implanted polarographic electrodes. J Appl Physiol 13:85-91.

Cohen Z, Ehret M, Maitre M, Hamel E (1995) Ultrastructural analysis of tryptophan hydroxylase immunoreactive nerve terminals in the rat cerebral cortex and hippocampus: their associations with local blood vessels. Neurosci 66:555-569.

Cohen Z, Bonvento G, Lacombe P, Hamel E (1996) Serotonin in the regulation of brain microcirculation. Prog Neurobiol 50:335-362.

Edvinsson L, Hardebo JE, MacKenzie ET, Stewart M (1977) Dual Action of Serotonin on Pial Arterioles *in situ* and the Effect of Propranolol on the Response. J Vasc Res 14:366-371.

Fuxe K, Dahlström AB, Jonsson G, Marcellino D, Guescini M, Dam M, Manger P, Agnati L (2010) The discovery of central monoamine neurons gave volume transmission to the wired brain. Prog Neurobiol 90:82-100.

Haas HL, Sergeeva OA, Selbach O (2008) Histamine in the nervous system. Physiol Rev 88:1183-1241.

Hamel E (2006) Perivascular nerves and the regulation of cerebrovascular tone. J Appl Physiol 100:1059-1064.

Harrison TC, Sigler A, Murphy TH (2009) Simple and cost-effective hardware and software for functional brain mapping using intrinsic optical signal imaging. J Neurosci Methods 182:211-218.

Hashemi P, Dankoski EC, Wood KM, Ambrose RE, Wightman RM (2011) In vivo electrochemical evidence for simultaneous 5-HT and histamine release in the rat substantia nigra pars reticulata following medial forebrain bundle stimulation. J Neurochem 118:749-759.

Herr NR, Daniel KB, Belle AM, Carelli RM, Wightman RM (2010) Probing presynaptic regulation of extracellular dopamine with iontophoresis. ACS Chem Neurosci 1:627-638.

Hosli E, Hosli L (1993) Receptors for Neurotransmitters on Astrocytes in the Mammalian Central-Nervous-System. Prog Neurobiol 40:477-506.

Iadecola C, Nedergaard M (2007) Glial regulation of the cerebral microvasculature. Nat Neurosci 10:1369-1376.

Inazu M, Takeda H, Ikoshi H, Sugiswa M, Uchida Y, Matsumiya T (2001) Pharmacological characterization and visualization of the glial serotonin transporter. Neurochem Intl 39:39-49.

Kiyatkin EA, Lenoir M (2012) Rapid fluctuations in extracellular brain glucose levels induced by natural arousing stimuli and intravenous cocaine: fueling the brain during neural activation. J Neurophysiol 108:1669-1684.

Kuczenski R, Segal D, Cho A, Melega W (1995) Hippocampus norepinephrine, caudate dopamine and serotonin, and behavioral responses to the stereoisomers of amphetamine and methamphetamine. J Neurosci 15:1308-1317.

Lauritzen M (2001) Relationship of spikes, synaptic activity, and local changes of cerebral blood flow. JCBFM 21:1367-1383.

Lincoln J (1995) Innervation of cerebral arteries by nerves containing 5-hydroxytryptamine and noradrenaline. Pharmacol Ther 68:473-501.

Martin GE, Williams M, Haubrich DR (1982) A pharmacological comparison of 6,7-dihydroxy-2-dimethylaminotetralin (TL-99) and N-n-propyl-3-(3-hydroxyphenyl)piperidine with (3-PPP) selected dopamine agonists. J Pharmacol Exp Ther 223:298-304.

Monassier L, Laplante MA, Ayadi T, Doly S, Maroteaux L (2010) Contribution of gene-modified mice and rats to our understanding of the cardiovascular pharmacology of serotonin. Pharmacol Ther 128:559-567.

Moukhles H, Bosler O, Bolam JP, Vallée A, Umbriaco D, Geffard M, Doucet G (1997) Quantitative and morphometric data indicate precise cellular interactions between serotonin terminals and postsynaptic targets in rat substantia nigra. Neurosci 76:1159-1171.

Park J, Takmakov P, Wightman RM (2011) In vivo comparison of norepinephrine and dopamine release in rat brain by simultaneous measurements with fast-scan cyclic voltammetry. J Neurochem 119:932-944.

Paulson PE, Robinson TE (1995) Amphetamine-induced time-dependent sensitization of dopamine neurotransmission in the dorsal and ventral striatum: A microdialysis study in behaving rats. Synapse 19:56-65.

Paxinos G, Watson C (2007) The Rat Brain in Stereotaxic Coordinates, 6 Edition. Amsterdam: Elsevier.

Peters JL, Miner LH, Michael AC, Sesack SR (2004) Ultrastructure at carbon fiber microelectrode implantation sites after acute voltammetric measurements in the striatum of anesthetized rats. J Neurosci Methods 137:9-23.

Rebec GV (1998) Real-time assessments of dopamine function during behavior: single-unit recording, iontophoresis, and fast-scan cyclic voltammetry in awake, unrestrained rats. Alcohol Clin Exp Res 22:32-40.

Richerson GB (2004) Serotonergic neurons as carbon dioxide sensors that maintain pH homeostasis. Nat Rev Neurosci 5:449-461.

Samanez-Larkin GR, Kuhnen CM, Yoo DJ, Knutson B (2010) Variability in nucleus accumbens activity mediates age-related suboptimal financial risk taking. J Neurosci 30:1426-1434.

Takmakov P, Zachek MK, Keithley RB, Bucher ES, McCarty GS, Wightman RM (2010) Characterization of local pH changes in brain using fast-scan cyclic voltammetry with carbon microelectrodes. Anal Chem 82:9892-9900.

Thompson JK, Peterson MR, Freeman RD (2003) Single-neuron activity and tissue oxygenation in the cerebral cortex. Science 299:1070-1072.

Venton BJ, Michael DJ, Wightman RM (2003) Correlation of local changes in extracellular oxygen and pH that accompany dopaminergic terminal activity in the rat caudate-putamen. J Neurochem 84:373-381.

Wikberg-Matsson A, Wikberg JE, Uhlen S (1998) Characterization of alpha1-adrenoceptor subtypes in the pig. Eur J Pharmacol 347:301-309.

Zimmerman JB, Wightman RM (1991) Simultaneous electrochemical measurements of oxygen and dopamine in vivo. Anal Chem 63:24-28.

Zimmerman JB, Kennedy RT, Wightman RM (1992) Evoked neuronal activity accompanied by transmitter release increases oxygen concentration in rat striatum in vivo but not in vitro. JCBFM 12:629-637.

Chapter 5

Controlled iontophoresis coupled with fast-scan cyclic voltammetry/ electrophysiology in awake, freely-moving animals

INTRODUCTION

The modulation of target neurons via neurotransmitter release is central to the regulation of an organism's behavior. Dopamine plays an extensive role in governing motivated behaviors and our groups have shown that its release coincides with learned associations for rewarding stimuli and drugs of abuse (Phillips et al., 2003; Robinson and Wightman, 2007; Owesson-White et al., 2009; Beyene et al., 2010; Day et al., 2010). Here, we describe a technique that is capable of monitoring extracellular dopamine release and postsynaptic cell activity in awake, behaving animals. At a single carbon-fiber electrode of micron dimensions, dopamine release is detected by fast-scan voltammetry and postsynaptic cell activity is monitored by single-unit recordings. The electrode is coupled to micropipettes that with the application of current locally deliver pharmacological agents to investigate the specific receptor(s) activated. This approach was first developed by Millar and coworkers who used fast-scan cyclic voltammetry and single-unit recording at a single carbon-fiber electrode (Millar et al., 1981). They combined these techniques with iontophoresis to compare the response of striatal medium spiny neurons (MSNs) to locally applied dopamine and endogenous dopamine released by electrical stimulation (Williams and Millar, 1990). Despite the utility of this approach, it has been used only rarely in behaving animals (Cheer et al., 2005; Cheer et al., 2007). Here we evaluate this approach in awake animals to probe the effects of dopamine in the nucleus accumbens (NAc), a

striatal subregion involved in reward processing, on evoked dopamine release and the electrical activity of MSNs.

Establishing the nature of dopamine responses proved difficult in early studies using iontophoresis combined with single-unit recording for several reasons (Grenhoff and Johnson, 1997). First, many of those recordings were in anesthetized animals and anesthesia is known to alter neuronal activity (Chiodo, 1988; Rebec, 1998). Second, the amount of drug delivered by iontophoresis was not quantifiable. Too little drug delivered results in a false negative whereas too much leads to nonspecific effects. Applied pump currents were commonly used to compare ejections (Pierce and Rebec, 1995; Kiyatkin and Rebec, 1996, 1999b), but the same pump current ejected different drug concentrations from barrel to barrel (Herr et al., 2008). To remedy this, we monitor the iontophoretic coejection of an electroactive molecule with the drug of interest from the same barrel. When the relative mobilities of the coejected substances are known, monitoring the concentration of the electroactive molecule with the carbon-fiber electrode provides an indirect measure of the relative concentration of the coejected nonelectroactive substance (Herr et al., 2008; Herr et al., 2010). Third, ionic and electrical artifacts can occur in iontophoresis. Since the chemical and physiological environments are monitored with the combined voltammetry/single-unit recording probe, these problems become apparent during the experiment and can be corrected. Finally, many studies were completed before the recognition of various subtypes of dopamine receptors and before investigators realized that dopamine receptors are coupled to second messenger systems that modulate the effects of classical neurotransmitters such as glutamate. In addition, MSNs have “up” and “down” states during which the cell’s response to dopamine may differ and are not discernible with single-unit recordings (O'Donnell, 2003; Nicola et al., 2004; Surmeier et al., 2007).

Interpretation of dopamine responses in prior studies were further complicated by the lack of understanding of the distribution of dopamine receptors. Dopamine neurons in the

NAc synapse onto dendrites and spines of MSNs (Yung et al., 1995). MSNs are GABAergic and comprise 95% of the cell bodies in this region (Chang and Kitai, 1985). Glutamatergic neurons that project from the cortex also form synapses on MSNs. Recent anatomical discoveries have shown that the predominant dopamine receptors, the D1 and D2 receptors, are segregated between two different MSN populations (Valjent et al., 2009; Gerfen and Surmeier, 2011). Early studies that focused exclusively on the dorsal striatum showed that some MSNs project axons to the output nuclei of the basal ganglia (substantia nigra and internal capsule of the globus pallidus [GPi]) and are termed the "direct pathway." Other MSNs project to the external capsule of the globus pallidus (GPe) and are termed the "indirect pathway" because they synapse with neurons that also project back to the output nuclei. Although this circuitry was originally characterized in the dorsal striatum, it is also found in the NAc (Ikemoto, 2007). In the NAc core 53% of MSN's comprise the direct pathway and have D1 receptors exclusively. Further, 41% of neurons in the NAc core comprise the indirect pathway and have D2 receptors exclusively. Thus, an estimated 6% of MSNs in the NAc have both D1 and D2 receptors.

In this work we describe the modifications made to the voltammetry/single-unit recording/iontophoresis probes for use in awake animals. These improvements enable examination of the distribution of dopamine receptor subtypes present on MSNs in the NAc. In addition, we have examined the immediate and prolonged cell firing effects of endogenous and exogenous dopamine and dopamine antagonists on the different types of MSNs. Our initial results agree with previously reported distributions of dopamine receptors on MSNs (Ikemoto, 2007), lending credence to our combined technique and supporting previous *in vitro* and indirect *in vivo* studies.

RESULTS & DISCUSSION

Voltammetry/single-unit/iontophoresis measurements

A diagram of the circuitry associated with these experiments is shown in Figure 5.1 (Takmakov et al., 2011a). In this work, the cyclic voltammograms were repeated at 5 Hz (once every 200 ms). With the scan rate employed (400 V/s), a single cyclic voltammogram is recorded in 8.5 ms. The total time with the current transducer connected (20 ms) includes 5.75 ms before the triangular wave to allow for dopamine adsorption and 5.75 ms after the triangular wave to allow the amplifiers to settle. For the remaining 180 ms between scans, the amplifier connected to the carbon-fiber electrode is switched (in <1µs) from a current transducer to a voltage follower to allow recording of unit activity. Iontophoresis occurs continuously during the switching between voltammetry and single-unit recordings via a separate circuit. The data from each measurement type is collected on separate computers along with time stamps allowing synchronization of the data to iontophoretic ejections or other events.

In prior work we used continuous iontophoresis over multiple minutes to affect cell firing frequency (Cheer et al., 2007). Shorter applications are advantageous because they restrict the drug to the local environment in which chemical changes and single-unit activity are measured. Here, we adopted two methods to monitor ejection effects. With the first method, we measured changes in cell firing or changes in electrically stimulated dopamine release shortly after a 15 s iontophoretic ejection. This approach has the advantage that the electrochemical signal arising from the ejected internal standard does not interfere with endogenous chemical measurements. With the second method we measured changes in cell firing during the 15 s ejections. This method was primarily used with electrophysiological recordings.

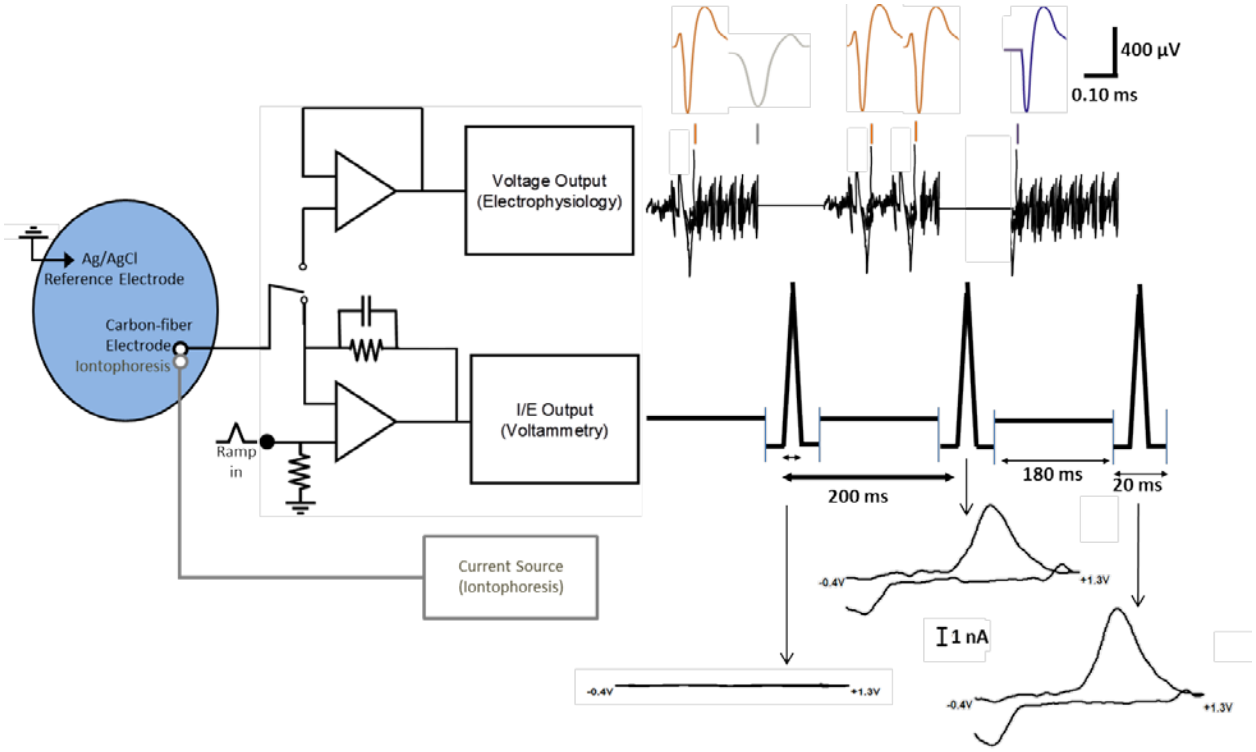

Figure 5.1. Diagram of the electronics and outputs for combined fast-scan cyclic voltammetry/electrophysiology. The same carbon-fiber electrode and reference electrode were used for both circuits and the reference electrode also served as ground for the iontophoresis circuit. The output of the carbon-fiber electrode was connected to a voltage follower to monitor cell firing (upper circuitry). Every 200 ms the carbon-fiber microelectrode was switched from the electrophysiology circuit to the lower voltammetry circuitry for 20 ms. In this position, the amplifier controlled the electrode potential and the current was monitored. The synchronized outputs for both circuits are shown to the right of the circuitry. When the lower circuit was completed, the electrode was held at -0.4 V then over 8.5 ms scanned from to +1.3 V and back to -0.4 V. The changes in current during each scan are indicated with arrows. During this time, there were no voltage changes seen in the electrophysiology (when circuit was open but program still recorded data). With the upper circuit connected, changes in voltage were monitored. The colored marks above the voltage read out indicate regions of the 180 ms that have been expanded above. Orange spikes are firing of the MSN of interest; purple spikes are firing that looks similar to the MSN of interest but are not included due to the horizontal portion at the start of the spike. The grey spike is an example of an excluded event.

Electrode Modifications

We have made several improvements to the construction of iontophoresis probes from the methods we previously described (Herr et al., 2008). First, we addressed the electrical coupling that sometimes occurred between the iontophoresis barrels and voltammetric barrel due to the inherent variability in the thickness of the glass pipettes. When the thickness of the glass between the adjacent barrels is thin or there are microfractures in the capillaries, electrical coupling between the iontophoresis barrels is likely to occur. Second, we improved the quality of the glass seal against the carbon fiber to help prevent large background currents during voltammetric recordings. Finally, we modified a commercially available manipulator to facilitate use of the probes in awake animals.

Reduced electrical coupling and improvements to the carbon fiber-glass seal were accomplished using a modified fabrication technique. First, a carbon fiber was inserted into in a single glass capillary, and this assembly was inserted into one barrel of a 4-barrel pre-fused glass assembly (Figure 5.2A). Heat-shrink tubing was applied to the ends of each multi-barrel glass capillary at the location where the chuck of the pipette puller was tightened onto the glass. Tack was placed at the lower end to prevent the inner glass capillary containing the carbon fiber from falling out. The assembly was pulled on a vertical micropipette puller in a two-step process that created two electrodes of the type shown in Figure 5.2B. The first pull elongated and narrowed the glass while the second pull formed the glass seal around the carbon fiber. The carbon fiber was then trimmed to have an exposed length of 50-75 µm. Before use, the heat-shrink was removed and an electrical connection to the carbon fiber was made with silver epoxy and an inserted silver wire. These procedures minimized the electrical coupling between the electrode and the iontophoresis barrels and resulted in improved carbon-glass seals.

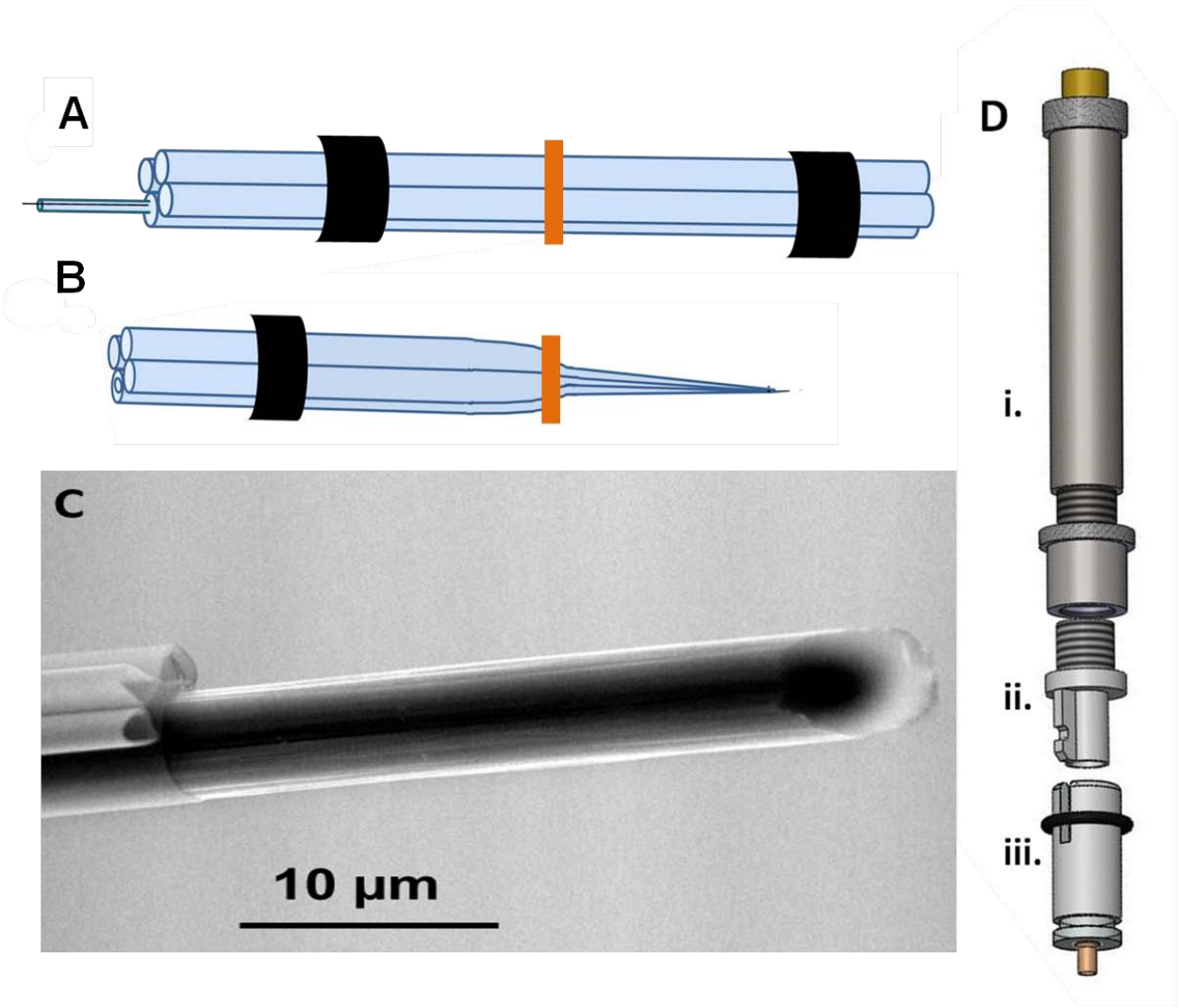

Figure 5.2. Modifications to probe construction and hardware for iontophoresis in freely moving animals. (A) 4-barrel pre-fused pipette ready for pulling with heat shrink on either end where the glass will contact the chucks of the puller. A smaller capillary containing a T-650 carbon fiber is loaded into one barrel. (B) One of the two electrodes created from the 2-pull electrode making technique. The vertical bar indicates the midpoint of the pipette before pulling. (C) Environmental scanning electron micrograph of the probe tip showing the glass iontophoresis barrels and carbon fiber. (D) Hardware used to attach and lower iontophoresis probe into the head of a freely-moving animal. (i) Commercially available Biela manipulator from Crist Instrument Co, (Part# 3-MMB-3D). (ii) Custom machined adapter that allows use of Biela manipulator with a guide cannula from Bioanalytical Systems, Inc. Fabricated by UNC Physics Machine Shop (Chapel Hill, NC). (iii) Commercially available guide cannula from Bioanalytical Systems.

To facilitate use of the voltammetry/single-unit/iontophoresis probe in awake animals and allow for lowering to a precise depth within the brain, the probe was inserted into a commercially available Biela micromanipulator (West and Woodward, 1984). The manipulator contains a metal tube (Figure 5.2Di) that has 4 inner grooves to hold a four-barrel pipette. This inner-most piece moves up and down as the two outer-most parts screw together. The Biela manipulators are designed for connection to the skull with a threaded guide cannula that requires a large diameter (1.5 mm) skull opening. The large hole tends to become blocked with blood clots, which increases the likelihood of pipette breakage. This problem is less frequent with the guide cannula that we use with single-barrel electrodes, which requires a 0.65 mm diameter hole (Figure 5.2Diii). This guide cannula uses a washer and groove system to attach the micromanipulator to the skull. The polyamide plastic cannula (2 mm long) extending beyond the hub was inserted in a hole drilled in the animal's brain and permanently affixed with dental cement during surgery. To mate the manipulator with the smaller diameter guide cannula, a custom-machined adapter was fabricated with threads to attach the adapter to the manipulator (UNC Physics Machine Shop, Chapel Hill, NC). The metal ridge of the adapter (Figure 5.2Dii) mates with the groove in the guide cannula and the washer on the cannula locks the pieces together. This allows for easy attachment on the animal's head under brief isofluorane anesthesia.

Modulation of dopamine evoked release by autoreceptors

Because stimulated release is modulated by D2 autoreceptors (Benoit-Marand et al., 2001; Wu et al., 2002), we used the improved probes to examine modulation of electrically stimulated (24 pulses, 60 Hz, 125 μA, repeated at 1 min intervals) dopamine release by agents active at D2 receptors in anesthetized animals. We first used microejections of dopamine (16 ± 1 μM) in an attempt to activate the D2 autoreceptor, but, there was no effect on electrically stimulated release (N = 4 animals) with three ejections carried out 5-7 minutes

apart. We then continuously delivered nomifensine (54 ± 2 μM), a dopamine transporter uptake inhibitor, while continuing stimulations at 1 min intervals. Under these conditions, the amplitude of electrically stimulated dopamine release was inhibited by 23 ± 6% ($p < 0.05$, paired t-test). This experiment is summarized in Figure 5.3. A lower concentration of dopamine (1.7 ± 0.5 μM) was also tested in 3 of the animals and showed the same inhibition of electrically stimulated dopamine release only during nomifensine application. By inhibiting uptake, nomifensine allowed dopamine to diffuse greater distances and remain in the extracellular space longer (Kelly and Wightman, 1987; Nicholson, 1995). Additionally, continuous inhibition of the transporter may alter autoreceptor function (Jones et al., 1999).

We also iontophoresed the D2 receptor antagonist raclopride in these same locations to ensure $[DA]_{max}$ responded as we previously showed to autoreceptor antagonism (Herr et al., 2010). The 15 s ejection consisted of 21 ± 11 μM raclopride and terminated 10 s before the stimulation. Ejections were repeated three times 7-10 minutes apart during which electrical stimulation occurred every 60 s. $[DA]_{max}$ was significantly increased by 151 ± 13% (N = 4 animals, $p < 0.05$, paired t-test). Even 70 s after the ejection, $[DA]_{max}$ was still increased by 132 ± 8% but returned to pre-raclopride levels 5 minutes after the conclusion of the raclopride ejection.

We also looked at the effect of autoreceptor antagonism on the amplitude of stimulated dopamine release in the NAc of awake, behaving animals. Awake animals were trained to press a lever that delivered an electrical stimulation to the VTA. Rats quickly learn this behavior termed intracranial self-stimulation (ICSS) that was discovered almost 60 years ago (Olds and Milner, 1954). To ensure dopamine release was not depleted by rapid lever pressing (Garris et al., 1999), a variable time out (VTO) paradigm, with lever availability 18-27s after a previous lever press was used. This VTO allowed for a 15 s drug ejection between presses as well.

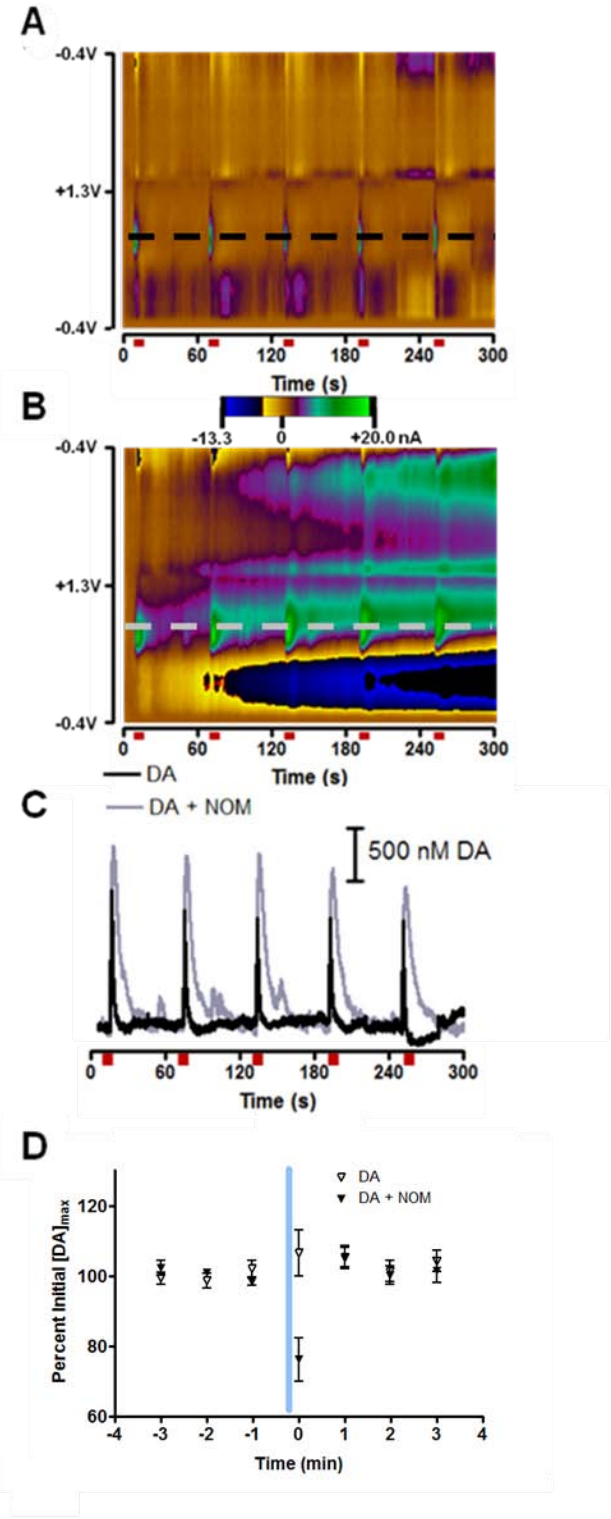

Figure 5.3. Effect of dopamine transporter on exogenous dopamine diffusion. (A) A two dimensional color plot where current is shown in false color on the potential vs. time axes is shown for current changes in the nucleus accumbens (NAc). The positive (green) currents are indicative of dopamine release. Anesthetized rats received a 24 pulse, 125 µA, 60 Hz electrical stimulation every 60 s and maximum dopamine concentration ($[DA]_{max}$) evoked with each stimulation recorded. Stimulations are indicated by red bars below the color plot. (B) In the same animal, the same experiment was carried out as in (A) but 54 ± 2 µM nomifensine (NOM) was constantly iontophoresed during the stimulations. (C) Dopamine (DA) oxidation currents as a function of time. Traces were taken from the potentials marked with dashed lines in panels A and B. (D) 15 s ejection of 16 ± 1 µM dopamine occurred at the vertical blue line and ended 10 s before electrical stimulation at t = 0 s. Open triangles indicate dopamine ejections while black triangles indicate dopamine ejections made during constant application of nomifensine. $[DA]_{max}$ evoked was greater in the presence of nomifensine but all data is presented as percent of pre-ejection $[DA]_{max}$ for each data set.

Data logging of $[DA]_{max}$ was initiated when it had reached a stable value (Owesson-White et al., 2008). After multiple lever-pressing trials, raclopride was ejected for 15 s and was terminated 3 s before the next lever extension. This caused an immediate increase in the maximum concentration of evoked dopamine that was observed after each lever press (Figure 5.4). This increase occurred at all locations tested, with raclopride increasing $[DA]_{max}$ at each location to 280 ± 130% the pre-raclopride $[DA]_{max}$ (N = 10 animals). This approach is an important improvement over systemic injections of dopamine receptor antagonists which can alter behavior and confound investigation of receptor mechanisms; localized iontophoretic application of raclopride allows modulation of receptors without affecting an animal's behavior (Ushijima et al., 1995).

Modulation of cell firing with D1 and D2 receptor antagonists

We did not attempt measurements of MSN unit activity in anesthetized animals because firing rates are so low under these conditions that investigators typically need to use glutamate to increase activity (White and Wang, 1986; Chiodo, 1988; Hu and Wang, 1988). In the awake rat, we examined the effects of the D1 antagonist, SCH 23390, the D2 antagonist, raclopride, and dopamine on MSN firing rate (dopamine results are described later). Representative histograms for responses to iontophoretic drug applications are shown in Figure 5.5, all measured at the same cell. Figure 5.5A shows a sample MSN waveform, shape of the waveform remained constant for all test conditions. In these experiments the same concentration of drug was applied to the cell for 15 s once every 60 s. The histograms are the average firing rate centered around these 30 drug applications with cell firing placed in 1.0 s bins. Drug was introduced for 15 s starting at t=0 s, and the average firing rate for 15 s before and after drug delivery also shown. The blue trace superimposed on each histogram is the average concentration of drug ejected over the time the histograms were collected. Figure 5.5B shows the average firing rate for the MSN over

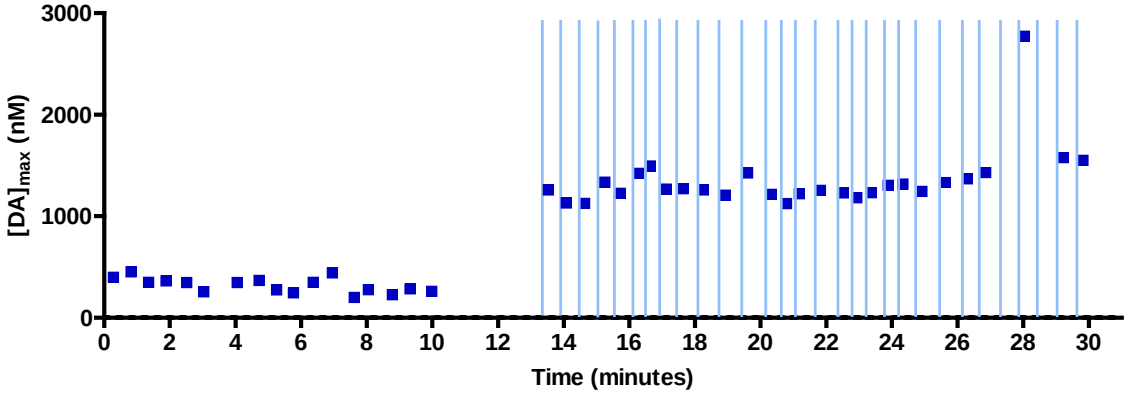

Figure 5.4. Consistent modulation of electrically evoked dopamine release with raclopride antagonism of the pre-synaptic D2 receptor during ICSS in a behaving rat. Stimulated release of dopamine occurred each time the animal pressed a lever, and the maximum amplitude was recorded as the maximum dopamine concentration ($[DA]_{max}$). The lever was made available to the animal once every 18-27 s. Raclopride iontophoretic ejections (15 s, 100 nM) began at 13 min. The ejections terminated 3 s before the lever became available (indicated by vertical lines).

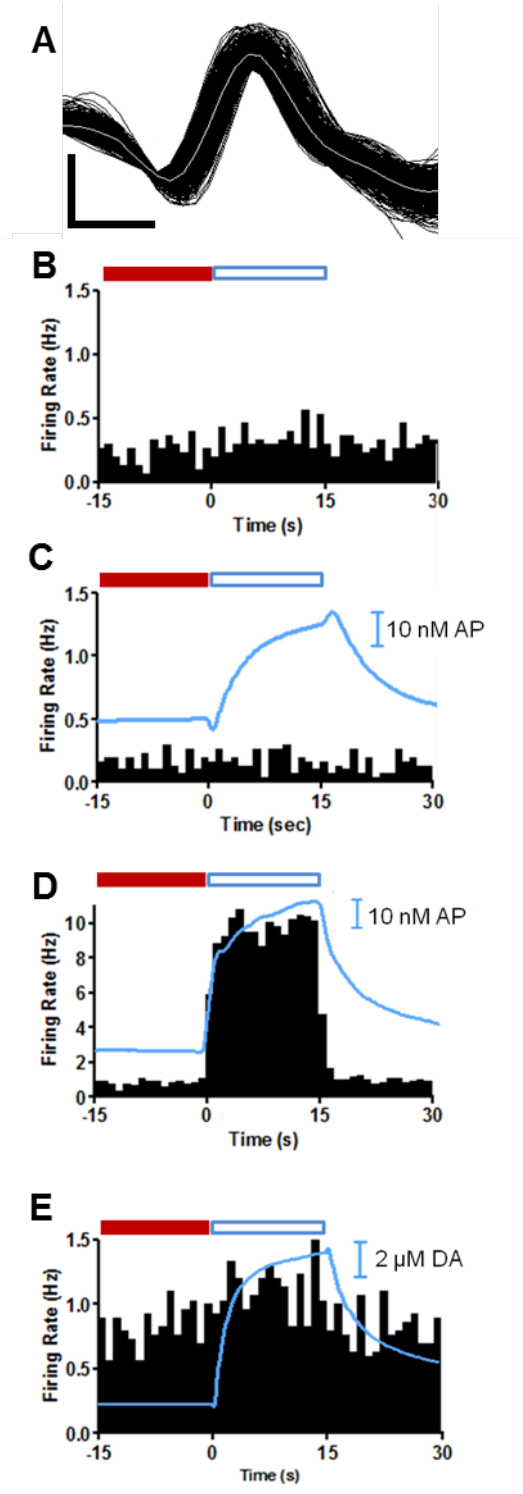

Figure 5.5. Immediate response of a single NAc MSN to iontophoretic application of dopamine receptor antagonists, SCH 23390 and raclopride, and dopamine in an awake animal. (A) Sample waveforms (150) shown in black with the average of the waveforms in grey for a NAc MSN collected in these experiments. The horizontal scale bar represents 0.3 ms and vertical scale bar is 300 µV. (B) MSN firing with no iontophoretic ejections. (C) MSN firing during iontophoresis of 23 nM SCH 23390 for 15 s starting at t = 0 s. (D) MSN firing with 40 nM raclopride iontophoresed for 15 s starting at t = 0 s. (E) MSN firing with 12 µM of dopamine iontophoresed for 15 s starting at t = 0 s. Histograms are the average of 30 consecutive trials (60 s duration) and each bar is the average frequency recorded during the indicated 1 s bin. All histograms were collected in the same location in the NAc of the same animal. The blue traces superimposed over histograms are the average concentration of acetaminophen (AP) (C, D) or dopamine (DA) (E) ejected during the 45 s window shown for all 30 trials. In panels C, D, and E iontophoretic drug delivery started at t = 0 s and ends at t = 15 s. Immediate changes in cell firing were determined by comparison of cell firing during a baseline period (-15 to 0 s, solid red bar) to the average firing rate during the ejection (blue boxed region, 0 to 15 s). A quotient that differed from the control by ± 0.5 was taken as an immediate change in cell firing rate.

30 trials during which no drug ejections occurred. This served to ensure that the cell was firing at a constant rate over a 30 minute period.

To evaluate the immediate effect of iontophoretic drug application on MSN firing rates we compared firing ratios. The firing ratio allows comparison of cell firing changes with respect to a defined baseline period. Here, baseline was defined as the average firing rate during the 15 s interval prior to each iontophoretic application (red bars in Figure 5.5). The firing ratio was determined by dividing the average firing rate during 30 consecutive drug ejections (the region shown by the blue open bars in Figure 5.5) by the baseline. The drug was deemed to have an immediate effect if it caused a change in firing ratio of 50% or more, a change never observed without drug application. At the location of the trials in Figure 5.5, the cell showed no immediate change in firing in response to application of 8.6 μM SCH 23390 (Figure 5.5C) whereas there was an abrupt increase in firing rate (and firing ratio) with the application of 14 μM raclopride (Figure 5.5D). This increase in cell firing is believed to be an excitation in response to blocking of the D2 mediate inhibition of MSN firing. The results from multiple units are summarized in Table 5.1 and show that only 12 out of the 30 cells that responded to one dopamine antagonist showed an immediate response.

The time required for a change in cell firing to occur is dependent on the time needed for ejected drug to diffuse to receptors on the MSN as well as the time delay between binding and the cascade of cell signaling that modulates MSN firing. Therefore, we also analyzed the data over a prolonged time scale. For prolonged firing ratios, baseline was taken as the average MSN firing rate during 30 trials with no drug ejections (red bar in Figure 5.6A). The prolonged firing ratio was then the average firing rate in the 15 s before and the 15 s after each of the 30 drug ejections (Figure 5.6B-E) divided the prolonged baseline. (The prolonged firing ratio purposely excludes cell firing during the 15 s period of drug ejection, which was used for determination of the immediate firing ratio.) Note that the

Table 5.1. Distribution of Prolonged and Immediate Responses of MSNs to Dopamine Antagonists

Type of Response	Number of Cells (%)	
	Raclopride	**SCH 23390**
Immediate		
Inhibitory	0 (0)	1 (3)
Excitatory	7 (23)	4 (13)
Prolonged		
Inhibitory	5 (17)	16 (53)
Excitatory	9 (30)	0 (0)

MSN = medium spiny neuron.
MSN responses are tabulated from n = 35 cells (units) from 19 rats. One cell did not respond to either drug and 4 cells responded to both. All 5 of these cells were excluded from the table.

-15 to 0 s period before an ejection, was also the time period 45 to 60 s after an ejection.

Representative firing patterns of another single unit are shown in Figure 5.6 along with the time periods used to calculate the prolonged firing ratio. Figure 5.6A shows the baseline for the prolonged measure (no drug was ejected), Figure 5.6B shows trials where SCH 23390 was ejected, and Figure 5.6C shows trials where raclopride was ejected. The immediate and prolonged firing ratios for each condition at this location are seen in Figure 5.6F. At this cell, SCH 23390 had a prolonged inhibition on cell firing but no immediate effect (Figure 5.6B, F). Raclopride had no significant effect on the firing ratio on either time scale in this MSN (Figure 5.6C, F). These responses classify this cell as a D1 responsive MSN.

This analysis was repeated for 35 cells, and the results are also summarized as the prolonged changes in Table 5.1. Out of 35 cells, all but one showed a prolonged response to receptor antagonists. While 4 units showed a prolonged response to both antagonists, 16 were only responsive to the D1 antagonist and 14 were only responsive to the D2 antagonist. This breakdown of cells is remarkably similar to the ratio of D1 and D2 cells established in the NAc by Girault and coworkers (Valjent et al., 2009). The 5 prolonged inhibitions evoked by raclopride all exhibited a robust, immediate excitation (like the example in Figure 5.5). The variability of the prolonged responses in MSNs that just responded to raclopride (5 out of 18 cells were inhibited while the remainder were excited) may have to do with the dual locations of D2 receptors (Usiello et al., 2000; Centonze et al., 2003; Centonze et al., 2004). Activation of D2 receptors on MSNs tends to inhibit cell firing whereas activation of D2 autoreceptors on dopamine neurons decreases dopamine release, minimizing this inhibition.

Modulation of cell firing with dopamine

At the same locations where the effects of raclopride and SCH 23390 were evaluated, we also evaluated the changes in firing rate induced by iontophoretically delivered dopamine and dopamine released by electrical stimulation (examples shown in Figure 5.6D and E). Iontophoresis of dopamine over a range of concentrations (10 nM to 20 μM) into the NAc caused no immediate change in MSN unit activity in 36 of the 40 cells tested (representative example in Figure 5.5E). However, only 18% of MSNs were unresponsive to either mode of dopamine delivery like the MSN in Figure 5.6. This means 82% of MSN showed a prolonged response to dopamine. In Table 5.2, the cells are grouped according to their prolonged responses to dopamine evoked by electrical stimulation or iontophoresis. Here, 75% of the MSNs monitored show the same type of prolonged response to both locally applied dopamine and electrical stimulation. Our result contrasts with that of Millar and coworkers who found electrically stimulated dopamine could excite or inhibit cell firing, but iontophoresed dopamine never excited cell firing (Williams and Millar, 1990). Our results also contrast with those of Gonon who found that transient electrical stimulations caused D1-mediated excitation of MSNs (Gonon, 1997). However, both of the prior reports were in anesthetized preparations. The changes in firing rate induced by increased extracellular dopamine concentration show that MSN firing rates can be modulated even in the absence of a coordinated surge of glutamate or GABA. For the 25% of the cells in which dopamine and the electrical stimulation do not cause the same firing rate changes, it may be that the stimulation releases other neurotransmitters besides dopamine that contribute to the observed effect. For example, GABA (Steffensen et al., 2001; Tritsch et al., 2012) and glutamate (Stuber et al., 2010) are released in conjunction with dopamine at some percentage of NAc synapses.

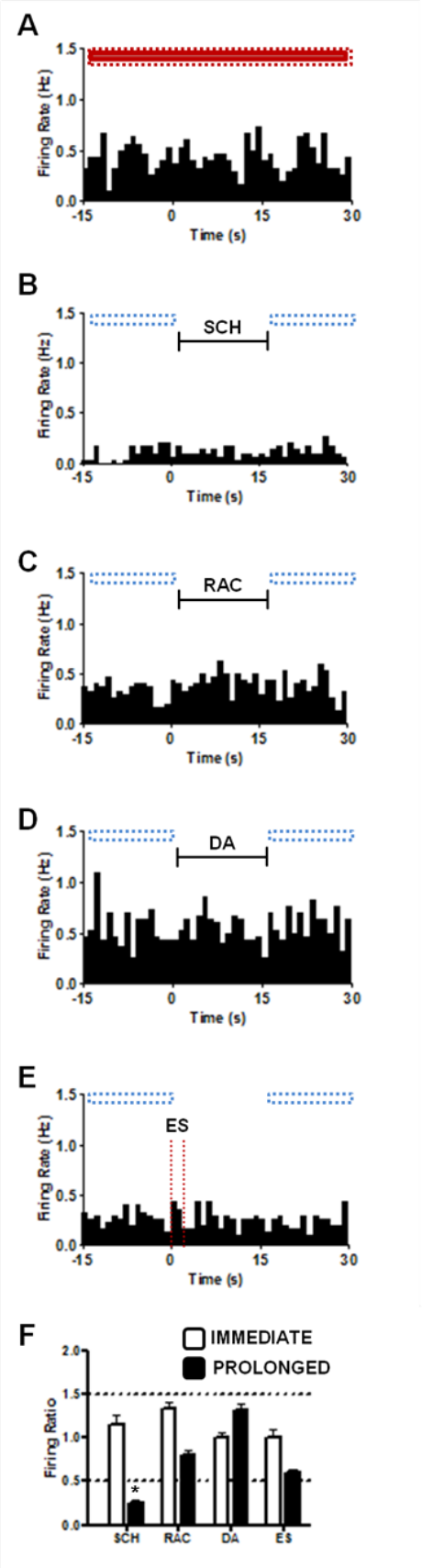

Figure 5.6. Firing rates measured at another MSN indicating the prolonged analysis method. Each histogram was constructed from the results of 30 trials for each condition, (A) Control where no event occurs (B) 15 s SCH 23390 (SCH) ejection, indicated by back bar (C) 15 s raclopride (RAC) ejection, indicated by back bar (D) 15s dopamine (DA) ejection, indicated by back bar (E) 60 Hz, 24 p electrical stimulation (ES), indicated with dashed vertical lines. The horizontal boxes above each histogram indicate where comparisons were made to determine prolonged changes in firing rate. Red indicates baseline (-15 to 30 s in panel A) and blue outlined boxes indicate regions compared to baseline (-15 to 0 s and 15 to 30 s). (F) Summary graph of immediate and prolonged changes in firing ratio from the single unit in panels A-E. Prolonged firing ratios were determined by dividing the average firing rate during periods with blue boxes over them in a panel by the red boxed region in panel A. Immediate firing ratios were determined as described in Figure 5.5 and the text. A quotient greater than 1.5 or less than 0.5 qualified as a change in frequency of cell firing. Horizontal dashed lines enclose the region where changes in firing ratio are less than 50% of the original signal. The only effect seen at this cell was a prolonged depression to SCH23390 as indicated by the * in Figure 5.6F.

Table 5.2. Medium Spiny Neuron Responses to Electrically Stimulated Dopamine and Locally Applied Dopamine

Type of Prolonged Response	Number of Cells (%)		
	ES & DA	DA only[a]	ES only[b]
Excitatory	12 (30)	5 (12)	3 (8)
Inhibitory	14 (35)	0 (0)	0 (0)
No response[c]	4 (10)	--	--
Mixed response[d]	2 (5)	--	--

DA = locally applied dopamine; ES = electrically stimulated release. MSN responses are tabulated from n = 40 cells (units) from 21 rats.

a Cells responded to DA only and had no response to ES.

b Cells responded to ES only and had no response to DA.

c Cells did not respond to ES or DA.

d Cells with a mixed response responded differently to ES vs DA. One of the cells had an inhibitory response to ES and an excitatory response to DA, while the other cell had an excitatory response to ES and an inhibitory response to DA.

CONCLUSIONS

Here we characterized an improved procedure to combine iontophoresis with voltammetric/single-unit recording that eliminates much of the unpredictability seen in earlier applications of this technique. We have established that drug ejections 15 s in duration can alter both chemical release and cell firing on different time scales. Previous experiments with iontophoresis showed that long ejections of SCH 23390 inhibited cell firing while both saline and raclopride caused no change in frequency of cell firing at the same cell (Cheer et al., 2007). These results are in agreement with the effects observed for a portion of MSNs tested here. However, for 40% of the MSNs we tested, raclopride significantly increased firing rate. We also see changes in firing rate after only 15 s of drug application (vs. several minutes). Additionally, we find that there are neurons that fire rapidly in response to raclopride and are unaffected by SCH 23390. This agrees with many prior experiments in anesthetized animals showing that dopamine may be both inhibitory and excitatory (White and Wang, 1986).

The results with raclopride on pre- and post-synaptic events differ in their onset time. Raclopride modulates dopamine release immediately and robustly after its application (Figure 5.3), but tends to be more effective in the prolonged modulation of MSN firing rate. These effects are mediated by two different isoforms of the D2 receptor that are found pre- and post-synaptically (Giros et al., 1989), and that exhibit similar pharmacology (Elsworth and Roth, 1997). They differ in that the post-synaptic D2 receptor has a longer third intracellular loop that requires the presence of $G_{\alpha i2}$ in order to inhibit adenylyl cyclase to the same extent that the pre-synaptic D2 receptor can with any $G_{\alpha i}$ protein (Montmayeur et al., 1993; Guiramand et al., 1995). Functionally, this means more binding may be required at post-synaptic receptors to elicit comparable adenylyl cylase inhibitions.

Our results provide an interpretable view of dopamine-receptor interactions because of our ability to monitor the applied drug concentration. In previous studies of dopamine's actions on MSNs, the dopamine concentration was not monitored directly but based on barrel concentrations and applied currents. The amount of dopamine applied in those experiments can be calculated to be approximately 50 times greater than the concentrations applied in this work (Kiyatkin and Rebec, 1999a). In studies where dopamine was exclusively inhibitory, the large concentrations of dopamine applied meant that uptake by the dopamine transporter could not make a significant change in the applied concentration.

Our initial iontophoresis experiments demonstrate at least three unique pharmacological responses that indicate the presence of different receptor populations on individual MSNs (Table 5.1) and these results are consistent with the current understanding of D1 and D2 receptors (Gerfen and Surmeier, 2011). This also supports the classic theory that the effect of dopamine on MSN intrinsic and synaptic channels will be excitatory at D1R MSNs and inhibitory at D2R MSNs (Albin et al., 1989; DeLong, 1990; Kreitzer and Berke, 2011). The prolonged effect of dopamine on MSN firing was independent of the receptor subtypes in animals not engaged in a specific task. The lack of immediate changes in cell firing with dopamine and, at some cells, with dopamine antagonists, may also be a result of physical distance between the tip of the iontophoresis barrel and receptors of interest.

We have presented a technique and methodology that is uniquely designed to determine not only what dopamine does in an awake animal under a number of conditions but that also has the potential to tease apart the role of other neurotransmitters in conjunction with dopamine. Characterization of this combined technique allows us to begin to differentiate between the function of MSNs based on their receptors. We can now investigate the argument that many different circuits within the NAc fire in different patterns specific to the aspect of goal-directed behavior for which they encode (Carelli and

Wightman, 2004). These initial data are very promising and show the potential of this combined technique to contribute to a broader understanding of neuronal signaling.

METHODS

Electrode Modifications

A capillary (Part # 624503, 0.60 mm o.d., 0.4 mm i.d., 4" long, A-M Systems, Sequim, WA) was loaded with a carbon fiber (T-650, Thornel, Amoco Corp., Greenville, SC) by aspiration and then loaded into one barrel of a pre-fused 4-barrel glass (Part # 4FB100-75-100, 1.0 mm OD, 0.75 mm ID, 100 mm L, 4-barrel omega dot tubing with filament, Friedrich and Dimmock, Millville, NJ). The 4-barrel glass with attached heat shrink (to prevent microfractures in the glass) was pulled on a vertical micropipette puller (Narashige, Tokyo, Japan). When pulling, it is important that the multi-barrel glass capillary is completely centered and straight within the coil of the puller. If the glass moved at all from the center of the coil when the chuck was rotated, the probe moved the same way when lowered into the brain. This greatly increased the likelihood of chipping or breaking the probe on the guide cannula or otherwise damaging the electrode seal.

In experiments described here, one iontophoresis barrel was filled with 5 mM dopamine dissolved in 5 mM NaCl. The additional two barrels were filled with either 5 mM of the D2-antagonist raclopride, 5 mM of the D1 antagonist SCH-23390, or 5 mM of the dopamine uptake inhibitor nomifensine. All drugs were dissolved in 5 mM NaCl containing 5 mM acetaminophen (Herr et al., 2010). Acetaminophen served as the electroactive marker that allowed ejections to be monitored and quantitated with FSCV the amount of electroinactive drug ejected was calculated indirectly from relative electrophoretic mobilities with respect to acetaminophen as done previously (Herr et al., 2008). Capillary electrophoresis and previously established methodology were used to determine that the relative electrophoretic mobilities of raclopride and SCH 23390 and nomifensine are 1.68,

1.90, and 2.24, respectively, compared to acetaminophen. Positive current was used to eject all drugs. The current was adjusted to during 'priming' (Herr et al., 2010) to deliver the appropriate micromolar concentration (detected with FSCV at the carbon-fiber) of dopamine or acetaminophen during a 15 s ejection. Between probes and from barrel to barrel, the amount of current required to achieve a desired concentration varied from 10 nA to 450 nA. During experiments, drug application was randomized.

After barrels were loaded with drug solutions, the probe was inserted connection side first, into the modified Biela manipulator and fastened to the manipulator with a strip of parafilm. A gold pin was then soldered to the end of the silver wire connected to the carbon-fiber electrode; separate silver wires were inserted into each pre-loaded iontophoresis barrel and all connections were secured to the probe with parafilm. A final check occurred to ensure that the electrode tip was centered and only moved straight up and down, not in circular motions, with turning of the manipulator.

For the range of acetaminophen concentrations used in these experiments, acetaminophen toxicity is considered unlikely. The first step in acetaminophen metabolism is its oxidation by cytochrome P450 2E1, which is predominately found in the liver (Lee et al., 1996). The enzyme is present in the brain but in smaller amounts (0.5 to 2% of liver concentration) (Upadhya et al., 2000; Hedlund et al., 2001) . This enzyme metabolizes acetaminophen into a toxic, reactive intermediate that under normal conditions is immediately broken down into a non-toxic compound by glutathione. The reactive intermediate can cause damage if there is an overexpression of the enzyme (normally due to chronic ethanol treatment) or if the glutathione concentration is low (Dong et al., 2000). Here, however, the plasma concentrations of acetaminophen were below 2 mM (the level for hepatoxicity) (Rumack and Peterson, 1978).

Cannula and Manipulator Modifications

Biela manipulators designed for 4-barrel glass were obtained commercially (Crist Instrument Co, Part# 3-MMB-3D). Before surgical implantation of the guide cannula, the custom made adapter was used to stretch the guide cannula (Bioanalytical Systems, West Lafayette, IL) slightly to ensure that the manipulator could easily slide into the cannula. Without this step, insertion of the manipulator into the cannula took more force which may stress the animal or electrode.

Combined Electrochemistry/Electrophysiology Instrumentation

A version of the custom build headstage (Takmakov et al., 2011a) with pins to connect the iontophoresis barrels to the current source was constructed by the UNC Electronics Facility. An iontophoretic constant current delivery system (NeuroPhore BH-2 System, Harvard Apparatus, Holliston, MA) was used for all iontophoretic ejections. All electrical signals were passed through an electrical swivel (Med-Associates, St. Albans, VT) that allowed the animal unrestrained movement within the behavioral chamber (Cheer et al., 2005).

Surgeries

For recovery surgeries, male Sprague-Dawley rats (225-350g; Charles River, Wilmington, MA) were anesthetized with isofluorane (rats were induced at 4% and maintained at 1.5 to 2.0% during surgery) and placed in a stereotaxic frame (Kopf, Tujunga, CA). Surgeries were performed as previously described (Cheer et al., 2004; Roitman et al., 2004; Owesson-White et al., 2008). The stretched guide cannula was implanted with the hub extending 2.5 mm into the brain directly above the NAc core (1.3 AP, 1.3 ML) or shell (1.7 AP, 0.8 ML, N = 4 animals and n = 8 cells) (Paxinos and Watson, 2007) and a bipolar stimulating electrode (Plastics One, Roanoke, VA) was lowered into the VTA (5.2 mm AP, 1.0 mm ML, and 7.8 mm DV). Coordinates for the bipolar stimulating electrode ensure

activation of the neurons projecting to the NAc (Ikemoto et al., 1997). A Ag/AgCl electrode was placed in the contralateral hemisphere to act as both reference for the carbon-fiber electrode and a ground for the iontophoresis barrels. All items were secured to the skull with stainless steel screws and dental cement. Rats inhaled 100% oxygen for a few minutes at the end of the surgery and were given ibuprofen (15mg/kg) to aid in their recovery.

Experiments with anesthetized animals were similar except for anesthesia used. Rats were anesthetized with 1.5 g/kg urethane (50% urethane/50% saline, w/w). Identical coordinates were used for implantation of electrodes. All procedures were approved by the Institutional Animal Care and Use Committee of the University of North Carolina.

Data acquisition

After at least a 3-day recovery period, rats were anesthetized in an isofluorane chamber (4% for ~2 minutes). Once lightly anesthetized, rats were removed from the chamber and the implanted cannula rinsed with 0.9% bacteriostatic saline (Animal Health International, Greely, CO). Isofluorane anesthetization lasts only for a few minutes and it has no measureable effect on an animal's ability to perform ICSS or on electrically stimulated $[DA]_{max}$ (Robinson and Carelli, 2008; Robinson et al., 2009). The loaded manipulator was then attached to the cannula, and the rat was placed into a behavioral chamber (Med Associates, St Albans, VT). Once in the chamber, the electrode and iontophoresis connections were made to the custom built headstage (Chemistry Department Electronics Facility, University of North Carolina, Chapel Hill).

The probe was slowly lowered to 6.0 mm in the brain (1 turn of the manipulator moved the electrode 0.4 mm). The electrode was then cycled for 15 min at 60 Hz from -0.4 to 1.3 V and back at 400 V/s (Heien et al., 2003) using custom-built software (Tarheel CV, LABVIEW, National Instruments, Austin, TX), and then cycled for 10 minutes with the same waveform applied at 10 Hz. The iontophoresis barrels were primed as described previously

(Herr et al., 2010) and pump currents to deliver the desired amount of each drug were determined at a depth of 6.2 mm into the brain. The electrode was then lowered into the NAc (7.0 mm DV) and the waveform was altered to allow FSCV and electrophysiological recordings (Owesson-White et al., 2008). Figure 5.1 shows the circuitry that allowed this switching to occur along with the simultaneous outputs from each circuit. A solid-state relay in the headstage alternated between the current amplifier for voltammetric scans and a voltage follower for unit recording. This complementary metal–oxide–semiconductor (CMOS) switch (MAX 319CSA) was chosen due to its low leakage, low charge transfer, low and matched input capacitance, low resistance (10 Ω), and fast (<1 μs) switching time (Takmakov et al., 2011b). The unit-recording interval had a 20-ms gap every 180 ms when voltammograms were collected. In the first 5 ms of this interval, a potential of -0.4 V was applied. The potential sweep for voltammetry remained the same as during the initial cycling.

Once in the NAc, data collection occurred at sites where a single unit was isolated. A single unit was classified as an MSN if baseline firing frequency was below 15 Hz and the waveform duration was less than 1.2 ms (Kish et al., 1999; Carelli and Ijames, 2001). After unit activity was monitored for 30 minutes to ensure a constant firing rate, drug was applied to the unit. The probe configuration allowed a maximum of three drugs applied per cell, so separate experiments were carried out prior to reported experiments where cell firing was monitored during ejections of 5 mM acetaminophen in 5 mM NaCl in rats during and prior to ICSS. Cell firing was not modulated by ejections of the neutral marker acetaminophen (N = 4 rats, n = 6 cells). Drugs were applied in a randomized order from cell to cell within an animal and from animal to animal to ensure affects were not due to the drug sequence. Positive currents were used for all ejections (10 to 450 nA). Multiple recording locations were used in a single animal provided they were at least 300 μm apart to ensure a new MSN was being recorded. Units recorded at carbon-fiber electrodes were amplified (x

1,000) and band-pass filtered (300–3,000 Hz). All signals were digitized with commercially available software (DIGITIZER, Plexon, Dallas, TX) and isolation of a unit was accomplished with principal component analysis in commercially available software (OFFLINE SORTER, Plexon, Dallas, TX). Med-Associates software (St. Albans, VT) controlled iontophoresis ejections and provided digital outputs synchronized to behavioral cues that were recorded in both Tarheel CV (fast-scan voltammetry) and Plexon (electrophysiology) records.

Data Analysis

Dopamine was identified from the background subtracted cyclic voltammograms (Michael et al., 1999). Current traces showed changes in dopamine concentration over time at the oxidation potential of dopamine from the cyclic voltammograms collected every 200 ms. Neural activity was characterized with raster displays and peri-event histograms (PEHs) across distinct time domains that bracketed the iontophoretic ejections. Each PEH was partitioned into three parts [baseline (15 s before the ejection), response (15 s during ejection), and recovery (15 s after the ejection)] to allow measurement of changes relative to the drug application. We use N to indicate number of animals and n to equal the number units.

REFERENCES

Albin RL, Young AB, Penney JB (1989) The functional anatomy of basal ganglia disorders. Trends in Neurosci 12:366-375.

Benoit-Marand M, Borrelli E, Gonon F (2001) Inhibition of dopamine release via presynaptic D2 receptors: time course and functional characteristics in vivo. J Neurosci 21:9134-9141.

Beyene M, Carelli RM, Wightman RM (2010) Cue-evoked dopamine release in the nucleus accumbens shell tracks reinforcer magnitude during intracranial self-stimulation. Neuroscience 169:1682-1688.

Carelli RM, Ijames SG (2001) Selective activation of accumbens neurons by cocaine-associated stimuli during a water/cocaine multiple schedule. Brain Research 907:156-161.

Carelli RM, Wightman RM (2004) Functional microcircuitry in the accumbens underlying drug addiction: insights from real-time signaling during behavior. Curr Opin Neurobiol 14:763-768.

Centonze D, Grande C, Usiello A, Gubellini P, Erbs E, Martín AB, Pisani A, Tognazzi N, Bernardi G, Moratalla R, Borrelli E, Calabresi P (2003) Receptor Subtypes Involved in the Presynaptic and Postsynaptic Actions of Dopamine on Striatal Interneurons. J Neurosci 23:6245-6254.

Centonze D, Gubellini P, Usiello A, Rossi S, Tscherter A, Bracci E, Erbs E, Tognazzi N, Bernardi G, Pisani A, Calabresi P, Borrelli E (2004) Differential contribution of dopamine D2S and D2L receptors in the modulation of glutamate and GABA transmission in the striatum. Neuroscience 129:157-166.

Chang HT, Kitai ST (1985) Projection neurons of the nucleus accumbens: an intracellular labeling study. Brain Res 347:112-116.

Cheer JF, Wassum KM, Heien ML, Phillips PE, Wightman RM (2004) Cannabinoids enhance subsecond dopamine release in the nucleus accumbens of awake rats. J Neurosci 24:4393-4400.

Cheer JF, Heien ML, Garris PA, Carelli RM, Wightman RM (2005) Simultaneous dopamine and single-unit recordings reveal accumbens GABAergic responses: implications for intracranial self-stimulation. Proc Natl Acad Sci USA 102:19150-19155.

Cheer JF, Aragona BJ, Heien ML, Seipel AT, Carelli RM, Wightman RM (2007) Coordinated accumbal dopamine release and neural activity drive goal-directed behavior. Neuron 54:237-244.

Chiodo LA (1988) Dopamine-containing neurons in the mammalian central nervous system: electrophysiology and pharmacology. NeurosciBiobehavRev 12:49-91.

Day JJ, Jones JL, Wightman RM, Carelli RM (2010) Phasic nucleus accumbens dopamine release encodes effort- and delay-related costs. Biol Psychiatry 68:306-309.

DeLong MR (1990) Primate models of movement disorders of basal ganglia origin. Trends in Neurosci 13:281-285.

Dong H, Haining RL, Thummel KE, Rettie AE, Nelson SD (2000) Involvement of human cytochrome P450 2D6 in the bioactivation of acetaminophen. Drug Metab Dispos 28:1397-1400.

Elsworth JD, Roth RH (1997) Dopamine Synthesis, Uptake, Metabolism, and Receptors: Relevance to Gene Therapy of Parkinson's Disease. Exp Neurol 144:4-9.

Garris PA, Kilpatrick M, Bunin MA, Michael D, Walker QD, Wightman RM (1999) Dissociation of dopamine release in the nucleus accumbens from intracranial self-stimulation. Nature 398:67-69.

Gerfen CR, Surmeier DJ (2011) Modulation of striatal projection systems by dopamine. Annu Rev Neurosci 34:441-466.

Giros B, Sokoloff P, Martres M-P, Riou J-F, Emorine LJ, Schwartz J-C (1989) Alternative splicing directs the expression of two D_2 dopamine receptor isoforms. Nature 342:923-926.

Gonon F (1997) Prolonged and extrasynaptic excitatory action of dopamine mediated by D1 receptors in the rat striatum in vivo. JNeurosci 17:5972-5978.

Grenhoff J, Johnson SW (1997) Electrophysiological Effects of Dopamine Receptor Stimulation. In: The Dopamine Receptors, 1st Edition (Neve KA, Neve RL, eds). Totowa, NJ: Humana Press.

Guiramand J, Montmayeur J-P, Ceraline J, Bhatia M, Borrelli E (1995) Alternative Splicing of the Dopamine D2 Receptor Directs Specificity of Coupling to G-proteins. J Biol Chem 270:7354-7358.

Hedlund E, Gustafsson JA, Warner M (2001) Cytochrome P450 in the brain; a review. Curr Drug Metab 2:245-263.

Heien ML, Phillips PE, Stuber GD, Seipel AT, Wightman RM (2003) Overoxidation of carbon-fiber microelectrodes enhances dopamine adsorption and increases sensitivity. Analyst 128:1413-1419.

Herr NR, Kile BM, Carelli RM, Wightman RM (2008) Electroosmotic flow and its contribution to iontophoretic delivery. Anal Chem 80:8635-8641.

Herr NR, Daniel KB, Belle AM, Carelli RM, Wightman RM (2010) Probing presynaptic regulation of extracellular dopamine with iontophoresis. ACS Chem Neurosci 1:627-638.

Hu X-T, Wang RY (1988) Comparison of effects of D-1 and D-2 dopamine receptor agonists on neurons in the rat caudate putamen: An electrophysiological study. JNeurosci 8:4340-4348.

Ikemoto S (2007) Dopamine reward circuitry: Two projection systems from the ventral midbrain to the nucleus accumbens-olfactory tubercle complex. Brain Res Rev 56:27-78.

Ikemoto S, Glazier BS, Murphy JM, McBride WJ (1997) Role of dopamine D1 and D2 receptors in the nucleus accumbens in mediating reward. JNeurosci 17:8580-8587.

Jones SR, Gainetdinov RR, Hu XT, Cooper DC, Wightman RM, White FJ, Caron MG (1999) Loss of autoreceptor functions in mice lacking the dopamine transporter. Nat Neurosci 2:649-655.

Kelly RS, Wightman RM (1987) Detection of dopamine overflow and diffusion with voltammetry in slices of rat brain. Brain Res 423:79-87.

Kish LJ, Palmer MR, Gerhardt GA (1999) Multiple single-unit recordings in the striatum of freely moving animals: effects of apomorphine and d-amphetamine in normal and unilateral 6-hydroxydopamine-lesioned rats. Brain Research 833:58-70.

Kiyatkin EA, Rebec GV (1996) Dopaminergic modulation of glutamate-induced excitations of neurons in the neostriatum and nucleus accumbens of awake, unrestrained rats. Journal of neurophysiology 75:142-153.

Kiyatkin EA, Rebec GV (1999a) Striatal neuronal activity and responsiveness to dopamine and glutamate after selective blockade of D1 and d2 dopamine receptors in freely moving rats. JNeurosci 19:3594-3609.

Kiyatkin EA, Rebec GV (1999b) Modulation of striatal neuronal activity by glutamate and GABA: iontophoresis in awake, unrestrained rats. Brain research 822:88-106.

Kreitzer AC, Berke JD (2011) Investigating striatal function through cell-type-specific manipulations. Neuroscience 198:19-26.

Lee SST, Buters JTM, Pineau T, Fernandez-Salguero P, Gonzalez FJ (1996) Role of CYP2E1 in the hepatotoxicity of acetaminophen. J Biol Chem 271:12063-12067.

Michael DJ, Joseph JD, Kilpatrick MR, Travis ER, Wightman RM (1999) Improving data acquisition for fast-scan cyclic voltammetry. Anal Chem 71:3941-3947.

Millar J, Armstrong-James M, Kruk ZL (1981) Polarographic assay of iontophoretically applied dopamine and low-noise unit recording using a multibarrel carbon fibre microelectrode. Brain Res 205:419-424.

Montmayeur JP, Guiramand J, Borrelli E (1993) Preferential coupling between dopamine D2 receptors and G-proteins. Mol Endocrinol 7:161-170.

Nicholson C (1995) Interaction between diffusion and Michaelis-Menten uptake of dopamine after iontophoresis in striatum. BiophysJ 68:1699-1715.

Nicola SM, Hopf FW, Hjelmstad GO (2004) Contrast enhancement: a physiological effect of striatal dopamine? Cell Tissue Res 318:93-106.

O'Donnell P (2003) Dopamine gating of forebrain neural ensembles. Eur J Neurosci 17:429-435.

Olds J, Milner P (1954) Positive reinforcement produced by electrical stimulation of septal area and other regions of rat brain. J Comp Physiol Psychol 47:419-427.

Owesson-White CA, Cheer JF, Beyene M, Carelli RM, Wightman RM (2008) Dynamic changes in accumbens dopamine correlate with learning during intracranial self-stimulation. Proc Natl Acad Sci USA 105:11957-11962.

Owesson-White CA, Ariansen J, Stuber GD, Cleaveland NA, Cheer JF, Wightman RM, Carelli RM (2009) Neural encoding of cocaine-seeking behavior is coincident with phasic dopamine release in the accumbens core and shell. Eur J Neurosci 30:1117-1127.

Paxinos G, Watson C (2007) The Rat Brain in Stereotaxic Coordinates, 6 Edition. Amsterdam: Elsevier.

Phillips PE, Stuber GD, Heien ML, Wightman RM, Carelli RM (2003) Subsecond dopamine release promotes cocaine seeking. Nature 422:614-618.

Pierce RC, Rebec GV (1995) Iontophoresis in the neostriatum of awake, unrestrained rats: differential effects of dopamine, glutamate and ascorbate on motor- and nonmotor-related neurons. Neuroscience 67:313-324.

Rebec GV (1998) Real-time assessments of dopamine function during behavior: single-unit recording, iontophoresis, and fast-scan cyclic voltammetry in awake, unrestrained rats. Alcohol ClinExpRes 22:32-40.

Robinson DL, Wightman RM (2007) Rapid dopamine release in freely moving rats. In: Electrochemical Methods for Neuroscience (Michael AC, Borland LM, eds), pp 17-36. Boca Raton, FL: CRC Press.

Robinson DL, Carelli RM (2008) Distinct subsets of nucleus accumbens neurons encode operant responding for ethanol versus water. Eur J Neurosci 28:1887-1894.

Robinson DL, Howard EC, McConnell S, Gonzales RA, Wightman RM (2009) Disparity between tonic and phasic ethanol-induced dopamine increases in the nucleus accumbens of rats. Alcohol Clin Exp Res 33:1187-1196.

Roitman MF, Stuber GD, Phillips PE, Wightman RM, Carelli RM (2004) Dopamine operates as a subsecond modulator of food seeking. J Neurosci 24:1265-1271.

Rumack BH, Peterson RG (1978) Acetaminophen overdose: Incidence, diagnosis and management in 416 patients. Pediatrics:898-905.

Steffensen SC, Lee R, Stobbs SH, Henriksen SJ (2001) Responses of ventral tegmental area GABA neurons to brain stimulation reward. Brain Res 906:190-197.

Stuber GD, Hnasko TS, Britt JP, Edwards RH, Bonci A (2010) Dopaminergic terminals in the nucleus accumbens but not the dorsal striatum corelease glutamate. J Neurosci 30:8229-8223.

Surmeier DJ, Ding J, Day M, Wang Z, Shen W (2007) D1 and D2 dopamine-receptor modulation of striatal glutamatergic signaling in striatal medium spiny neurons. Trends Neurosci 30:228-235.

Takmakov P, McKinney CJ, Carelli RM, Wightman RM (2011a) Instrumentation for fast-scan cyclic voltammetry combined with electrophysiology for behavioral experiments in freely moving animals. Rev Sci Instrum 82:074302.074301-074302.074306.

Takmakov P, McKinney CJ, Carelli RM, Wightman RM (2011b) Instrumentation for fast-scan cyclic voltammetry combined with electrophysiology for behavioral experiments in freely moving animals. Review of Scientific Instruments 82:074302.

Tritsch NX, Ding JB, Sabatini BL (2012) Dopaminergic neurons inhibit striatal output through non-canonical release of GABA. Nature 490:262-266.

Upadhya S, Tirumalai P, Boyd M, Mori T, Ravindranath V (2000) Cytochrome P4502E (CYP2E) in brain: constitutive expression, induction by ethanol and localization by fluorescence in situ hybridization. Arch Biochem Biophys 373:23-34.

Ushijima I, Carino MA, Horita A (1995) Involvement of D1 and D2 dopamine systems in the behavioral effects of cocaine in rats. Pharmacol Biochem Behav 52:737-741.

Usiello A, Baik J-H, Rouge-Pont F, Picetti R, Dierich A, LeMeur M, Piazza PV, Borrelli E (2000) Distinct functions of the two isoforms of dopamine D2 receptors. Nature 408:199-203.

Valjent E, Bertran-Gonzalez J, Herve D, Fisone G, Girault JA (2009) Looking BAC at striatal signaling: cell-specific analysis in new transgenic mice. Trends Neurosci 32:538-547.

West MO, Woodward DJ (1984) A technique for microiontophoretic study of single neurons in the freely moving rat. J Neurocsci Meth 11:179-185.

White FJ, Wang RY (1986) Electrophysiological evidence for the existence of both D-1 and D-2 dopamine receptors in the rat nucleus accumbens. J Neurosci 6:274-280.

Williams GV, Millar J (1990) Differential actions of endogenous and iontophoretic dopamine in rat striatum. EurJNeurosci 2:658-661.

Wu Q, Reith ME, Walker QD, Kuhn CM, Carroll FI, Garris PA (2002) Concurrent autoreceptor-mediated control of dopamine release and uptake during neurotransmission: an in vivo voltammetric study. J Neurosci 22:6272-6281.

Yung KK, Bolam JP, Smith AD, Hersch SM, Ciliax BJ, Levey AI (1995) Immunocytochemical localization of D1 and D2 dopamine receptors in the basal ganglia of the rat: light and electron microscopy. Neuroscience 65:709-730.

Chapter 6

Role of medium spiny neurons in intracranial self-stimulation

INTRODUCTION

Dopaminergic neurons exhibit a transient increase in firing rate (or bursting) in response to unexpected rewards and cues that predict reward (Schultz et al., 1997). These changes in firing rate are accompanied by transient increases in extracellular dopamine in terminal regions revealed by *in vivo* voltammetric recordings (Robinson et al., 2002; Phillips et al., 2003; Day et al., 2007; Sombers et al., 2009). Consistent with the mediation of reward, animals will self-administer dopaminergic agonists directly into brain regions that contain dopaminergic terminals (Ikemoto, 2007). Dopamine deficient mice will starve even though food is readily available indicating that dopamine is associated with the reward aspects of feeding behavior (Szczypka et al., 1999; Szczypka et al., 2001). Furthermore, genetically altered mice, whose dopaminergic neurons lack the ability to burst fire, show impaired ability to learn associations between cues and a reward (Zweifel et al., 2009). Taken together, these data indicate that dopamine is a neuromodulator that exerts profound effects on reward-based behaviors (Wise, 2004).

The dopaminergic neurons associated with reward are termed mesolimbic projections and extend from the ventral tegmental area (VTA) to several regions including the nucleus accumbens (NAc) core (Ikemoto, 2007). In the NAc, dopaminergic neurons synapse on the necks of medium spiny neurons (MSNs), GABAergic neurons, that also receive glutamatergic inputs from the cortical and thalamic regions of the brain (Hersch et al., 1995). Three dopamine receptor populations are expressed on MSNs (Gerfen and

Surmeier, 2011): in the NAc the majority express either D1- or D2-like dopamine receptors exclusively, while a minority (5-10 %) of MSNs have both D1- and D2-like dopamine receptors (Valjent et al., 2009). The family of D1-like receptors (D1Rs) include D_1 and D_5 dopamine receptors while the D2-like family of dopamine receptors (D2Rs) includes D_2, D_3, and D_4 receptor subtypes (Neve et al., 2004). The D1-like MSN's are referred to as the direct pathway because they project back to dopamine cell bodies where they provide an inhibitory input (Gerfen and Surmeier, 2011). In contrast, MSN containing the D2-family of receptors comprise the indirect pathway that projects to the ventral pallidum (for a review see (Sesack and Grace, 2010)). Cholinergic neurons in the ventral pallidum project back to dopamine cell bodies via the subthalamic nucleus and thus provide an excitatory influence as a consequence of disinhibition (Gerfen and Surmeier, 2011).

The modulation by dopamine of glutamatergic neurotransmission at MSNs has been the subject of considerable investigation. The prevalent view is that activation of D2Rs on MSNs (Gerfen and Surmeier, 2011) or on the glutamatergic corticostriatal terminals (Wang and Pickel, 2002) suppress excitation of MSNs. Consistent with this, glutamatergic transmission in the striatum is facilitated in D2R-deficient mice (Cepeda et al., 2001). Activation of D1Rs in the striatum potentiates NMDA receptor function (Gerfen and Surmeier, 2011). Here, we investigated the role of dopaminergic receptors in a reward based behavior, intracranial self-stimulation (ICSS). In ICSS, an animal depresses a lever to deliver an electrical stimulation to select regions of the brain. This paradigm has been characterized extensively and is often used to investigate brain reward (Wise, 2002). We used a single carbon-fiber electrode that is concurrently used to measure cyclic voltammograms, providing measurements of local dopamine concentrations, and single-unit activity arising from adjacent neurons (Millar and Barnett, 1988; Takmakov et al., 2011). When iontophoretic barrels attached to the carbon-fiber electrode are filled with specific receptor agonists or antagonists, the roles of dopamine receptor subtypes on MSNs can be

determined in behaving animals (Belle et al., 2013). In prior work we demonstrated that this approach can be used to identify D1-like and D2-like MSNs in the NAc, and that their incidence is similar to that obtained by traditional anatomical characterization. Here we show that specific cue-mediated changes in neural activity are associated either with D2- or D1-like receptors.

METHODS

Electrode Preparation

Iontophoresis probes were fabricated, filled with drugs, and loaded into a modified Biela manipulator as previously described (Belle et al., 2013). Combinations of the following drugs were loaded into the three iontophoresis barrels of the probe: 5 mM raclopride, 5 mM SCH 23390, 5 mM SKF 38393, or 5 mM quinpirole. All drugs were dissolved in 5 mM acetaminophen containing 5 mM NaCl, a vehicle shown to have no effect on stimulated dopamine release or MSN cell firing (Herr et al., 2010; Belle et al., 2013). Acetaminophen serves as an electroactive marker to indicate the performance of the iontophoretic barrels. The electrophoretic mobility of each compound relative to acetaminophen was used to determine ejected drug concentrations (Herr et al., 2010). Positive current was used to eject all drugs. Between probes and from barrel to barrel, the amount of current required to achieve a desired concentration varied from 10 nA to 450 nA. During experiments, the order of drug application was randomized.

Combined Electrochemistry/Electrophysiology Instrumentation

A custom built headstage (Takmakov et al., 2011) with pins to connect the iontophoresis barrels to the current source was constructed by the UNC Electronics Facility. An iontophoretic constant current delivery system (NeuroPhore BH-2 System, Harvard

Apparatus, Holliston, MA) was used for iontophoretic ejections. Electrical signals were passed through an electrical swivel (Med-Associates, St. Albans, VT) that allowed the animal unrestrained movement within the behavioral chamber (Cheer et al., 2005).

Surgeries

For recovery surgeries, male Sprague-Dawley rats (225-350g; Charles River, Wilmington, MA) were anesthetized with isoflurane (induced with 4% and maintained at 1.5 to 2.0% during surgery) and placed in a stereotaxic frame (Kopf, Tujunga, CA). Surgeries were performed as previously described (Owesson-White et al., 2008). The guide cannula was implanted with the hub extending 2.5 mm into the brain directly above the NAc core (1.3 AP, 1.3 ML) or shell (1.7 AP, 0.8 ML) (Paxinos and Watson, 2007) and a bipolar stimulating electrode (Plastics One, Roanoke, VA) was lowered into the VTA (5.2 mm AP, 1.0 mm ML, and 7.8 mm DV). A Ag/AgCl electrode in the contralateral hemisphere served as both the reference electrode for electrochemistry/electrophysiology and the return for the iontophoresis barrels. Implanted items were secured to the skull with stainless steel screws and dental cement. Rats inhaled 100% oxygen for a few minutes at the end of the surgery and were given ibuprofen orally (15 mg/kg) to aid in recovery. All procedures were approved by the Institutional Animal Care and Use Committee of the University of North Carolina.

Training

After at least 3 days of recovery, rats were trained on a fixed-ratio (FR-1) schedule, with the lever continuously presented. Upon lever press, a stimulus train (24 biphasic pulses, 60 Hz, 125-150 μA, 2 ms per phase) was delivered to the stimulating electrode on average 200 ms later. Once rats learned this association, they were trained to lever press on a variable-time out (VTO) schedule, FR-1. For the first 50 trials the audiovisual cue was

presented at the same time as the lever, with a VTO of 9-16 s between trials. For trials 51-200, the audiovisual cue preceded lever availability by 2 s (Figure 6.1A). The animal then pressed 50 times on an extended VTO (eVTO) paradigm with 16-25 s between trials (Figure 6.2A).

Data acquisition

Once fully trained, rats were briefly anesthetized with isoflurane (4% for ~2 minutes, shown to have no effect on ICSS performance (Robinson and Carelli, 2008; Robinson et al., 2009)) for insertion of the iontophoresis assembly and micromanipulator into the implanted cannula. The iontophoresis probe was slowly lowered to 6.2 mm in the brain. The electrode was cycled for 15 min at 60 Hz from -0.4 to 1.3 V and back at 400 V/s (Heien et al., 2003) using custom-built software (HDCV, LABVIEW, National Instruments, Austin, TX). After this the waveform was applied at 10 Hz during priming of the iontophoretic barrels as described previously (Herr et al., 2010).

Following priming, the electrode was lowered into the NAc (7.0 mm DV) and the same waveform applied at 5 Hz to allow electrophysiological recordings in between potential scans (Owesson-White et al., 2008; Belle et al., 2013). Data collection occurred at sites where a single unit was isolated; multiple recording locations were used in a single animal provided they were at least 300 µm apart. Single units were amplified (x 1,000), band-pass filtered (300-3,000 Hz), and digitized with commercially available software (DIGITIZER, Plexon, Dallas, TX). Isolation of units employed principal component analysis with commercially available software (OFFLINE SORTER, Plexon, Dallas, TX).

Single units were considered MSNs if they had a baseline firing rate below 15 Hz and a waveform duration of less than 1.2 ms (Carelli and Ijames, 2001). Baseline firing rate was measured during 30 trials of the eVTO paradigm. Next, trials occurred where a drug

was iontophoresed for 15 s during the extended time-out period. Iontophoretic barrels were used with a randomized order of drug application. The firing pattern of a MSN was defined as responsive to the lever or the cue based on the magnitude of the z-score to each event. It was classified as increasing in firing rate if the firing rate during the baseline ICSS period had a z-score of +1.65 with respect to the cue onset or lever availability period. MSNs were considered to decrease in firing rate if the z-score was less than -1.65. For MSNs that had z-scores fitting multiple response categories, the MSN was classified based on the z-score of greatest magnitude. MSNs without significant changes in firing rate were termed non-phasic. Med-Associates software (St. Albans, VT) controlled iontophoresis ejections and provided digital outputs synchronized to behavioral cues that were recorded in both HDCV (fast-scan cyclic voltammetry) and Plexon (electrophysiology) records.

Data Analysis

Dopamine was identified from the background subtracted cyclic voltammograms with principal component analysis (Michael et al., 1999). Neural activity was characterized with raster displays and peri-event histograms (PEHs) across distinct time domains that bracketed the iontophoretic ejections. We use N to indicate number of animals and n to equal the number of units.

RESULTS

Neuronal Responses during Behavior

In trained animals executing an ICSS program, we simultaneously measured dopamine release and neuronal firing at sites within the NAc where MSNs were isolated. The animals expected lever extension into the behavioral chamber 2 s after the initiation of an audiovisual cue that was delivered at random times (Figure 6.1A). Pressing the lever activated an electrical stimulation of dopamine cell bodies in the VTA. MSNs showed four

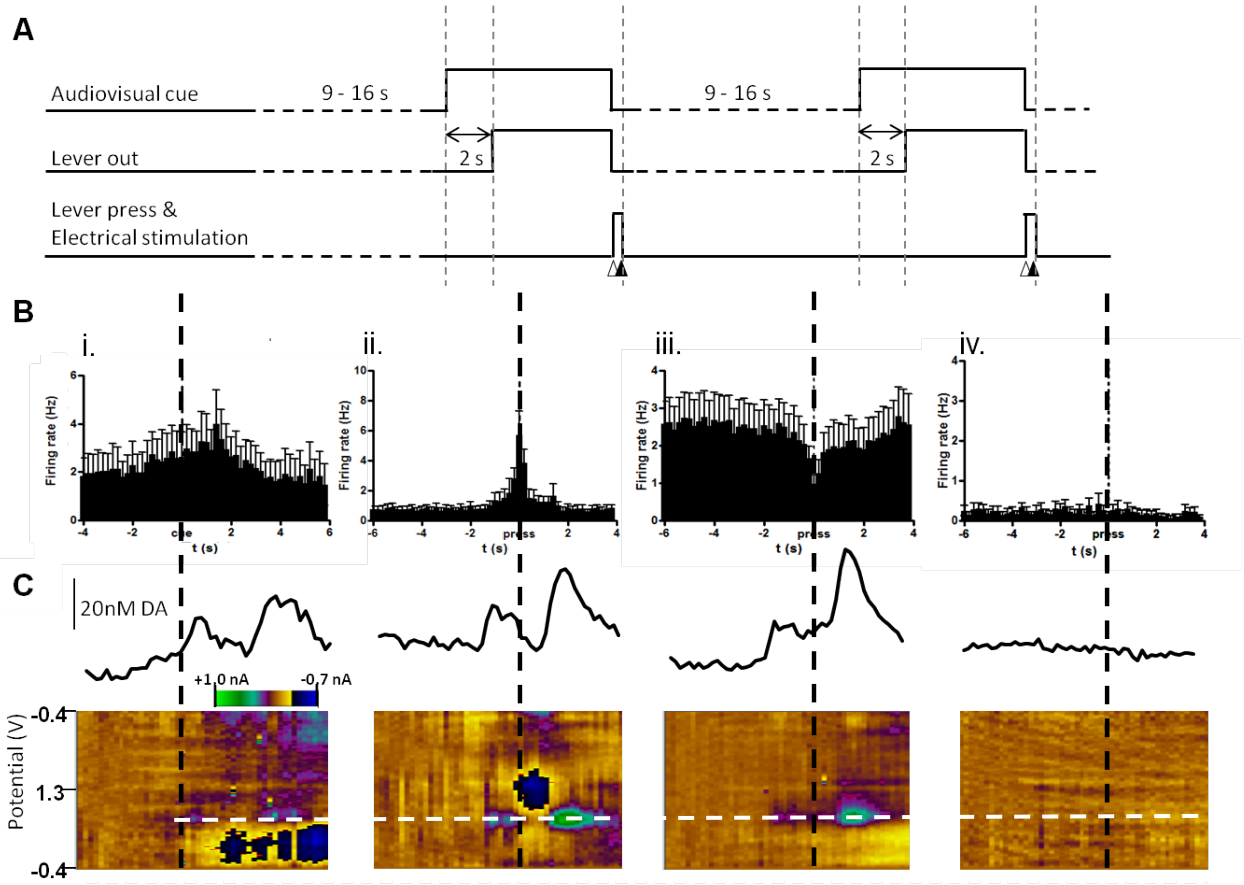

Figure 6.1. Neuronal responses seen during VTO ICSS. A) Timing diagram for VTO ICSS (Upper) The audiovisual cue (house light and tone) turns on and (Middle) 2 s later the lever is presented to the animal. (Lower) The stimulation was delivered (black triangle) 200 ms following lever press (white triangle) and the lever retracted after press. After a variable time out of 9-16 s the audiovisual cue was presented and the cycle reinitiated. B & C) 4 distinct MSN firing responses seen during behavior in (A): increase in cell firing to cue presentation (i), increase in cell firing to lever press (ii), decrease in cell firing to lever press (iii), no change in cell firing during behavior (iv). The black vertical dashed line marks the time of cue onset (i) or lever press (ii-iv). B) Average PEH for each MSN type. Firing events are collected in 200 ms bins. PEHs are the average of 6 MSNs (i), 17 MSNs (ii), 38 MSNs (iii), or 9 MSNs (iv). C) Colorplot representation of voltammetric data collected over the 10 s including cue presentation and lever press. Each colorplot is the average of 30 trials within a single location. The white dashed line indicates the potential at which the dopamine is oxidized.

different responses (Figure 6.1C). Firing rate increased immediately following cue presentation (9 %), increased immediately before the lever press (24 %), or decreased immediately before the lever press (54 %). In 13 % of locations firing rate did not change in response to the cue or lever extension, and these were locations where dopamine release timelocked to the behavior was not observed. At the other locations, a transient increase in dopamine concentration occurred following lever presentation, followed by a second dopamine surge at the electrical stimulation, consistent with our prior findings (Owesson-White et al., 2008).

Identification of MSNs by Dopamine Receptor Subtype

MSNs were classified as D1, D2 or D1/D2 cells based on their firing rate changes during iontophoretic introduction of D1R and D2R antagonists. The VTO interval was increased to 16-25 s, and the predrug firing rate was taken over a 15 s interval 1 s prior to cue onset for 30 consecutive trials (Figure 6.2A). Next, the D1R antagonist raclopride or D2R antagonist SCH 23390 were iontophoresed during the 15 s interval 1 s prior to cue onset in each trial. Average changes during antagonist application relative to predrug firing rate were taken as an indicator of the specific dopamine receptor subtype present. The majority (76%) of MSNs showed altered cell firing to only one receptor antagonist, 5% responded to both D1R and D2R antagonism, and 19% of MSNs were unresponsive to either antagonist. As seen previously (Belle et al., 2013), D2 responsive MSNs increased their firing rate in response to raclopride while D1 responsive MSNs decreased their firing rate in response to SCH 23390 (Figure 6.2B). D1 responsive MSNs also showed the highest predrug firing rate, while non-phasic cells had the lowest baseline firing rate (Figure 6.2B).

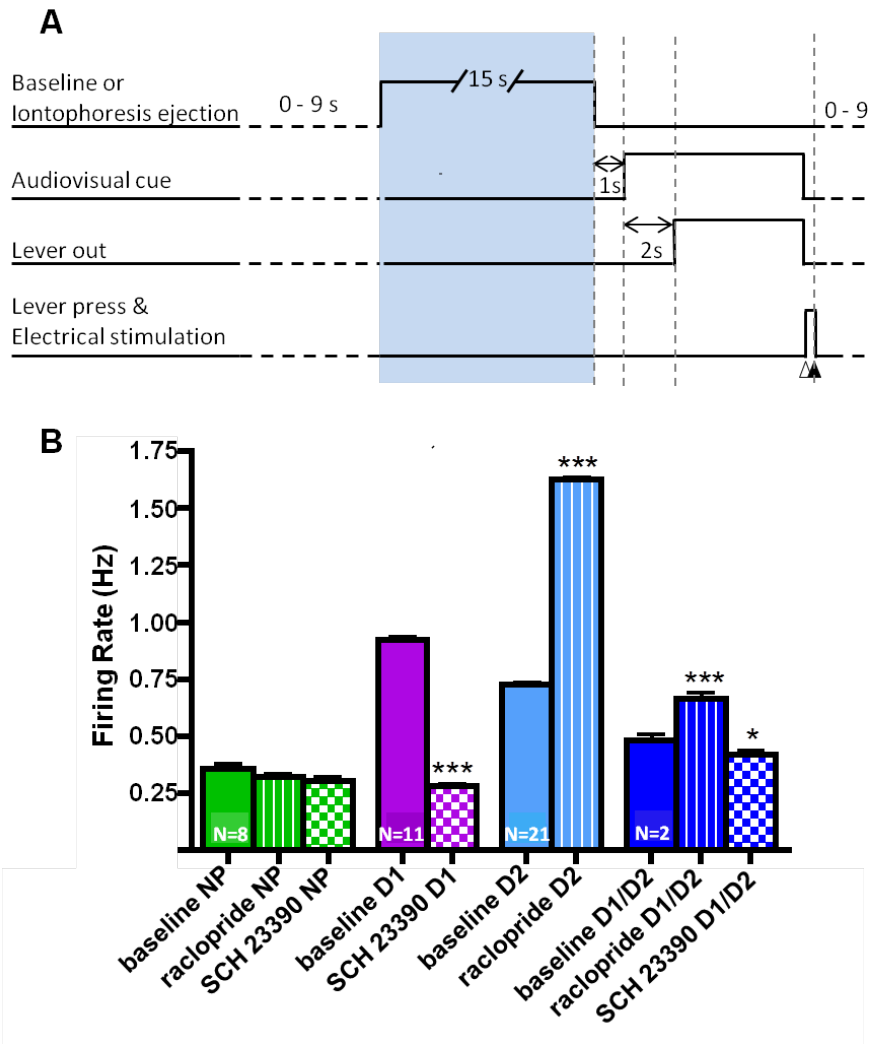

Figure 6.2. Firing rates for MSNs sorted by dopamine receptor subtype. A) Timing diagram for eVTO with highlighted region showing the period during which firing rates in (B) are compared. Timing is the same as in Figure 6.1, but with a variable time out between trials of 16- 25 s, to allow a collection of baseline firing rate or iontophoretic ejection (Top). B) Baseline firing for D1, D2 and D1/D2 MSNs along with firing during application of receptor subtype specific antagonists, SCH 23390 for D1 MSNs, raclopride for D2 MSNs, and both for D1/D2 MSNs. Baseline cell firing is significantly different between all cell types (one-way ANOVA, Tukey post test, $p<0.001$). All pharmacological manipulations significantly alter baseline firing rates (paired t-test, *** $p<0.001$ * $p<0.05$).

Dopamine modulation of MSN firing patterns

We investigated whether iontophoresis of dopamine receptor antagonists affected firing patterns of MSNs during ICSS. MSNs were sorted by both dopamine receptor type and ICSS response. Interestingly, cells that were unresponsive to pharmacological challenge also were not timelocked in their firing during ICSS responses. All MSNs that had a timelocked increase in cell firing following the cue responded only to D2R antagonism (Table 6.1). Most of the cells timelocked to (but proceeding) the press were D1 responsive cells. Populations of D1, D2, and D1/D2 responsive MSNs showed decreases in firing rate timelocked, but preceding, the press.

Role of D2 Receptors in Increased Firing Rate of MSNs to Cue Presentation

MSNs that show excitations immediately after the cue all respond solely to D2R antagonism. In addition to their response to raclopride, the increase in firing rate was depressed by D2R agonist quinpirole (Figure 6.3A) and was unaffected by D1R selective drugs (Figure 6.3B). The relative increase in firing rate (i.e. signal-to-baseline) after cue onset remained constant following raclopride but decreased following quinpirole (Figure 6.3C).

Role of D1 Receptors in Increased Firing Rate of MSNs in Anticipation of Lever Press

The majority (86%) of MSNs that showed an increased firing rate in anticipation of the lever press responded exclusively to D1R antagonism as reported in Table 6.1. But, the six cells showing this behavior do not show statistically significant differences in firing rate during ICSS when averaged together (Figure 6.4) due to the variation in predrug MSN firing frequencies between cells. Further collection of MSN responses will hopefully create a statistically significant depression of the anticipatory increase in MSN firing with SCH 23390

Table 6.1. MSN Cell-type and Firing Pattern During ICSS

	Number of Cells (%)[a]		
Type of Response	**D1**	**D2**	**D1+D2**
Excitatory to cue[b]	0 (0)	16 (36)	0 (0)
Excitatory to press[c]	6 (14)	1 (2)	0 (0)
Inhibitory to press[d]	4 (9)	4 (9)	2 (5)
TOTAL	10 (23)	21 (47)	2 (5)

[a]Percentages are calculated from N = 44 cells (units) from 14 rats. 11 (25%) non-phasic units are not listed in the table. These units did not respond to either antagonist and showed no time-locked response to behavior

[b]z-score of ≥1.65 for the 1.8 s cue firing period compared to 2.4 s baseline, when all firing is aligned to cue presentation

[c]z-score of ≥1.65 for the 0.6 s lever anticipation firing period compared to 2.4 s baseline when firing was aligned to lever presentation

[d] z-score of ≤-1.65 for the 0.6 s lever anticipation firing period compared to 2.4 s baseline when firing was aligned to lever presentation

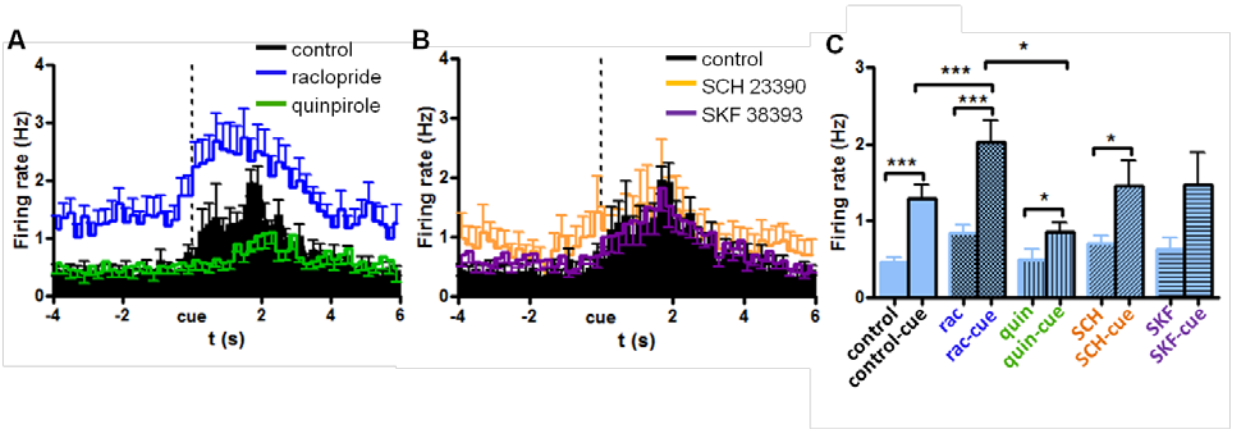

Figure 6.3. Pharmacological manipulation of cue cells during behavior. A) Manipulation of cell firing with D2R selective drugs. Average cell firing of MSNs during control sessions (black boxes, n=27), a session where the D2R antagonist raclopride (rac) was iontophoresed before cue presentation (blue trace, n=27) and a session where the D2R agonist quinpirole (quin) was iontophoresed before cue presentation (green trace, n=11). All session conditions showed a significant change in cell firing with the cue, and there was a significant change in cell firing between session conditions (two-way ANOVA, $p<0.001$). B) Manipulation of cell firing with D1R selective drugs. Average cell firing of MSNs during control sessions (black boxes, n=27), a session where the D1R antagonist SCH 23390 was iontophoresed before cue presentation (orange trace, n=13) and a session where the D1R agonist SKF 38393 was iontophoresed before cue presentation (purple trace, n=11). All session conditions showed a significant change in cell firing with the cue but no significant change in cell firing between conditions (two-way ANOVA, $p<0.001$). C) Summary average firing rate before onset of the cue and during the 1.8 s cue presentation window (-cue) for all pharmacological manipulations of cue responsive cells (one-way Anova $P < 0.001$ *** (df=9)).

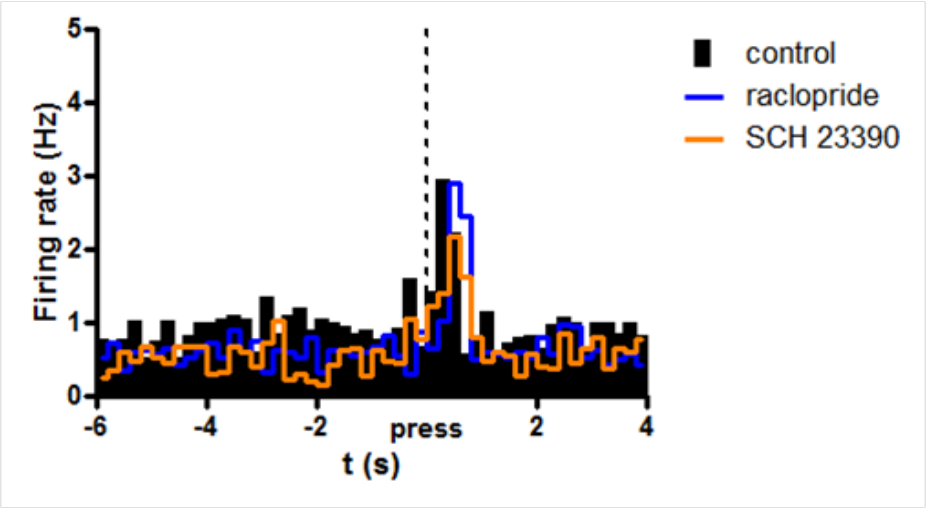

Figure 6.4. Pharmacological manipulation of D1 MSNs that increased firing frequency immediately before lever press. Average cell firing of MSNs during control sessions (black boxes, n=6), a session where the D2R antagonist raclopride was iontophoresed before cue presentation (blue trace, n=6) and a session where the D1R antagonist SCH 23390 was iontophoresed before cue presentation (orange trace, n=6). CURRENTLY: There was no statistical difference in the firing patterns between session conditions, but within each session condition there was a significant change in cell firing to the lever press (two-way ANOVA, $p<0.001$).

application and no alteration with raclopride. The MSNs that showed inhibition immediately before the press responded to both D1R and D2R agents.

DISCUSSION

In this work we examined the electrochemical and electrophysiological events that occur in the NAc during execution of the operant, rewarding behavior, ICSS. We combined these measurements with a novel iontophoretic procedure that allows delivery of known amounts of pharmacologically active substances (Belle et al., 2013). Iontophoresis of dopamine antagonists enable the distinction of MSNs modulated by D1-like receptors, the direct pathway, from MSNs that are modulated by D2-like receptors, the indirect pathway. Consistent with prior work (Day et al., 2007; Owesson-White et al., 2008; Howe et al., 2013), we find that cues that predict impending reward availability induce a transient dopamine concentration surge that is followed by a second dopamine surge evoked by the electrical stimulation. Simultaneous single-unit recordings reveal that these neurochemical events coincide with electrophysiological changes in firing rate. MSNs that increased their firing rate to cue onset exclusively responded to a D2R agonist or antagonist. Less than two seconds later, but prior to the lever press, a population of MSNs, primarily D1 responsive, exhibit a more rapid increase in firing rate. Another distinct (but heterogeneous) population of MSNs exhibits a transient decrease in firing immediately preceding the lever press.

The major glutamatergic inputs to NAc MSNs are from the ventral hippocampus, basal lateral amygdala, and prefrontal cortex (Sesack and Grace, 2010). Dopamine in the NAc modulates the effects of these excitatory inputs rather than directly driving neuronal activity (O'Donnell et al., 1999; Nicola et al., 2000). Thus, when dopamine is transiently introduced into the NAc of an awake but quiescent animal, either exogenously with iontophoresis or endogenously with electrical stimulation of dopaminergic neurons, it is

relatively ineffective in causing an immediate change in the firing of MSNs (Belle et al., 2013). In contrast, in active reward-seeking, glutamatergic terminals are activated and the modulatory effects of dopamine are apparent. Indeed, there was sufficient neuronal activity in the time in between behavioral trials that we could evaluate the effects of dopamine antagonists on firing rate. From the results in Figure 6.2B we conclude that dopamine predominantly increases the firing rate of D1 responsive MSNs and decreases the firing of D2 responsive MSNs. These data are consistent with measurements of the modulatory effects of dopamine at MSNs that are in the "up" state as determined with patch clamp recording in brain slices or anesthetized preparations (Bamford et al., 2004; Brady and O'Donnell, 2004; Andre et al., 2010; Wang et al., 2012).

Even though it only has a modulatory role, considerable evidence shows that dopamine release is critically important for optimum performance of reward related responses (Schultz, 2007; Tripp and Wickens, 2012). In particular, evidence from ICSS experiments strongly supports the view that dopamine release is an important component of this behavior (Wise, 2004). For example, genetically modified rats that express opsin in dopamine neurons will work to deliver optical pulses that evoke the neuronal release of dopamine in much the same way as the animals described here work for electrical stimulation to the VTA (Witten et al., 2011). However, subsequent research using optogenetics has also revealed that mice will work to receive optical excitation of MSNs containing opsin (Britt et al., 2012). These optogenetic results concur with the previous neurochemical result that ICSS can occur without dopamine release (Garris et al., 1999). Rather, dopamine appears to filter the responses of NAc MSNs to cortical (O'Donnell, 2003), hippocampal, and amgydalar inputs (Mogenson et al., 1988; Pennartz et al., 1994; O'Donnell et al., 1999; Floresco et al., 2001). One proposal is that dopamine modulates these different inputs via alteration of the signal-to-baseline ratio of MSN firing (Kiyatkin and Rebec, 1996; O'Donnell and Grace, 1996; Nicola et al., 2000). Our combined

neurochemical and electrophysiological results in the NAc of a rat pressing for ICSS reward directly confirm this hypothesis. In the presence of a D2R antagonist, both the baseline firing rate and the burst immediately following the cue increase their firing rate, thus resulting in a decreased signal (the burst) relative to the noise (the baseline, Figure 6.4A). Overall firing frequency also changes, suggesting that *changes* in MSN firing modulate behavior.

During ICSS a minority of MSNs show no phasic changes in firing rate. These cells are in locations lacking detectable dopamine release during ICSS (Figure 6.1Biv), a previously reported phenomenon (Owesson-White et al., 2009; Cacciapaglia et al., 2011). In this behavioral paradigm, non-phasic cells have significantly suppressed baseline firing rates compared to phasic MSNs, supporting the idea that the circuit containing these NAc MSNs is not activated during ICSS.

There have been prior attempts to separate the roles of D1R and D2R containing MSNs on behavior. Kravitz and coworkers used selective optogenetic activation of dopamine D1R- or D2R–expressing striatal MSNs to evaluate their influence on reinforcement learning in mice (Kravitz et al., 2012). Stimulating D1R–expressing neurons induced persistent reinforcement, whereas stimulating D2R–expressing neurons induced transient punishment. Additionally, microinfusion of the D2R agonist quinpirole into the NAc (Yawata et al., 2012) inhibited acquisition of aversive behaviors. In agreement with these findings we observed that increased MSN firing at the cue was suppressed with D2R agonism while D2R antagonism decreased the signal-to-baseline ratio for the increase in firing rate by increasing baseline firing (Figure 6.4). In contrast, we hope to find that MSNs showing an anticipatory increase to the lever press show enhanced firing in the presence of D1R agonists. The concept that activation of both types of MSNs is required to coordinate responses during reward seeking is supported by the work of Cui and coworkers. Using viral expression of a calcium indicator selective for D1 or D2 MSNs, they showed that both pathways are activated in mice executing an operant task (Cui et al., 2013).

D1 MSN responses are required for behavioral reinforcement (Kravitz et al., 2012) and increased cell firing during reward based behaviors involves D1R activation of the direct pathway (Cheer et al., 2007). Our experiments reveal that the dopamine surge following the cue does not result in a D1R mediated response until almost 2 seconds later in anticipation of lever availability. This is consistent with the initiation of MSN firing by glutamatergic inputs while dopamine serves a modulatory role. Indeed, dopamine is known to exert its effects 2 to 3 seconds after its release (Schultz, 2007).

Consistent with our findings, microinfusions of D2R antagonists into the NAc block responding to reward predicting cues (Yun et al., 2004). Using a second order reinforcement schedule for cocaine self-administration, Di Ciano and coworkers found that cue evoked reinstatement of drug seeking was attenuated by a selective D_3R antagonist given systemically (Di Ciano et al., 2003) and lever pressing was inhibited by microinfusions of the D_3R antagonist directly into the basal lateral amygdala (Di Ciano, 2008). These results were replicated by Gal and coworkers who also showed that haloperidol, a nonspecific D2R antagonist blocked reinstatement of cocaine taking (Gal and Gyertyan, 2006). In both studies, cue-controlled responding for sucrose was unaffected by these antagonists. Others have shown that D2 MSNs are linked to motivation (Trifilieff et al., 2013) or updating a learned response (Yawata et al., 2012).

The occurrence of increased firing rate at cue presentation exclusively in D2 MSNs indicates an inhibition of the indirect circuit. Consistent with this, the effects of glutamate release on D2R responsive MSNs in the slice preparation is attenuated by dopamine (Wang et al., 2012). D2 MSNs also have been shown to participate in long term depression (Grueter et al., 2010). Stimulating D2R–expressing neurons induced transient punishment, indicating that activation of these circuits is sufficient to modify the probability of performing future actions (Kravitz et al., 2012). Suppression of D2 MSN firing by dopamine (or quinpirole, Figure 6.4) would attenuate this affect.

In conclusion, the dopamine surge following the cue has a dual role. First, it prevents responding or encoding of aversive circuits to cue presentation by inhibiting the firing frequency of D2 MSNs. Second, 2-3 s later dopamine activates low affinity D1Rs in anticipation of the press. With further experiments to examine alteration of MSN firing patterns with D1R agonism and in behavioral extinction paradigms the measurements made here will help provide a clarified view of the interplay between the direct and indirect pathways in reward driven behavior.

REFERENCES

Andre VM, Cepeda C, Cummings DM, Jocoy EL, Fisher YE, William Yang X, Levine MS (2010) Dopamine modulation of excitatory currents in the striatum is dictated by the expression of D1 or D2 receptors and modified by endocannabinoids. Eur J Neurosci 31:14-28.

Bamford NS, Zhang H, Schmitz Y, Wu NP, Cepeda C, Levine MS, Schmauss C, Zakharenko SS, Zablow L, Sulzer D (2004) Heterosynaptic dopamine neurotransmission selects sets of corticostriatal terminals. Neuron 42:653-663.

Belle AM, Owesson-White C, Herr NR, Carelli RM, Wightman RM (2013) Controlled Iontophoresis Coupled with Fast-Scan Cyclic Voltammetry/Electrophysiology in Awake, Freely Moving Animals. ACS Chem Neurosci.

Brady AM, O'Donnell P (2004) Dopaminergic modulation of prefrontal cortical input to nucleus accumbens neurons in vivo. J Neurosci 24:1040-1049.

Britt JP, Benaliouad F, McDevitt RA, Stuber GD, Wise RA, Bonci A (2012) Synaptic and behavioral profile of multiple glutamatergic inputs to the nucleus accumbens. Neuron 76:790-803.

Cacciapaglia F, Wightman RM, Carelli RM (2011) Rapid Dopamine Signaling Differentially Modulates Distinct Microcircuits within the Nucleus Accumbens during Sucrose-Directed Behavior. J Neurosci 31:13860-13869.

Carelli RM, Ijames SG (2001) Selective activation of accumbens neurons by cocaine-associated stimuli during a water/cocaine multiple schedule. Brain Res 907:156-161.

Cepeda C, Hurst RS, Altemus KL, Flores-Hernandez J, Calvert CR, Jokel ES, Grandy DK, Low MJ, Rubinstein M, Ariano MA, Levine MS (2001) Facilitated glutamatergic transmission in the striatum of D2 dopamine receptor-deficient mice. J neurophysiol 85:659-670.

Cheer JF, Heien ML, Garris PA, Carelli RM, Wightman RM (2005) Simultaneous dopamine and single-unit recordings reveal accumbens GABAergic responses: implications for intracranial self-stimulation. Proc Natl Acad Sci U S A 102:19150-19155.

Cheer JF, Aragona BJ, Heien ML, Seipel AT, Carelli RM, Wightman RM (2007) Coordinated accumbal dopamine release and neural activity drive goal-directed behavior. Neuron 54:237-244.

Cui G, Jun SB, Jin X, Pham MD, Vogel SS, Lovinger DM, Costa RM (2013) Concurrent activation of striatal direct and indirect pathways during action initiation. Nature 494:238-242.

Day JJ, Roitman MF, Wightman RM, Carelli RM (2007) Associative learning mediates dynamic shifts in dopamine signaling in the nucleus accumbens. Nat Neurosci 10:1020-1028.

Di Ciano P (2008) Drug seeking under a second-order schedule of reinforcement depends on dopamine D3 receptors in the basolateral amygdala. Behav Neurosci 122:129-139.

Di Ciano P, Underwood RJ, Hagan JJ, Everitt BJ (2003) Attenuation of cue-controlled cocaine-seeking by a selective D3 dopamine receptor antagonist SB-277011-A. Neuropsychopharmacol 28:329-338.

Floresco SB, Blaha CD, Yang CR, Phillips AG (2001) Modulation of hippocampal and amygdalar-evoked activity of nucleus accumbens neurons by dopamine: cellular mechanisms of input selection. J Neurosci 21:2851-2860.

Gal K, Gyertyan I (2006) Dopamine D3 as well as D2 receptor ligands attenuate the cue-induced cocaine-seeking in a relapse model in rats. Drug Alcohol Depend 81:63-70.

Garris PA, Kilpatrick M, Bunin MA, Michael D, Walker QD, Wightman RM (1999) Dissociation of dopamine release in the nucleus accumbens from intracranial self-stimulation. Nature 398:67-69.

Gerfen CR, Surmeier DJ (2011) Modulation of striatal projection systems by dopamine. Ann Rev Neurosci 34:441-466.

Grueter BA, Brasnjo G, Malenka RC (2010) Postsynaptic TRPV1 triggers cell type-specific long-term depression in the nucleus accumbens. Nat Neurosci 13:1519-1525.

Heien ML, Phillips PE, Stuber GD, Seipel AT, Wightman RM (2003) Overoxidation of carbon-fiber microelectrodes enhances dopamine adsorption and increases sensitivity. Analyst 128:1413-1419.

Herr NR, Daniel KB, Belle AM, Carelli RM, Wightman RM (2010) Probing presynaptic regulation of extracellular dopamine with iontophoresis. ACS Chem Neurosci 1:627-638.

Hersch SM, Ciliax BJ, Gutekunst CA, Rees HD, Heilman CJ, Yung KK, Bolam JP, Ince E, Yi H, Levey AI (1995) Electron microscopic analysis of D1 and D2 dopamine receptor proteins in the dorsal striatum and their synaptic relationships with motor corticostriatal afferents. J Neurosci 15:5222-5237.

Howe MW, Tierney PL, Sandberg SG, Phillips PE, Graybiel AM (2013) Prolonged dopamine signalling in striatum signals proximity and value of distant rewards. Nature 500:575-579.

Ikemoto S (2007) Dopamine reward circuitry: Two projection systems from the ventral midbrain to the nucleus accumbens-olfactory tubercle complex. Brain Res Rev.

Kiyatkin EA, Rebec GV (1996) Dopaminergic modulation of glutamate-induced excitations of neurons in the neostriatum and nucleus accumbens of awake, unrestrained rats. J Neurophysiol 75:142-153.

Kravitz AV, Tye LD, Kreitzer AC (2012) Distinct roles for direct and indirect pathway striatal neurons in reinforcement. Nat Neurosci 15:816-818.

Michael DJ, Joseph JD, Kilpatrick MR, Travis ER, Wightman RM (1999) Improving data acquisition for fast-scan cyclic voltammetry. Anal Chem 71:3941-3947.

Millar J, Barnett TG (1988) Basic instrumentation for fast cyclic voltammetry. J Neurosci Methods 25:91-95.

Mogenson GJ, Yang CR, Yim CY (1988) Influence of dopamine on limbic inputs to the nucleus accumbens. Ann NY Acad Sci 537:86-100.

Neve KA, Seamans JK, Trantham-Davidson H (2004) Dopamine receptor signaling. J Receptor Signal Transduct Res 24:165-205.

Nicola SM, Surmeier J, Malenka RC (2000) Dopaminergic modulation of neuronal excitability in the striatum and nucleus accumbens. Annu Rev Neurosci 23:185-215.

O'Donnell P (2003) Dopamine gating of forebrain neural ensembles. Eur J Neurosci 17:429-435.

O'Donnell P, Grace AA (1996) Dopaminergic reduction of excitability in nucleus accumbens neurons recorded in vitro. Neuropsychopharmacol 15:87-97.

O'Donnell P, Greene J, Pabello N, Lewis BL, Grace AA (1999) Modulation of cell firing in the nucleus accumbens. Ann N Y Acad Sci 877:157-175.

Owesson-White CA, Cheer JF, Beyene M, Carelli RM, Wightman RM (2008) Dynamic changes in accumbens dopamine correlate with learning during intracranial self-stimulation. Proc Natl Acad Sci U S A 105:11957-11962.

Owesson-White CA, Ariansen J, Stuber GD, Cleaveland NA, Cheer JF, Wightman RM, Carelli RM (2009) Neural encoding of cocaine-seeking behavior is coincident with phasic dopamine release in the accumbens core and shell. Eur J Neurosci 30:1117-1127.

Paxinos G, Watson C (2007) The Rat Brain in Stereotaxic Coordinates, 6 Edition. Amsterdam: Elsevier.

Pennartz CM, Groenewegen HJ, Lopes da Silva FH (1994) The nucleus accumbens as a complex of functionally distinct neuronal ensembles: an integration of behavioural, electrophysiological and anatomical data. ProgNeurobiol 42:719-761.

Phillips PE, Stuber GD, Heien ML, Wightman RM, Carelli RM (2003) Subsecond dopamine release promotes cocaine seeking. Nature 422:614-618.

Robinson DL, Carelli RM (2008) Distinct subsets of nucleus accumbens neurons encode operant responding for ethanol versus water. Eur J Neurosci 28:1887-1894.

Robinson DL, Heien ML, Wightman RM (2002) Frequency of dopamine concentration transients increases in dorsal and ventral striatum of male rats during introduction of conspecifics. J Neurosci 22:10477-10486.

Robinson DL, Howard EC, McConnell S, Gonzales RA, Wightman RM (2009) Disparity between tonic and phasic ethanol-induced dopamine increases in the nucleus accumbens of rats. Alcohol Clin Exp Res 33:1187-1196.

Schultz W (2007) Multiple dopamine functions at different time courses. Annu Rev Neurosci 30:259-288.

Schultz W, Dayan P, Montague PR (1997) A neural substrate of prediction and reward. Science 275:1593-1599.

Sesack SR, Grace AA (2010) Cortico-Basal Ganglia reward network: microcircuitry. Neuropsychopharmacol 35:27-47.

Sombers LA, Beyene M, Carelli RM, Wightman RM (2009) Synaptic overflow of dopamine in the nucleus accumbens arises from neuronal activity in the ventral tegmental area. J Neurosci 29:1735-1742.

Szczypka MS, Rainey MA, Kim DS, Alaynick WA, Marck BT, Matsumoto AM, Palmiter RD (1999) Feeding behavior in dopamine-deficient mice. Proceedings of the National Academy of Sciences of the United States of America 96:12138-12143.

Szczypka MS, Kwok K, Brot MD, Marck BT, Matsumoto AM, Donahue BA, Palmiter RD (2001) Dopamine production in the caudate putamen restores feeding in dopamine-deficient mice. Neuron 30:819-828.

Takmakov P, McKinney CJ, Carelli RM, Wightman RM (2011) Instrumentation for fast-scan cyclic voltammetry combined with electrophysiology for behavioral experiments in freely moving animals. Rev Sci Instrum 82:074302.

Trifilieff P, Feng B, Urizar E, Winiger V, Ward RD, Taylor KM, Martinez D, Moore H, Balsam PD, Simpson EH, Javitch JA (2013) Increasing dopamine D2 receptor expression in the adult nucleus accumbens enhances motivation. Mol Psychiatry.

Tripp G, Wickens J (2012) Reinforcement, dopamine and rodent models in drug development for ADHD. Neurotherapeutics 9:622-634.

Valjent E, Bertran-Gonzalez J, Herve D, Fisone G, Girault JA (2009) Looking BAC at striatal signaling: cell-specific analysis in new transgenic mice. Trends Neurosci 32:538-547.

Wang H, Pickel VM (2002) Dopamine D2 receptors are present in prefrontal cortical afferents and their targets in patches of the rat caudate-putamen nucleus. J Comp Neurol 442:392-404.

Wang W, Dever D, Lowe J, Storey GP, Bhansali A, Eck EK, Nitulescu I, Weimer J, Bamford NS (2012) Regulation of prefrontal excitatory neurotransmission by dopamine in the nucleus accumbens core. J Physiol 590:3743-3769.

Wise RA (2002) Brain reward circuitry: insights from unsensed incentives. Neuron 36:229-240.

Wise RA (2004) Dopamine, learning and motivation. Nat Rev Neurosci 5:483-494.

Witten IB, Steinberg EE, Lee SY, Davidson TJ, Zalocusky KA, Brodsky M, Yizhar O, Cho SL, Gong S, Ramakrishnan C, Stuber GD, Tye KM, Janak PH, Deisseroth K (2011) Recombinase-driver rat lines: tools, techniques, and optogenetic application to dopamine-mediated reinforcement. Neuron 72:721-733.

Yawata S, Yamaguchi T, Danjo T, Hikida T, Nakanishi S (2012) Pathway-specific control of reward learning and its flexibility via selective dopamine receptors in the nucleus accumbens. Proc Natl Acad Sci U S A 109:12764-12769.

Yun IA, Wakabayashi KT, Fields HL, Nicola SM (2004) The ventral tegmental area is required for the behavioral and nucleus accumbens neuronal firing responses to incentive cues. J Neurosci 24:2923-2933.

Zweifel LS, Parker JG, Lobb CJ, Rainwater A, Wall VZ, Fadok JP, Darvas M, Kim MJ, Mizumori SJ, Paladini CA, Phillips PE, Palmiter RD (2009) Disruption of NMDAR-dependent burst firing by dopamine neurons provides selective assessment of phasic dopamine-dependent behavior. Proc Natl Acad Sci U S A 106:7281-7288.